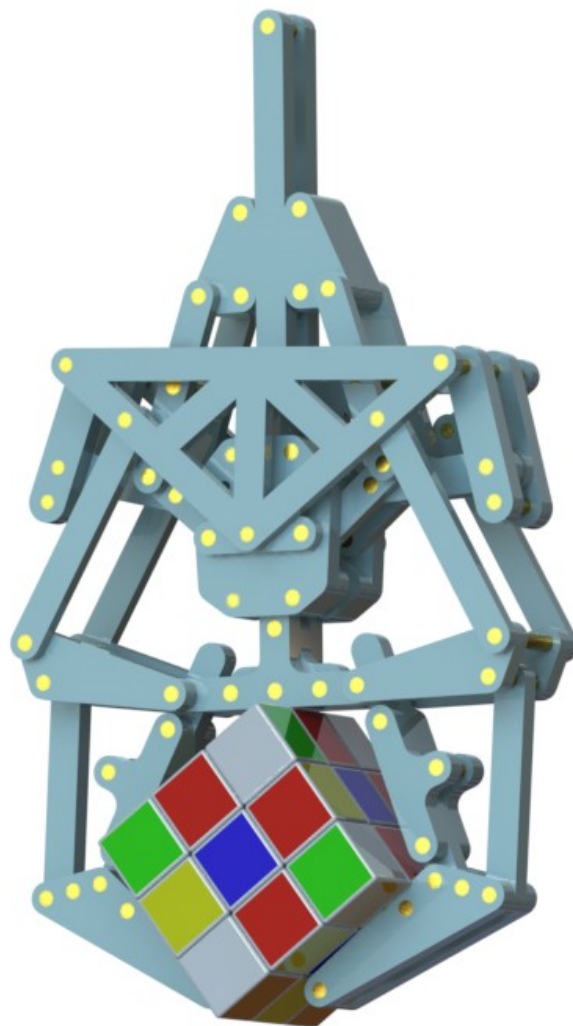


Design of an underactuated grasper with adjustable compliance

R.A.J. Stavenuiter

1359568

Master of Science Thesis



Design of an underactuated grasper with adjustable compliance

MASTER OF SCIENCE THESIS

For the degree of Master of Science in Mechanical Engineering at Delft
University of Technology

May 21, 2013

Author: R.A.J. Stavenuiter
Student number: 1359568

Board of examiners: Prof.Dr.Ir. J.L. Herder, Delft University of Technology
Dr.Ir. L. Birglen, Polytechnique Montreal
Dr.Ir. M. Wisse, Delft University of Technology
Ir. E.A. Arkenbout, Delft University of Technology

Faculty of Mechanical, Maritime and Materials Engineering (3mE) · Delft University of
Technology

Preface

This thesis consists of the research I have performed at the Interactive Mechanisms Research Lab of the department of BioMechanical Engineering. Spring balanced, compliant and underactuated mechanisms are the main research fields studied at this lab which in my opinion have one thing in common; obtaining functionality by means of a clever mechanical design instead of sophisticated control. These topics have always intrigued me during my study, therefore the choice was easily made to perform my graduation research at this lab. One of the topics that drew my attention was underactuated grasping; simplistic multi degree of freedom mechanisms that are able to grasp any kind of object using only a single actuator. This type of graspers has a high level of self-adaptability which is advantageous when picking up objects but limits the robustness of the grasper. I challenged myself to increase the robustness of an underactuated grasper by only adjusting the mechanical design.

The first part of my research consisted of a literature study on variable stiffness actuator designs. The purpose of this study was to identify working principles used to mechanically adjust the robustness of a mechanism and get inspired for the design of my grasper. The second part of my research began abroad at Polytechnique Montreal. Here I performed the conceptual design process and started the analytical modeling of the final concept. After 3.5 memorable months I returned to Delft to complete the analytical modeling and to build and test a prototype of my final design.

I would like to thank my supervisors Just Herder and Lionel Birglen for their advice during this research. Furthermore I would like to thank my friends, family, my girlfriend Roos Veenkamp and my roommates: Thomas Dekker, Marjolein van Osch, Vincent Koenders, Roxanne Kiel, Rowan Ton, Frank Vester and Claire den Boer with whom I could share my moments of glory and distress during this research.

Delft, University of Technology
May 21, 2013

R.A.J. Stavenuiter

Table of Contents

Preface	i
1 Paper: Design of an underactuated grasper with adjustable compliance	1
A Conceptual Design	11
A-1 Task analysis	12
A-2 Requirements	13
A-3 Identify locations	13
A-4 Morphological overview	16
A-5 Concept solutions	17
A-6 Concept selection	27
A-7 Proof of concept	28
A-8 Final concept	36
B Analytical Modeling	39
B-1 Experiments	40
B-2 Optimization	43
C Experiments	49
C-1 Prototype	50
C-2 Measurement setup	52
D Literature study: Performance quantification of variable stiffness actuator designs	57
Bibliography	87

Chapter 1

Paper: Design of an underactuated grasper with adjustable compliance

Submitted to *Transactions on Robotics*

Design of an Underactuated Grasper with Adjustable Compliance

Ronald A.J. Stavenuiter, Lionel Birglen and Just L. Herder

Abstract—Underactuated graspers are known for their self-adaptability. The final configuration of the grasper in which it obtains a stable grasp relies on the static equilibrium of the grasper and object. An external or inertial force that acts on the object disturbs this static equilibrium and can cause a change in the configuration of the grasper. The self-adaptability therefore reduces the robustness against external perturbations. This paper introduces the concept design of an underactuated grasper with the ability to adjust its level of self-adaptability by changing the rotational stiffness of an internal differential mechanism. By implementing a bi-stable mechanism the grasper is able to transfer from a compliant state to a stiff state once the actuator force overcomes a threshold value. Experimental validation of the concept design shows that the lateral compliance of the grasper in the stiff state is reduced by a factor of 7 compared to the compliant state. The lateral pull-out force of the grasper in the stiff state is increased by a factor of 1.9 compared to the compliant state. As a result a grasper was designed which uses the benefits of self-adaptability to grasp an object and increases its robustness once a stable grasp is obtained without the need of an additional actuator.

Index Terms—Underactuated grasping, robustness.

I. INTRODUCTION

UNDERACTUATED grasping is a research topic that is widely studied. Many grasper designs have been proposed, such as the SARAH hands [1], SDM hand [2], TWIX hand [3], Delft Hand III [4], SRI hand [5] and others as can be found in [6]. An underactuated grasper distributes an actuation force between the phalanges of its fingers. When an actuator force is applied and the fingers enclose an object a number of contact forces arise between the phalanges and the object. Because of the self-adaptability of the grasper these contact forces change the configuration of the grasper until a configuration is found in which the grasper and object are in static equilibrium. The general advantage of this working principle is that a large variety of objects can be grasped without sophisticated control algorithms. In the case that an external force is applied to the object the static equilibrium is perturbed. As a response to this force perturbation the configuration of the grasper is adjusted and the object position changes. If the object position stays within the stable region of the grasper a new static equilibrium position can be found. If it does not then the external force leads to an instable grasp.

One could say that instead of resisting external forces the grasper adjusts to them due to its self-adaptability. This behavior can be troublesome, for example during a pick and place task in which the grasper undergoes high accelerations. The inertial forces that act on the object can change the configuration of the grasper which could lead to instability. It

may therefore be beneficial if the grasper could use the self-adaptability while grasping and increase its robustness once a stable grasp is obtained.

In literature previous work can be found that has focused on improving the stability and the robustness of underactuated graspers. Stability can be improved by optimizing the dimensional design of a grasper [7] or by adding a second actuator [8]. Other work has focused on improving the robustness of an underactuated finger during a precision grasp by varying the transmission ratio between proximal and distal phalanx [9]. This variable transmission ratio is obtained by actively changing the pulley radius of the proximal joint. Another way to increase the robustness of a grasper is to remove degrees of freedom (DOF) of the grasper using joint locks such as electrostatic brakes as applied in [5] or friction based brakes as applied in [10] [11]. Another possibility is to implement a friction based coupling mechanism as applied in [12]. This design increases the robustness by restricting the rotation of a pulley that connects two tendon driven fingers.

Instead of removing DOF to increase the robustness of a grasper another approach is to mechanically adjust the rotational stiffness of the available DOF. This method is widely applied in the designs of variable stiffness actuators such as the MACCEPA 2.0 [13], AwAS II [14], DLR FSJ [15] and others as can be found in [16]. This type of actuators make use of passive elements and by changing the characteristics of these elements the rotational stiffness of the actuator can be adjusted. A similar method has been applied in underactuated grasping to obtain the ability of adjusting grasp styles by varying spring preloads of the fingers of the grasper [17]. Mechanically adjusting the rotational stiffness can also be used to adjust the robustness of a grasper.

This research proposes the design of an underactuated grasper which increases its robustness against external force perturbations by adjusting the rotational stiffness of an internal differential mechanism. By changing the actuation type of the differential from a point force to an antagonistic couple the rotational stiffness of the differential is adjusted. Using a preloaded bi-stable mechanism the grasper requires only a single actuator and transfers between a compliant and a stiff state once the actuator force overcomes a threshold value. Analytical and experimental validation of the design will be done to quantify the robustness of the grasper.

The paper is constructed as follows: section II describes the design method and the methods used to analytically and experimentally validate the concept. Section III shows the analytical and experimental results, which will be discussed in section IV. Conclusions are drawn in section V.

II. METHODS

A. Design framework

In order to restrict the solution space of this research a number of limitations were applied. The actuation force was set at a constant value of 3.9N and no mass or inertia of the links and object was considered. It was considered not to model the spring that connects the proximal and distal phalanx. The robustness of the grasper was defined as the ability of the grasper to resist lateral forces that are applied to the center of the object in the direction parallel to the palm. The lateral compliance of the grasper was used as a metric to quantify the robustness and was defined as follows:

$$\frac{1}{k_{lat}} = \frac{\Delta X_{obj,lat}}{\Delta F_{obj,lat}} \quad (1)$$

where the lateral compliance of the grasper is denoted by $\frac{1}{k_{lat}}$ in which k_{lat} represents the lateral stiffness of the grasper. $\Delta X_{obj,lat}$ represents the change in lateral displacement of the object in meters and $\Delta F_{obj,lat}$ represents the change in the resulting lateral force of the object in Newton, both in the direction parallel to the palm of the grasper. Because of the nonlinear relation of eq. (1) the lateral compliance as applied in this research was calculated only during the first grasp type, starting at zero object displacement up to the point where a transition to another grasp type takes place. The lateral direction was chosen because the experimental data of the Delft hand III as shown in [4] indicated that the robustness of the grasper was approximately three times higher in the case that the forces applied to the object were directed perpendicular to the palm compared to the case where forces were applied at an angle of $\frac{1}{4}\pi$ radians. Throughout this paper the directions parallel and perpendicular to the palm of the grasper will be referred to as lateral and axial respectively.

B. Conceptual design

1) *Requirements:* In order to set up the requirements of the grasper a task analysis of an underactuated grasper was done. A distinction was made between three basic tasks: grasp, hold and release the object and for each task the desired lateral compliance was determined. As a result it was stated that the grasper should only have a high compliance during the grasping action to passively adjust its configuration to the shape and size of the object. Once a stable grasp is obtained the compliance should decrease and be maintained up to the point where the next object has to be grasped. The mechanism that adjusts the compliance should therefore be triggered at two instances, when the grasping action starts and once a stable grasp is obtained. It was also stated that adjusting the compliance should not interfere with the force distribution between the phalanges. A change in the force distribution between the phalanges disturbs the static equilibrium and therefore results in reconfiguration of the grasper. Furthermore it was considered desirable that a single actuator was used to control both the motion of the grasper as well as adjusting the compliance.

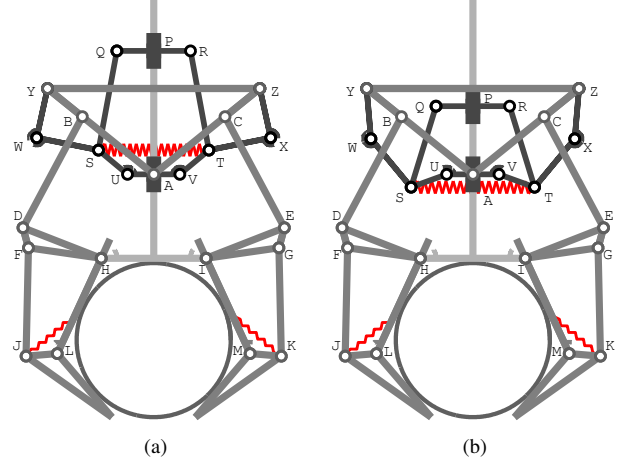


Fig. 1. Schematic representation of the final concept in its compliant (a) and stiff (b) state.

2) *Concept generation:* As a tool to generate conceptual solutions a literature study was done on variable stiffness actuator designs to identify possible working principles of adjusting the stiffness of a mechanism [18]. The findings of this study were used to form the basis of a morphological table describing solutions to obtain and trigger adjustable compliance. Conceptual solutions were generated using two different approaches, consisting of a total redesign of underactuated fingers with implemented adjustable compliance and designing mechanisms that work parallel to conventional grasper designs. No focus was put on a specific actuation principle, therefore linkage, pulley-tendon and gear driven concepts were found. As a result a total of 24 conceptual solutions were found of which the most promising concept was chosen and further developed which led to the final grasper design illustrated in Fig.1. Appendix A elaborates more on each step of the concept design process that led to the final concept.

C. Final concept

Fig. 1 is a schematic representation of the final conceptual design. A conventional grasper design was used as a basis and a mechanism was added to adjust the compliance of the grasper. The grasper design which was used as a basis consists of two fingers with each two phalanges. The angular rotation of the phalanges is restricted by mechanical stops at joints H , I , L and M . The input links of the two fingers (DFH and EGI) are connected to a differential (AYZ) which is connected to joint A . This joint consists of a rotational and prismatic joint which allows the differential to rotate and translate axially along the ground link which is attached to the palm (HI).

A bi-stable mechanism ($SUVT$) is attached to prismatic joint A of the grasper and is connected to a second prismatic joint P . The rotation angles of the links SU and TV are restricted by mechanical stops in joints U and V . The two rotational joints S and T of the bi-stable mechanism are connected by a preloaded tension spring. Two pairs of links ($SW-WY$ and $TX-XZ$) connect the bi-stable mechanism

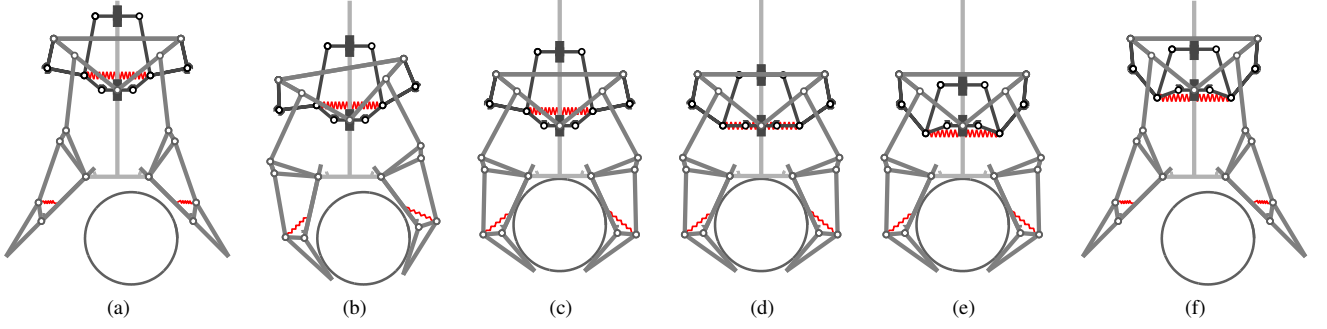


Fig. 2. Grasping sequence of the final concept in which (a) to (c) illustrate the object being grasped in the compliant state and (c) to (e) illustrate the transfer between the compliant and stiff state. Once the grasper opens it stays in the stiff state as shown in (f) and transfers back to the compliant state shown in (a) once the actuator force overcomes a threshold value.

to the differential. The angular rotation of both pairs of links is restricted by mechanical stops in joints W and X . The actuation force of the grasper should be applied at prismatic joint P in the direction coaxial to the prismatic joint. The two stable positions of the bi-stable mechanism result in either a compliant or a stiff state. A transition between states occurs when the actuator force overcomes the spring preload.

Fig. 1a illustrates the compliant state in which the preloaded spring pulls links SU and VT against the mechanical stops. In this state the actuation force applied at prismatic joint P is distributed via the bi-stable mechanism to joint A of the differential. As a result the actuation force is similar to a point-force located in joint A . This allows the differential to freely rotate around joint A and distribute the actuation force between the two fingers.

Fig. 1b illustrates the stiff state in which the preloaded spring pulls the two pairs of links $SW-WY$ and $TX-XZ$ against their mechanical stops. The actuation force applied at prismatic joint P is distributed via the bi-stable mechanism and the two pairs of links to joints Y and Z of the differential. This way the actuation force is applied to the differential as an antagonistic couple which increases the rotational stiffness of the differential around joint A . This antagonistic couple results in an equilibrium position of the differential in which link YZ is parallel to the palm.

In Fig. 2 the grasping sequence of the final concept is illustrated. It shows how a cylindrical object is grasped which is located eccentric with reference to the center of the palm. Fig. 2a shows the grasper in its compliant state and in its opened position. Once an actuation force is applied to prismatic joint P the fingers enclose the object (Fig. 2b). When the contact forces increase the object is lifted from the ground and directed to the center of the palm (Fig. 2c). As the contact forces further increase the preload of the spring of the bi-stable mechanism is overcome and the grasper transfers from the compliant to the stiff state (Fig. 2d and 2e). When the sign of the actuator force changes the grasper opens (Fig. 2f). The grasper remains in the stiff state up to the point that the actuator force overcomes the spring preload and then transfers to the compliant state. This brings the grasper back into its initial state (Fig. 2a).

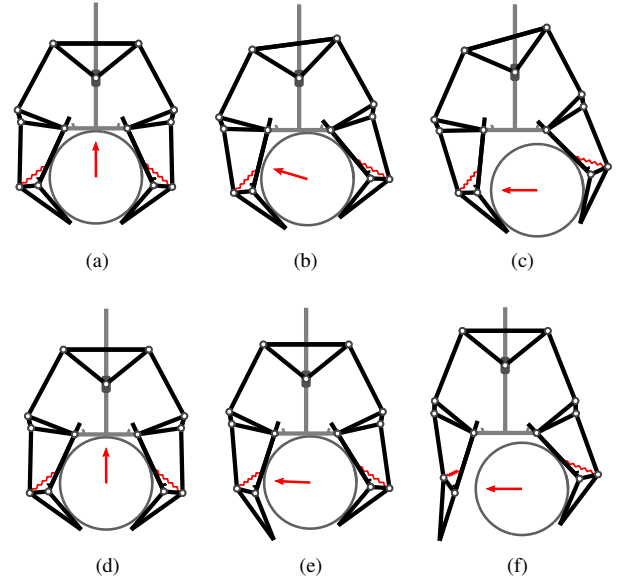


Fig. 3. Schematic representation of the static equilibrium position of the grasper and object for different lateral object displacements. Different grasp types are illustrated that occur in both the compliant state: P1-D1-Palm-P2-D2 (a), P1-Palm-P2-D2 (b), P1-P2-D2(MS) (c) and the stiff state P1-D1-Palm-P2-D2 (d), Palm-P2-D2 (e), P2-D2(MS) (f). The grasp types are labeled according to the phalanges that exert a force on the object, where P and D stand for the proximal and distal phalanx and 1 and 2 stand for the left and right finger respectively. MS indicates whether the proximal phalanx is at its maximum angle and makes contact with the mechanical stop. The arrow indicates the direction of the resulting force of the object.

D. Analytical model

An analytical model was made and implemented into Matlab to describe the behavior of the grasper when the object undergoes a lateral displacement. Fig. 3 illustrates the grasp types that occur during this object displacement for both the stiff and compliant state. It shows that in the compliant state the differential rotates and both fingers maintain contact with the object as it undergoes a lateral displacement. However in the stiff state the differential does not rotate when the object undergoes a lateral displacement. The bi-stable mechanism was designed in such a way that it prevents the differential from rotating and instead the actuation force is counteracted

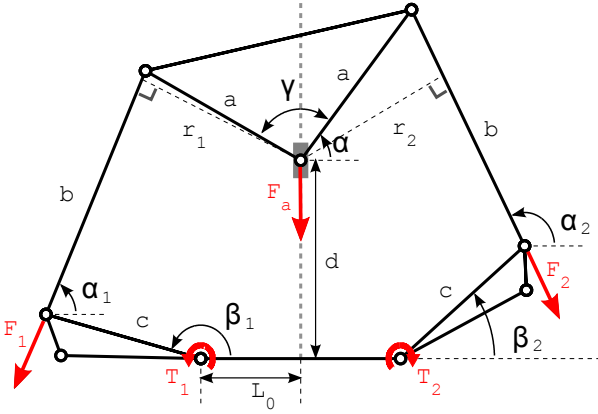


Fig. 4. Schematic representation of the differential, illustrating the angle of the differential α , angles of the input links β_1, β_2 , link lengths a, b, c , the actuator force F_a , the input forces of the left and right finger F_1 and F_2 which result in the input torques T_1 and T_2 and other geometric information.

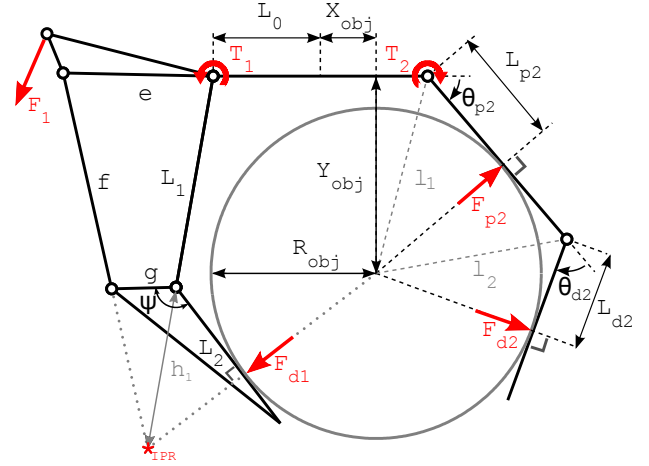


Fig. 5. Schematic representation of the fingers grasping an object, illustrating the actuation torques T_i , proximal and distal contact forces F_{pi}, F_{di} , Phalanx lengths L_1, L_2 , half the palm width L_0 , the fixed angle ψ , phalanx angles θ_{pi}, θ_{di} and other geometric information. The asterisk indicates the instantaneous point of rotation (IPR) of the left finger.

and the entire differential translates axially. As a result only the finger in the direction of the lateral object displacement maintains contact with the object.

A general set of equations was set up describing the configuration of the grasper, the contact forces of the phalanges and the resulting force of the object based on the position of the object. Each of the grasp types illustrated in Fig. 3 could be described by selectively combining equations from this general set. Using the nonlinear solver `fmincon` the static equilibrium position of the grasper and object could be determined for a given lateral object displacement. An automatic transition between grasp types was modeled by detecting the presence of negative forces in the solution of the solver and proposing a new grasp type based on the found solution. In the case that the object did not make contact with the palm of the grasper a solution was found in which the axial resulting force of the object was equal to 0N. In order to validate the Matlab model a similar experiment was modeled in MSC Adams.

Appendix B elaborates more on the Matlab model. The general set of equations will be discussed in the following sections.

1) *Contact forces*: Fig. 4 illustrates a schematic representation of the differential and input links of the grasper. In the compliant state the actuator force F_a results in two forces F_1 and F_2 which are dependent of the angles of the differential α and input links α_1 and α_2 as described by eq. 2 to 5:

$$\begin{bmatrix} F_1 \\ F_2 \end{bmatrix} = \frac{F_a}{p} \begin{bmatrix} r_2 \\ r_1 \end{bmatrix} \quad (2)$$

with

$$p = r_1 \sin \alpha_2 + r_2 \sin \alpha_1 \quad (3)$$

$$r_1 = -a \sin(\alpha_1 - \alpha - \gamma) \quad (4)$$

$$r_2 = a \sin(\alpha_2 - \alpha) \quad (5)$$

In the stiff state the actuation force and the spring force of the bi-stable mechanism prevent the differential from rotating. In the case of a lateral object displacement the actuation force is distributed between the two fingers in such a way that the entire actuation force is distributed to a single finger. In the case of an object displacement as shown in Fig. 3e and 3f the entire actuation force is distributed to the right finger. In this case the axial component of F_2 is equal to the actuation force and the magnitude of F_2 can therefore be determined by:

$$F_2 = \frac{F_a}{\sin \alpha_2} \quad (6)$$

Using the expressions of F_1 and F_2 the actuation torques of the fingers T_1 and T_2 can be calculated. These actuation torques relate to the contact forces according to equation (7) to eq. (14) as described in [6]:

$$F_{pi} = -\frac{L_1(-L_{di} + h_i \cos \theta_{di})}{L_{pi}L_{di}(h_i + L_1)} T_i \quad (7)$$

$$F_{di} = \frac{h_i}{L_{di}(h_i + L_1)} T_i \quad (8)$$

with

$$h_i = g(\cos(\theta_{di} - \psi) - \sin(\theta_{di} - \psi) \cot \beta_i) \quad (9)$$

with

$$\cot \beta_i = \frac{g \sin(\theta_{di} - \psi) S_i + M_i(L_1 + g \cos(\theta_{di} - \psi))}{-(L_1 + g \cos(\theta_{di} - \psi)) S_i + M_i g \sin(\theta_{di} - \psi)} \quad (10)$$

with

$$M_i = -L_1(L_1 + 2g \cos(\theta_{di} - \psi)) + e^2 - f^2 - g^2 \quad (11)$$

$$S_i = \sqrt{4e^2 f^2 - N_i^2} \quad (12)$$

$$(13)$$

with

$$N_i = L_1(L_1 + 2g \cos(\theta_{di} - \psi)) - e^2 - f^2 + g^2 \quad (14)$$

where $i = 1, 2$ represents the left and right finger respectively. The resulting lateral and axial contact forces were used to describe the resulting forces of the object. The angles of the proximal phalanges of the grasper θ_{pi} were bounded at $\frac{1}{4}\pi$ by a mechanical stop. The effect of the mechanical stop on the proximal contact force was included in the model in the case that the object did not make contact with the palm and the resulting axial force of the object was directed towards the palm of the grasper. This was done by increasing the value of the proximal contact force up to the point where the resulting axial force of the object was compensated.

2) *Phalanx geometry equations*: For a single finger two ways of making contact with the object were considered: contact with both phalanges or contact with only the distal phalanx. Fig. 5 illustrates these two types. In the case that both phalanges make contact with the object, the moment arms of the contact forces and the angles of the phalanges were calculated based on the position of the object as described in eq.(15) to (20)

$$L_{p2} = \sqrt{(L_0 - X_{obj})^2 + Y_{obj}^2 - R_{obj}^2} \quad (15)$$

$$L_{d2} = L_1 - L_{p2} \quad (16)$$

$$\theta_{p2} = \pi - \left(\cos^{-1} \left(\frac{L_0 - X_{obj}}{l_1} \right) + \cos^{-1} \left(\frac{L_{p2}}{l_2} \right) \right) \quad (17)$$

$$\theta_{d2} = \pi - 2 \cos^{-1} \left(\frac{L_{d2}}{l_2} \right) \quad (18)$$

with

$$l_1 = \sqrt{(L_0 - X_{obj})^2 + Y_{obj}^2} \quad (19)$$

$$l_2 = \sqrt{R_{obj}^2 + L_{d2}^2} \quad (20)$$

In the case that a finger makes contact with the object with only its distal phalanx, a static equilibrium position can be found when the line of force of the distal phalanx intersects the equilibrium point of the finger. In the case that no proximal contact force is present and the influence of the spring between the proximal and distal phalanx is not considered, this equilibrium point is indicated by the instantaneous point of rotation (IPR) of the proximal phalanx and link FJ or GK of the transmission linkage for the left and right finger respectively. Fig. 5 illustrates the case in which the left finger is in its equilibrium point. This configuration of the finger can be found by solving the set of loop closure equations described by eq. (21) and (22), where eq.(21) describes the loop of the phalanges, the center of the object and the palm and eq.(22) describes the loop of the proximal phalanx, the equilibrium point, the center of the object and the palm.

$$\begin{pmatrix} -L_1 \cos \theta_{p1} - L_{d1} \cos(\theta_{p1} + \theta_{d1}) \\ -L_1 \sin \theta_{p1} - L_{d1} \sin(\theta_{p1} + \theta_{d1}) \end{pmatrix} = \begin{pmatrix} L_0 + X_{obj} - r_{obj} \sin(\theta_{p1} + \theta_{d1}) \\ -Y_{obj} + r_{obj} \cos(\theta_{p1} + \theta_{d1}) \end{pmatrix} \quad (21)$$

$$\begin{pmatrix} -(L_1 + h_1) \cos \theta_{p1} \\ -(L_1 + h_1) \sin \theta_{p1} \end{pmatrix} = \begin{pmatrix} L_0 + X_{obj} - (h_1 \sin \theta_{d1} + R_{obj}) \sin(\theta_{p1} + \theta_{d1}) \\ -Y_{obj} + (h_1 \sin \theta_{d1} + R_{obj}) \cos(\theta_{p1} + \theta_{d1}) \end{pmatrix} \quad (22)$$

3) *Differential geometry equations*: In the case that the grasper is in the compliant state the configuration of the differential can be found solving loop closure equations eq.(23) and (24), where eq.(23) describes the geometrical loop of the input link of the left finger, the left half of the differential and the palm and (24) describes the loop of both input links, the differential and the palm.

$$\begin{pmatrix} -L_0 + c \cos \beta_1 + b \cos \alpha_1 \\ c \sin \beta_1 + b \sin \alpha_1 \end{pmatrix} = \begin{pmatrix} a \cos(\alpha + \gamma) \\ a \sin(\alpha + \gamma) + d \end{pmatrix} \quad (23)$$

$$\begin{pmatrix} -L_0 + c \cos \beta_1 + b \cos \alpha_1 - a \cos(\alpha + \gamma) \\ c \sin \beta_1 + b \sin \alpha_1 - a \sin(\alpha + \gamma) \end{pmatrix} = \begin{pmatrix} L_0 + c \cos \beta_2 + b \cos \alpha_2 - a \cos \alpha \\ c \sin \beta_2 + b \alpha_2 - a \sin \alpha \end{pmatrix} \quad (24)$$

In the case that the grasper is in the stiff state the angle of the differential is known and the rest of the configuration of the differential can be calculated using geometric equations.

E. Experimental Analysis

1) *Experimental setup*: A prototype of the final design was made and is illustrated in Fig. 6. A laser cutting machine was used to cut all the components out of a plate of acrylic. The components were connected to each other using brass axles with a diameter of 4mm. Ball bearings were used to create the prismatic joints A and P . The bi-stable mechanism was designed to have a threshold value of 3,5N.

An overview of the experimental setup is illustrated in Fig. 7. The ground link and the palm of the grasper were rigidly connected to the base plate. A THK prismatic joint was also connected to the base plate and was aligned with prismatic joint P of the grasper. The sliders of the two prismatic joints were rigidly connected to each other. By connecting a constant weight of 400 grams via a pulley to the prismatic joints a constant force actuation of 3.9N was obtained.

The cylindrical object was made out of acrylic disks with a diameter of 35mm which were bolted on an aluminum frame. Ball bearings were used to allow the frame to rotate along a central axis. A Graupner electric motor with an eccentric load was mounted on top of the object and was used to induce vibrations. These vibrations were used to overcome static friction in the joints of the grasper and allowing the object to move to its static equilibrium position.

Two THK prismatic joints were mounted on top of each other to create a planar joint for the object. This planar joint was attached to the base plate in such a way that the two prismatic joints were aligned perpendicular and parallel to the palm of the grasper. A PI linear actuator with a Futek load cell was aligned parallel to the palm of the grasper and connected to the planar joint using a threaded rod. This way the resulting lateral force of the object could be measured with the load cell and the lateral object displacement could

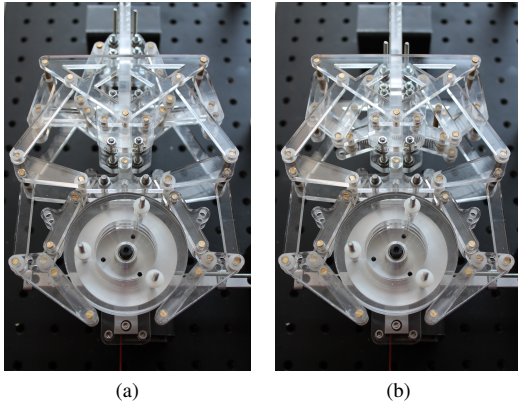


Fig. 6. Grasper prototype in its compliant (a) and stiff (b) state while grasping an object

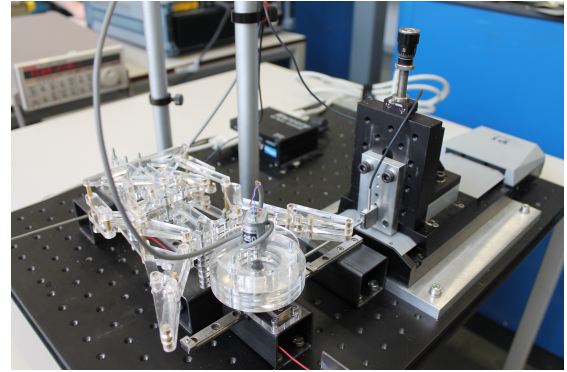


Fig. 7. Experimental setup illustrating the grasper and the object on its planar joint which is connected to a linear actuator via a load cell

be adjusted by controlling the position of the linear actuator. Because of the planar joint the object could freely translate in the axial direction. It was assumed that any torque caused by the resulting lateral force of the object was counteracted by the planar joint and did not have an effect on the force measured by the load cell.

A labview program was used to control the position of the linear actuator, to induce vibrations to overcome static friction and to read the value of the load cell. A more detailed description of the measurement setup can be found in Appendix C.

2) *Experiment protocol:* Two types of experiments were done to quantify the compliance of the grasper. In the beginning of both experiments the actuation force was applied to the grasper. The object position in which the load cell measured a resulting force of approximately 0N was found and considered to be the center of the palm. With experiment A the linear actuator moved the object laterally with a constant velocity of 1 mm/s up to a maximum displacement of 25 and 22mm with reference to the center of the palm for the compliant and stiff state respectively. Once the final position was obtained, the linear actuator moved the object back to the center of the palm to close the loop. During both movements the actuator position and the force measured by the load cell were obtained with a sampling frequency of 20 Hz.

With experiment B the object was moved step by step with a step size of 1 mm. After each step vibrations with a frequency of 100 Hz were generated for 1 second to overcome static friction and allow the grasper and object to move to the static equilibrium position. Once the vibrations stopped the value of the load was manually read and stored. When the maximum displacement was obtained the actuator moved the object back to the center of the palm. Again the object was moved step by step, applying vibrations after each step and measuring the resulting force for each object position.

With both experiments the procedure was repeated five times for the grasper both its compliant and stiff state. The actuation force used in the experiments exceeded the threshold force of the bi-stable mechanism. Therefore in order to prevent the transfer from the compliant to the stiff state the links of

the bi-stable mechanism were secured during the experiments in which the grasper was in its compliant state.

III. RESULTS

Fig. 8a and 8d illustrate the results of the static analysis in Matlab and the simulation in Adams. It shows the resulting lateral force of the object for a lateral object displacement in the compliant and stiff state for 120 data points. The root mean square error (RMSE) of the Matlab and Adams results was found 0.013N and 0.012N for the compliant and stiff state respectively. The lateral object displacement on which a transition takes place between two grasp types can be identified from the characteristic of the graphs. Table I shows the grasp type corresponding to each lateral object displacement during the stiff and compliant state. The graph of the compliant state starts in the origin and initially has a close to linear behavior during the first grasp type. The graph of the stiff state also begins in the origin but transfers immediately to the second grasp type once the object undergoes a lateral displacement. As a result of this displacement the resulting lateral force of the object almost instantly increases to 3.65N. The lateral compliance of both states was determined during the first grasp type starting from the position in which the object is in the center of the palm up to the point in which the grasper transfers to the second grasp type. As a result the theoretical lateral compliance in the compliant and stiff state was found 0.0 and 4.15mm/N respectively. The maximum lateral pull-out force which leads to the loss of contact between the grasper and the object was indicated by the absolute maximum force of the graph. Fig. 8a and 8d show that the magnitude of the lateral pull-out force in the stiff state has increased by a factor of 1.7 compared to the compliant state.

The results of experiment A in which the object was displaced with a constant velocity for the compliant and stiff state are shown in Fig. 8b and 8e respectively. The figures show the analytical results of the Matlab model and the experimental results of the resulting lateral force of the object corresponding to a lateral object displacement. For both states a large hysteresis loop can be seen. In the upper part of the graph the object is moved away from the palm and in the

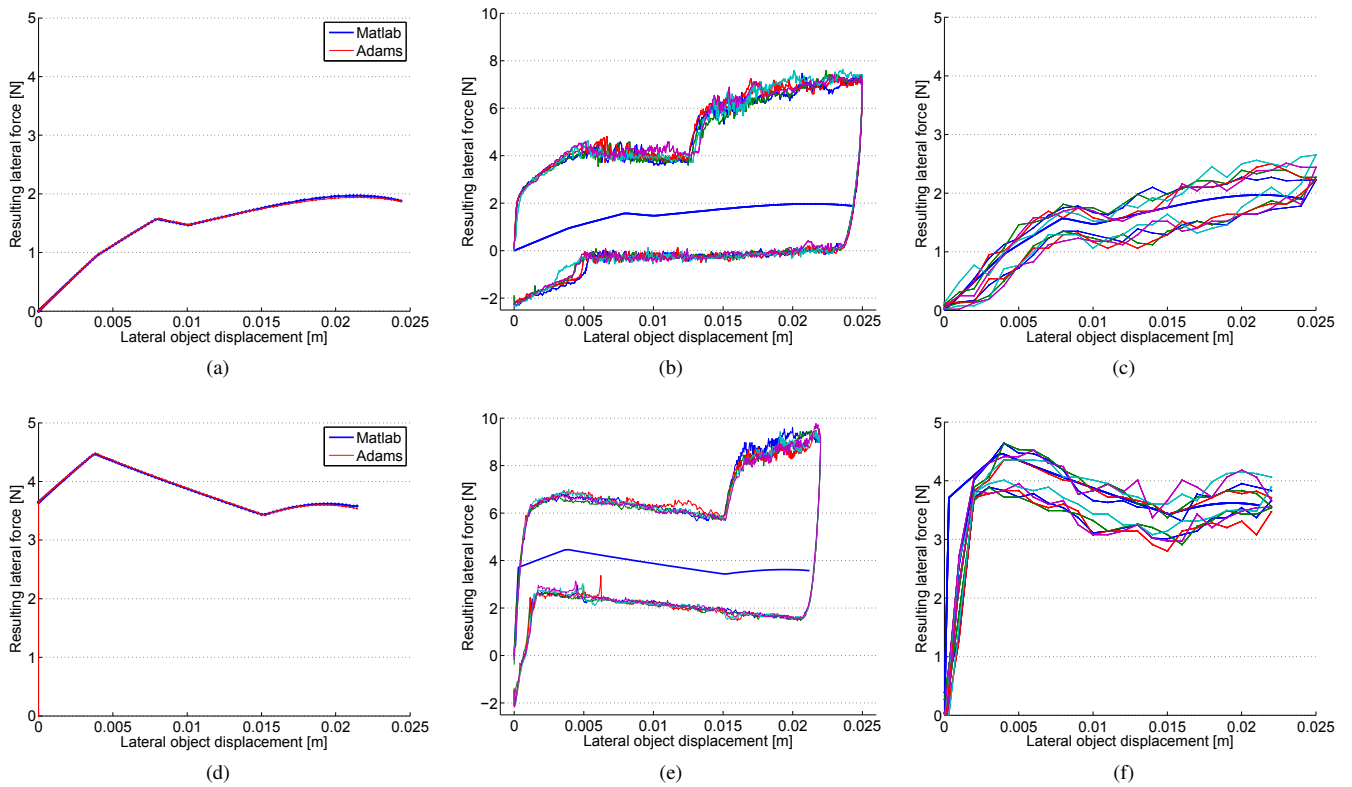


Fig. 8. Results of the analytical analysis in Matlab compared to: the analysis in Adams (a)(d), the results of experiment A (b)(e) and the results of experiment B (c)(f) for the stiff and compliant state respectively. In all graphs the thick lines illustrate the analytical results, where the thin lines illustrate the experimental results

lower part of the graph the object is moved towards the palm. The large increase in force in the upper part of both graphs at $X_{obj}=0.013m$ and $X_{obj}=0.015m$ for the compliant and stiff state respectively is due to the contact between the proximal phalanx and the mechanical stop. In both graphs it can be seen that in the case that the object is moved back to the palm, the resulting force of the object becomes negative.

Fig. 8c and 8f show the results of experiment B in which the object position was changed with a step size of 1mm and vibrations were generated to overcome static friction. In both states a hysteresis loop is visible. The root mean square error of the analytical and experimental results was found 0.29N and 0.53N for the compliant and stiff state respectively. The lateral compliance was calculated during the initial grasp type starting in the origin up to $X_{obj}=0.004m$ for the compliant and $X_{obj}=0.002m$ for the stiff state by means of a linear regression. This resulted in a lateral compliance of 3.40 and 0.48 mm/N for the compliant and stiff state respectively. The transition from the compliant to the stiff state has therefore reduced the compliance by a factor of 7. In order to determine the lateral pull-out force the average resulting force at $X_{obj}=0.025m$ and $X_{obj}=0.004m$ for the compliant and stiff state respectively was determined. As a result the transition from the compliant to the stiff state has increased the lateral pull-out force of the grasper by a factor of 1.9 from 2.36N to 4.48N.

TABLE I
GRASP TYPES FOR EACH OBJECT DISPLACEMENT

Compliant state		
Grasp type	$X_{obj}[mm]$	
P1-D1-Palm-P2-D2	0	$\leq x \leq 4.5$
P1-Palm-P2-D2	4.5	$< x \leq 7.5$
P1-P2-D2	7.5	$< x \leq 10$
P1-P2-D2 (MS)	10	$< x$
Stiff state		
Grasp type	$X_{obj}[mm]$	
P1-D1-Palm-P2-D2	0	$= x$
Palm-P2-D2	0	$< x \leq 4.5$
P2-D2	4.5	$< x \leq 16$
P2-D2 (MS)	16	$< x$

IV. DISCUSSION

The results obtained with Matlab and Adams illustrated in Fig. 8a and 8d show only minor discrepancy as indicated by the values of the RMSE. It was therefore stated that the Matlab model was validated. The hysteresis loop that was found in the results of experiment A shows that the prototype was strongly subjected to friction. Fig. 8b illustrates that in the compliant state when the object is moved back to the center of the palm the resulting force of the object is negative for the largest part of this movement. This indicates that the actuator is actually pushing the object back to the center of the palm. The results of experiment B as shown in Fig. 8c and 8f show that applying vibrations to the object has reduced the effect of

friction on the measured results. There is still an amount of friction present indicated by the hysteresis loop. Despite the error indicated by the RMSE Fig. 8c and 8f illustrate that the characteristics of the experimental results show resemblance with the characteristics of the analytical model. It is expected that the value of the RMSE can be reduced by improving the mechanical design of the prototype and the experimental setup.

The concept design as presented in this research is able to discretely adjust its lateral compliance between two states. This was done to be able to adjust the lateral compliance of the grasper without the need of an additional actuator. The bi-stable mechanism was designed in such a way that the lowest lateral compliance was obtained in the stiff state. In the case that it is possible to adjust the characteristics of the bi-stable mechanism it could be possible to obtain any lateral compliance between the minimum and maximum values of 0.48mm/N and 3.40mm/N respectively for the stiff state. Another option is to be able to adjust the preload of the linear spring of the bi-stable mechanism to adjust the threshold force of the grasper.

The method of adjusting the rotational stiffness of the differential to adjust the lateral compliance of the grasper can be discussed. The main disadvantage of this working principle is that the grasper is less able to adapt to the shape of the object in the stiff state compared to the compliant state. In the stiff state the differential is forced to its symmetric position which results in a symmetric position of the input links of the fingers. In the case that the grasper picks up an object in the compliant state and obtains a stable grasp in which the differential of the grasper is not in its symmetric position, then the transition from the compliant to the stiff state will change the configuration of the grasper until the differential is in its symmetric position. As a result the phalanx angles and the contact forces change and a new static equilibrium position has to be found.

Forcing the differential into its symmetric position could also have its benefits. Since the exact configuration of the grasper is unknown once an object has been grasped, it is also unknown where the object is located with respect to the center of the palm. For pick and place tasks it is desirable to have a reference where the object is located to be able to accurately place the object. By forcing the differential to a symmetric position, one might be able to have a better reference of the position of the object with respect to the center of the palm.

The link lengths of the grasper as proposed in this research were chosen to obtain a self-centering behavior of the grasper which requires a resulting lateral force in the case of an object displacement. This was done such that the grasper was able to transfer from the compliant to the stiff state once a stable grasp was obtained. However, in the stiff state the antagonistic couple that is applied to the differential also results in a self-centering behavior of the grasper. Therefore instead of changing states once a stable grasp is obtained, the transition between states can also be done once the fingers enclose the object and can be used to obtain the self-centering behavior of the grasper. This way the self-centering feature of the fingers would be redundant and it might be possible to design the link lengths of the fingers in such a way that would increase the

level of compliance in the compliant state, or even increase the stability of the grasper. Also if the transition between states is done once the fingers have enclosed the object, objects that would have led to an asymmetric grasp will immediately be guided to their final position. It would therefore be interesting to study the dynamic behavior of the grasper to see if these characteristics can be beneficial.

During this research the closing time of the grasper was not considered as a design criterion. In practice it is beneficial to minimize this to increase the capacity of the grasper. Adjusting the compliance should therefore not increase the closing time of the grasper. Otherwise the increased allowable acceleration might only compromise the lower closing time of the grasper.

An advantage of a grasper with adjustable compliance compared to a grasper with a fixed compliance would be that the grasper is both self-adaptable and robust. In the case of a grasper with a fixed compliance a compromise has to be made between self-adaptability and robustness.

V. CONCLUSION

This research proposed the concept design of an underactuated grasper which is able to adjust its robustness against external lateral force perturbations. Using a bi-stable mechanism a transition can take place between two types of actuation of an internal differential mechanism; a point force in the compliant state which allows free rotation of the differential and an antagonistic couple in the stiff state which increases the rotational stiffness of the differential. The compliant and stiff states respectively result in a high and low lateral compliance of the grasper. A transition between states takes place once the actuator force overcomes a certain threshold value. Therefore the lateral compliance of the grasper can be adjusted without the need of an additional actuator.

Theoretically this working principle can be used to reduce the lateral compliance of the grasper to 0 mm/N for external forces up to a certain threshold value. Experimental results that were obtained with a prototype showed that a transition from the compliant to the stiff state decreased the lateral compliance of the grasper by a factor of 7 from 3.40mm/N to 0.48mm/N. This transition also increased the lateral pull-out force of the grasper by a factor of 1.9 from 2.36N to 4.48N.

REFERENCES

- [1] T. Laliberte, L. Birglen, and C. Gosselin, "Underactuation in robotic grasping hands," *Machine Intelligence & Robotic Control*, vol. 4, no. 3, p. 111, 2002.
- [2] A. M. Dollar and R. D. Howe, "The highly adaptive sdm hand: Design and performance evaluation," *The international journal of robotics research*, vol. 29, no. 5, pp. 585–597, 2010.
- [3] V. Begoc, S. Krut, E. Dombre, C. Durand, and F. Pierrot, "Mechanical design of a new pneumatically driven underactuated hand," in *Robotics and Automation, 2007 IEEE International Conference on*. IEEE, 2007, pp. 927–933.
- [4] G. A. Kragten, "Underactuated hands: fundamentals, performance analysis and design," Ph.D. dissertation, Delft University of Technology, 2011.
- [5] D. Aukes, S. Kim, P. Garcia, A. Edsinger, and M. R. Cutkosky, "Selectively compliant underactuated hand for mobile manipulation," in *Robotics and Automation (ICRA), 2012 IEEE International Conference on*. IEEE, 2012, pp. 2824–2829.
- [6] L. Birglen, T. Lalibert, and C. M. Gosselin, *Underactuated robotic hands*. Springer, 2008, vol. 40.

- [7] L. Birglen and C. Gosselin, "Optimal design of 2-phalanx underactuated fingers," in *Proc. of IMG2004: IEEE international conference on Intelligent Manipulation and Grasping*, 2004, p. 110116.
- [8] L.-A. Demers and C. Gosselin, "Kinematic design of an ejection-free underactuated anthropomorphic finger," in *IEEE International Conference on Robotics and Automation, 2009. ICRA '09*, 2009, pp. 2086–2091.
- [9] S. A. Spanjer, R. Balasubramanian, J. L. Herder, and A. M. Dollar, "Improved grasp robustness through variable transmission ratios in underactuated fingers," in *Intelligent Robots and Systems (IROS), 2012 IEEE/RSJ International Conference on*, 2012, p. 22892294.
- [10] B. Peerdeman, G. Pieterse, S. Stramigioli, H. Rietman, E. Hekman, D. Brouwer, and S. Misra, "Design of joint locks for underactuated fingers," in *2012 4th IEEE RAS EMBS International Conference on Biomedical Robotics and Biomechatronics (BioRob)*, 2012, pp. 488–493.
- [11] R. Pape, "The effect of joint locks in underactuated hand prostheses," MSc thesis Msc Thesis, Delft University of Technology, 2011.
- [12] J. T. Belter and A. M. Dollar, "Underactuated grasp acquisition and stability using friction based coupling mechanisms," in *Robotics and Automation (ICRA), 2011 IEEE International Conference on*, 2011, p. 30353040.
- [13] B. Vanderborght, N. G. Tsagarakis, C. Semini, R. Van Ham, and D. G. Caldwell, "Macepa 2.0: Adjustable compliant actuator with stiffening characteristic for energy efficient hopping," in *Robotics and Automation, 2009. ICRA'09. IEEE International Conference on*. IEEE, 2009, pp. 544–549.
- [14] A. Jafari, N. G. Tsagarakis, and D. G. Caldwell, "Awas-ii: A new actuator with adjustable stiffness based on the novel principle of adaptable pivot point and variable lever ratio," in *Robotics and Automation (ICRA), 2011 IEEE International Conference on*. IEEE, 2011, pp. 4638–4643.
- [15] S. Wolf, O. Eiberger, and G. Hirzinger, "The dlr fsj: Energy based design of a variable stiffness joint," in *Robotics and Automation (ICRA), 2011 IEEE International Conference on*. IEEE, 2011, pp. 5082–5089.
- [16] R. v. Ham, T. Sugar, B. Vanderborght, K. Hollander, and D. Lefeber, "Compliant actuator designs," *Robotics & Automation Magazine, IEEE*, vol. 16, no. 3, pp. 81–94, 2009.
- [17] D. Aukes, B. Heyneman, V. Duchaine, and M. R. Cutkosky, "Varying spring preloads to select grasp strategies in an adaptive hand," in *Intelligent Robots and Systems (IROS), 2011 IEEE/RSJ International Conference on*. IEEE, 2011, pp. 1373–1379.
- [18] R. Stavenuiter, "Performance quantification of variable stiffness actuator designs," MSc thesis literature study, Delft University of Technology, 2012.

Appendix A

Conceptual Design

A-1 Task analysis

In order to set up the requirements the total task of an underactuated grasper was analyzed. A division was made between three basic tasks: grasp, hold and release the object. During these tasks the actions that occur and the desired level of compliance during the task were determined and will be discussed in the next paragraphs.

Grasp

When the actuator applies a force, this force is distributed between the phalanges and the grasper starts closing. Both fingers sequentially enclose the object and therefore adapt to its shape. When the contact forces increase the object is lifted from the ground and the force distribution between the phalanges causes a change in the configuration of the grasper which guides the object to the center of the palm. This is only possible if the configuration of the grasper can easily be changed. Therefore the level of compliance during the grasping action should be high. In the case that the grasper is stiff the fingers do not enclose the object before increasing the contact force and as a result the object is pushed away from the moment that first contact is made. This reduces the chance of obtaining a stable grasp. A high level of compliance is therefore beneficial when grasping.

Hold

Once the object and the grasper are in static equilibrium with each other a stable grasp is obtained. This stable grasp should be maintained while the object is moved to its requested location. When the object is subjected to inertial forces due to accelerations or to other external force perturbations these forces interfere with the static equilibrium.

When the grasper is compliant these forces will result in reconfiguration of the grasper until a new equilibrium position is found. An advantage of this reconfiguration is that the magnitude of the contact forces between the object and the phalanges are only slightly adjusted. However when the amount of reconfiguration is too high, the grasper could lose contact with the object. In the case that the grasper is infinitely stiff the external forces do not result in reconfiguration of the grasper. In this case the contact forces will be changed to counteract the external forces such that a new static equilibrium is obtained. Whether a compliant or stiff grasper is desired is strongly dependent of the type of object that is grasped. When dealing with delicate objects it is desired to reduce the contact forces as much as possible to minimize the chance of damaging the object. In this case a high level of compliance would be beneficial. However In this research it is assumed that the contact forces are not an issue and the focus is put on increasing the robustness of the grasper to resist external perturbations. Therefore a high stiffness is considered the best while holding an object.

Release

Once the object is at its final position the grasper can release it. If the actuator reduces the actuation force the contact forces also reduce. In both the compliant and stiff case the fingers sequentially open and guide the object back onto the ground. Once the grasper is in its open

position it can move to the next object. During this movement the inertial forces that act on the fingers of the grasper itself could also result in reconfiguration of the grasper. It is therefore beneficial to have a stiff grasper when moving it in the open position.

A-2 Requirements

A number of requirements can directly be derived from the task analysis. It showed that the stiffness of the grasper should increase once a stable grasp is obtained and this high stiffness should be maintained when holding the object, releasing the object and while the grasper is moved to the next object. Therefore the grasper should only be compliant during the grasping action to allow the actuation force to be distributed between all the phalanges and result in the shape adaption and self-centering feature. The stiffness of the grasper should therefore be triggered to increase once the grasp is complete and to decrease once the grasping action begins. Furthermore the increase in stiffness should not interfere with the force distribution between the phalanges. A change in the force distribution between the phalanges disturbs the static equilibrium and therefore results in reconfiguration of the grasper. Another requirement that was set concerned the level of underactuation, which is described as the difference between the number of degrees of freedom and the number of actuators. Adjustable stiffness should be implemented while maintaining the level of underactuation or preferably even increase this level. Furthermore it was desired to obtain a simplistic solution which passively adjusts the stiffness without the need of extra control.

A-3 Identify locations

By adjusting the stiffness of a few components of the linkage of an underactuated grasper, the stiffness of the entire grasper can be changed. This chapter shows an analysis that was done to identify whether the stiffness of the entire grasper could be adjusted by adjusting the stiffness between one or two pairs of links of each finger.

Fig. A-1 shows a schematic of an underactuated grasper where each link is numbered. All possible connections between two links of a finger were visualized by drawing lines between the numbered links. For each of the lines it was determined if the 2 DOF of the finger would be removed when the relative movement between the two links connected by the line would be locked. A similar analysis was done where it was determined if the 2 DOF of the finger would be removed when relative movement between two pairs of linkages would be locked. The results of these analyses can be found in Table A-1 together with two more analyses. In total 56 possible solutions were found to adjust the stiffness of a single finger and 2 solutions were found to adjust the stiffness of the entire grasper by connecting two links of the left and right finger.

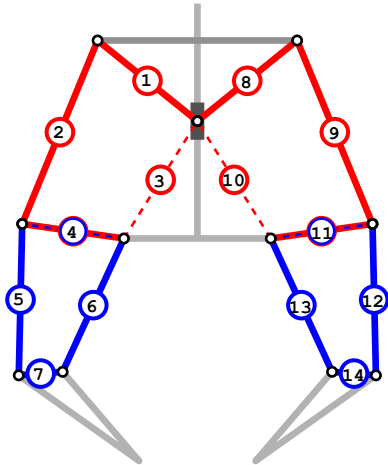


Figure A-1: Schematic representation of grasper where each link is numbered

Table A-1: Possible combinations of linkages

Schematic	Notes	Combinations
	<p>The finger of an underactuated grasper is seen as two four-bar-linkages on top of each other. Each four bar linkage has one DOF and six possible ways of combining two links:</p> <ul style="list-style-type: none"> - 4 combinations between adjacent links - 2 combinations between opposing links <p>By adjusting the stiffness of two pairs of links, the stiffness of the entire finger can be adjusted. This results in $6*6=36$ possible ways of adjusting the stiffness.</p>	<p>1-2 & 4-5 1-3 & 4-6 1-4 & 4-7 2-3 & 5-6 2-4 & 5-7 3-4 & 6-7</p>
	<p>The stiffness of the entire finger can be adjusted by adjusting the stiffness of the relative movement between two links of each four bar linkage. 8 possible solutions were found</p>	<p>1-5 1-6 1-7 2-5 2-6 2-7 3-5 3-7</p>

Schematic	Notes	Combinations
	<p>If the links 3 and 6 are connected, the remaining mechanism has 1 free DOF. There are 12 ways by connecting adjacent/opposing links of the two four-bar linkages in order to adjust the stiffness of the remaining DOF.</p> <p>This results in 12 possible ways of adjusting the stiffness of the entire finger.</p>	<p>1-2 & 3-6 1-3 1-4 2-3 2-4 3-4 4-5 4-6 4-7 5-6 5-7 6-7</p>
	<p>Adjusting the stiffness of the relative movement between two links of different fingers can also adjust the stiffness of the entire grasper. Two solutions were found based on this principle</p>	<p>5-12 7-14</p>

A-4 Morphological overview

A literature study was done on adjustable stiffness actuators to identify working principles of adjusting the rotational stiffness of a joint. This study can be found in Appendix D. Four main working principles of adjusting stiffness can be distinguished according to [1]:

- **Equilibrium-controlled stiffness (ECS):** A fixed stiffness spring is connected in series with a stiff actuator. By actively changing the equilibrium position of the spring the output force which relates to the desired stiffness can be controlled.
- **Antagonistic controlled stiffness (ACS):** Two actuators in series with two nonlinear springs are coupled antagonistically. Both the output position and stiffness settings are controlled by the two actuators.
- **Structure controlled stiffness (SCS):** The stiffness is controlled by changing the physical structure of a spring by means of changing the effective length.
- **Mechanically controlled stiffness (MCS):** The stiffness is controlled by changing the preload or the effective moment arm of a spring, always using the full length of the spring.

A morphological table was set up containing these four and other working principles that were found. The table was complemented with methods to trigger the adjustable stiffness mechanism and with methods to actuate an underactuated grasper. The morphological overview can be found in Table A-2. A distinction was made between two ways of adjusting stiffness: continuous and discrete. Continuously adjusting stiffness meant that the stiffness setting could vary within a certain range from compliant to stiff, where discretely adjusting stiffness meant that only two stiffness settings could be obtained: either compliant or stiff.

A number of solutions was found for triggering the mechanism to transfer between the compliant and stiff state. A second actuator can be used to control the stiffness setting. Also contact forces or angular displacement of joint angles can be used to trigger the mechanism once they exceed a certain threshold. The overall working principle of concept solutions can be found by combining elements from the morphological table. These solutions will be discussed in the next section.

Table A-2: Morphological overview containing solutions to actuate a grasper and to obtain and trigger adjustable stiffness

Function	Solutions		
Actuation	Pulley-tendon	Gears	Linkage
Obtain stiffness	Continuous	Discrete	
	<i>Adjustable moment arm</i>	<i>Mechanical stop</i>	
	<i>Effective length</i>	<i>Worm gear</i>	
	<i>Preload</i>	<i>Screw-nut</i>	
	<i>Antagonistic couple</i>	<i>One-way-valve</i>	
	<i>Friction brakes</i>	<i>Ratchet</i>	
Trigger mechanism	threshold force	Link angles	Seperate actuator

A-5 Concept solutions

By combining elements from Table A-2 conceptual solutions were generated on three different levels: joint, finger and grasper level. In this chapter an overview of the conceptual solutions for each level is given. For each concept a schematic illustration is given in combination with additional information concerning the working principle.

A-5-1 Joint level concepts

As mentioned in section A-3 the stiffness of the entire grasper can be changed by changing the stiffness between pairs of links of the fingers. When changing the stiffness between two adjacent links, the joint that connects the two links can be used. Therefore a number of concept solutions for joints with adjustable stiffness was generated.

#1. Friction brakes

One way of increasing the rotational stiffness of a joint is by increasing the friction forces of the joint. Conventional mechanisms based on friction are drum, disk and band brakes as illustrated in Fig.A-2. The downside of friction based mechanisms is that they are often subjected to wear and in most cases there is no equilibrium point to which the mechanism returns after a perturbation. In the case of implementing friction brakes into a grasper, the brakes should be idle during the grasping action and should be enabled once the grasp is complete.

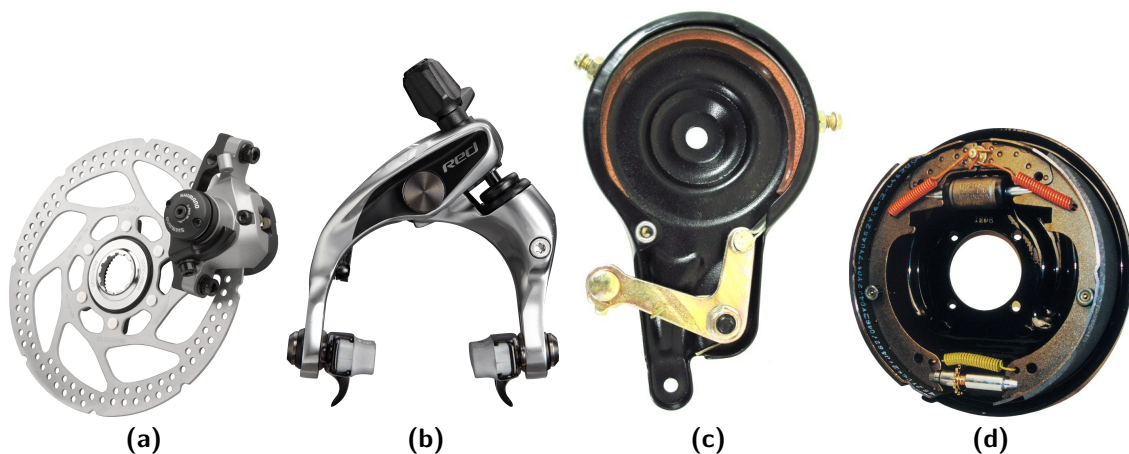
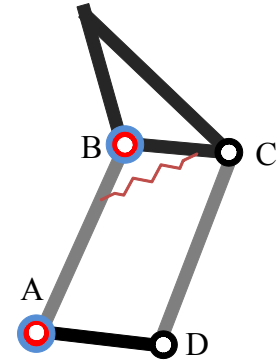


Figure A-2: Conventional brake types: disk(a), rim (b), band (c) and drum (d) brake

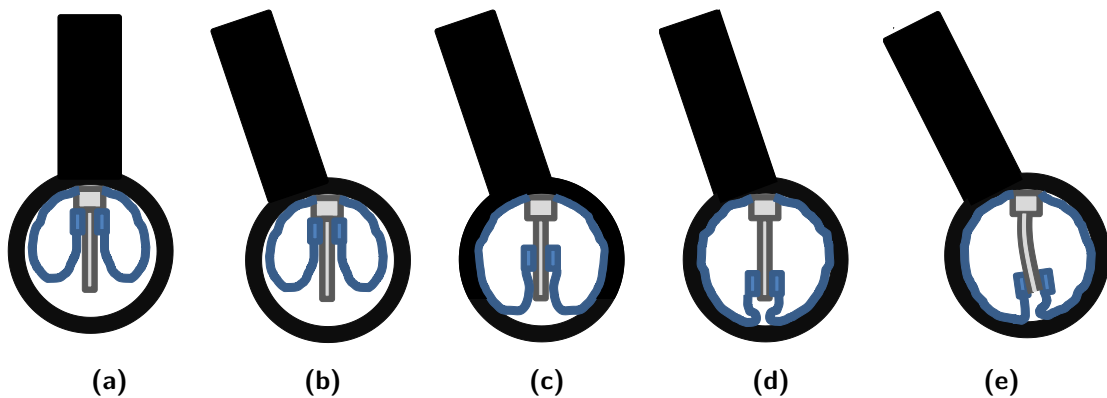
#2. Magnetic joint

This concept uses the attraction between two electromagnets to obtain rotational stiffness of the joint. By controlling the current flowing through the two magnets the attraction between the two magnets can be controlled, and therefore the rotational stiffness of the joint can be controlled. For the implementation of this principle in an underactuated finger two magnets should be attached to the two adjacent links. During the grasp action there should be no current flowing through the magnets in order to allow the joint to rotate freely. Once a stable grasp is obtained, a current should be applied to the magnets to obtain stiffness.



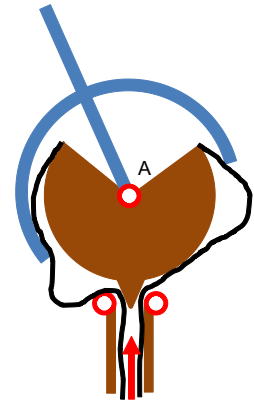
#3. Effective length lever

This concept uses the effective length of a cantilever beam to adjust the rotational stiffness of a joint. The following figure illustrates the concept. The concept consists of an outer ring that is connected to one link and a cantilever beam that is connected to the adjacent link. The ring and cantilever beam are connected by a slider with a flexible membrane. In (a) the two parts are not connected and can freely rotate with respect to each other. Once the final position is obtained (b) an actuator moves the slider and the membrane connects the cantilever beam to the outer ring. The position of the slider determines the effective length of the cantilever beam and thus the rotational stiffness of the joint (c)(d). When an external torque is applied to the finger the cantilever beam deflects and a rotational stiffness of the joint can be noticed (e).



#4. Buckling of flexible member

This concept uses buckling of a flexible member to obtain stiffness. The joint consists of three main parts: a ground part (brown), a link (blue) that is connected to the ground part by rotational joint A and a flexible member (black) that is attached to the ground part. When no force is applied to the flexible member it follows the contour of the ground part and does not make any contact with the blue link. Therefore the blue link can freely rotate around joint A. When a force is applied to the flexible member as illustrated, the flexible member starts to buckle and makes contact with the two extensions of the link. In order to rotate the link the flexible member has to be deformed and because of that stiffness is added to the joint. However, it is unknown if buckling occurs in this manner and if it provides enough stiffness to resist an external torque.



A-5-2 Finger level concepts

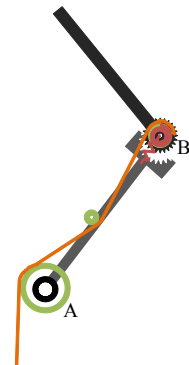
The second level in which concept ideas were generated was the finger level. This section discusses the working principle of a list of concepts of underactuated fingers with adjustable stiffness by explaining the closing sequence of the finger. The concepts are named according to the following format: Concept number / Driving working principle of the finger/mechanism used to adjust stiffness / mechanism used to trigger mechanism.

#5 / Pully-tendon / mechanical stop, joint / threshold force

This concept makes use of toothed surfaces of the joint that connects the proximal and the distal phalanx.

- When a force is applied to the tendon the entire finger rotates around joint A and there is no contact between the object and the phalanges.
- When the proximal phalanx makes contact with the object, the preload of the rotational spring in B is overcome and the distal phalanx rotates around B.
- When the distal phalanx makes contact with the object the preload of the linear spring in B is overcome and the toothed surfaces of joint B lock.

Note: Joint A has to be locked as well or the tendon force should prevent rotation around joint A. Joint B also needs some kind of linear sliding joint

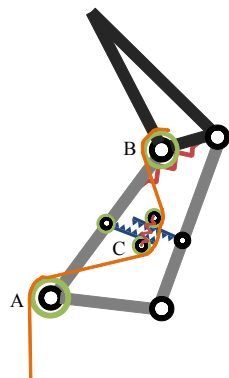


#6. Pully-tendon / mechanical stop, links / threshold force

This concept makes use of a toothed prismatic joint that connects two links of a finger.

- When tendon is pulled the entire finger rotates around A .
- When the proximal phalanx makes contact with the object the preload of the linear spring at B is overcome and the distal phalanx rotates around B.
- When the distal phalanx makes contact with the object, the preload of the linear spring in C is overcome and the links of the prismatic joint lock.

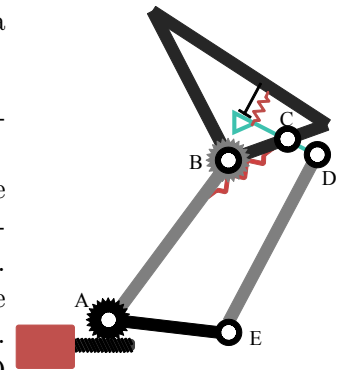
Note: Joint A still has to be locked. Other locking mechanisms can be used and different combinations of links can be locked.



#7. Linkage / non-backdrivable, ratchet / Threshold force

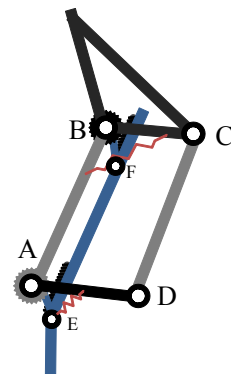
This concept uses a ratchet with a preloaded spring in joint B and a non-backdrivable actuator that actuates joint A.

- The entire finger rotates around joint A when the non-backdrivable actuator applies a torque to link AE.
- When the proximal phalanx makes contact with the object, the preload of the linear spring between the proximal and distal phalanx is overcome and the distal phalanx rotates around joint B.
- When the distal phalanx makes contact with the object, the preload of the linear spring in the distal phalanx is overcome. Link AE continues rotating and link DE enables ratchet CD which locks into the gear mounted on link AB.

**#8. Linkage / Mechanical stop / Threshold force**

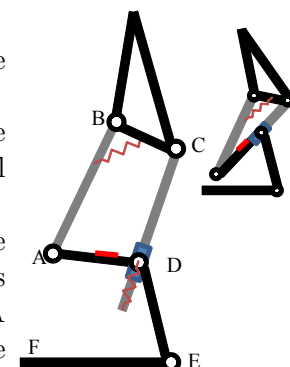
This concept uses toothed surfaces in joints A and B which can lock the joints once they make contact with a secondary link EF.

- The entire finger rotates around joint A when a torque is applied to link AD.
- When the proximal phalanx makes contact with the object, the preload of the linear spring at B is overcome and the distal phalanx rotates around B.
- The distal phalanx makes contact and an equilibrium position is found.
- The hand and object are lifted by pulling bar EF. Due to the pulling force and the weight of the hand and object the preload of the spring at E is overcome and the joints A and B lock.

**#9. Linkage / Mechanical stop / Phalanx angles, angles between links**

This concept uses a singular position of the transmission linkage to remove a degree of freedom.

- The entire finger rotates around joint A when an input torque is applied to link AD at joint D.
- When the proximal phalanx makes contact with the object the preload of the linear spring at joint B is overcome and the distal phalanx starts to rotate around joint B.
- When the distal phalanx makes contact with the object the preload of the spring at joint D is overcome and joint D starts to slide over link CD, until a singular position is obtained. A mechanical stop on link AD prevents the mechanism to rotate any further.



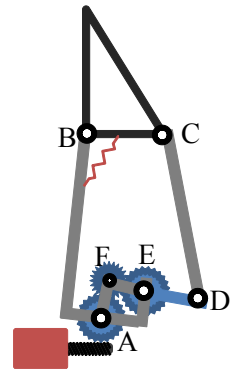
Note: The exact behavior of the slider and the rest of the mechanism once a mechanical lock is achieved is unknown. Joint A should still be locked.

#10. Gear / Non-backdrivable, worm gear / Threshold force

This concept makes use of a force controlled non-backdrivable actuator.

- The entire finger rotates around joint A when a torque is applied to the gear at joint A.
- When the proximal phalanx makes contact with the object the preload of the linear spring at joint B is overcome and the distal phalanx starts to rotate around joint B.
- When the distal phalanx makes contact with the object the actuator should reach its maximum torque and stall.

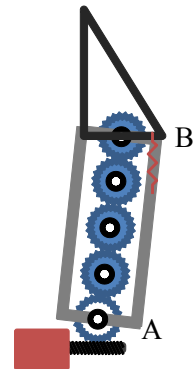
Note: A coupled movement of the proximal and distal phalanx is still possible.

**#11. Gear / Non-backdrivable, worm gear / Threshold force**

This concept uses a non-backdrivable actuator and a set of gears to distribute the actuation torque.

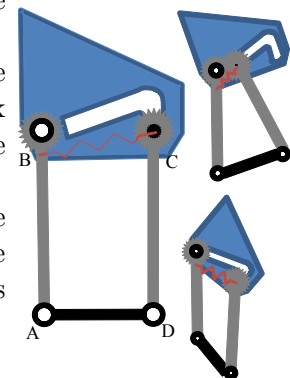
- The entire finger rotates around joint A when a torque is applied to the gear at joint A.
- When the proximal phalanx makes contact with the object, the preload of the linear spring at joint B is overcome and the distal phalanx starts to rotate around joint B.
- When the distal phalanx makes contact with the object, the motor should reach its maximum torque and stall.

Note: A coupled movement of the proximal and distal phalanx is still possible.

**#12. Linkage / Mechanical stop / Threshold force**

This concept uses a pin-hole joint in C and toothed surfaces at joints B and C.

- The entire finger rotates around joint A when an input torque is applied to link AD.
- When the proximal phalanx makes contact with the object, the preload of the linear spring that connects the proximal phalanx and joint C is overcome and the distal phalanx starts to rotate around joint B.
- When the distal phalanx makes contact with an object the force exerted by the linear spring to restrict the movement of the pin-hole joint C is overcome and the joint moves. The linear spring pulls joint C against joint B to lock the angle of the distal phalanx.

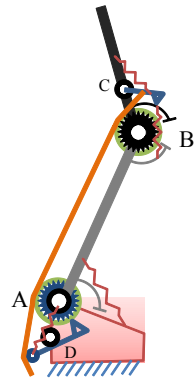


NOTE: It is unsure whether the distal phalanx maintains position when joint C slides through the slot and if the mechanism can be unlocked when link AD is rotated clockwise. Also the link lengths, slot design and placement of the spring have to be chosen precisely in order to make this concept work.

#13. Pully-tendon / mechanical stop / threshold force

This concept uses ratchet-like mechanisms in the joints of the proximal and distal phalanx that lock the joints once a threshold force is overcome.

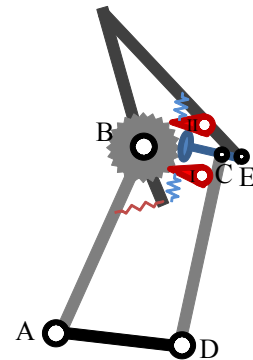
- The entire finger rotates around A when tendon is pulled.
- When the proximal phalanx makes contact with the object, the preload of the linear spring in B is overcome and the distal phalanx rotates around B.
- When the distal phalanx makes contact with the object, the preload of the linear spring at C is overcome and joint B locks.
- When tendon force increases the preload of the linear spring at D is overcome and joint A locks.

**#14. Linkage / Non-backdrivable / Actuation torque**

This concept uses a non-backdrivable ratchet-like mechanism to lock a joint.

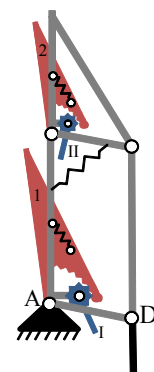
- When a torque is applied to link AD the entire finger rotates around joint A.
- When the proximal phalanx makes contact with the object, link CD pushes pawl II up which unlocks the distal phalanx. The distal phalanx then rotates around joint B.
- When the distal phalanx makes contact with the object the actuation force should be kept constant.

Note: Joint A still has to be locked which can be done by implementing a similar mechanism in joint A. In the case that no actuation torque is applied the finger is infinitely stiff.

**#15. Linkage / Mechanical stop / threshold force**

This concept uses variable mechanical stops that are actuated when the phalanges make contact with an object.

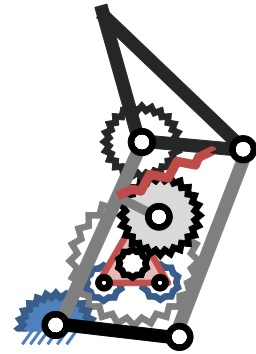
- When a torque is applied to link AD the entire finger rotates around joint A.
- When the proximal phalanx touches the object the preload of the linear spring between the proximal phalanx and block 1 is overcome and block 1 rotates around joint A. This causes pawl I to rotate until it touches the ground.
- The preload of the linear spring connecting the proximal and distal phalanx is overcome and the distal phalanx rotates around joint B.
- When the distal phalanx touches the object the preload of the linear spring between the distal phalanx and block 2 is overcome and block 2 rotates around joint B. This causes pawl II to rotate until it touches link AB.



#16. Linkage / non-backdrivable / Phalanx angles, joint angles

In many cases when the distal phalanx is more than 90 degrees with reference to the ground a force-closed grasp is obtained. In this case no force needs to be exerted to the object to maintain a stable grasp as long as the angles of the phalanges are maintained. The concept uses the information of the angular rotation of both phalanges to trigger a non-backdrivable mechanism once the angle of the distal phalanx is more than 90 degrees with reference to the ground. A possible way to determine the angle of the distal phalanx is by using a geared mechanism which receives an input from both the angles of the proximal and distal phalanx and has an output which corresponds to the angle of the distal phalanx with reference to the ground.

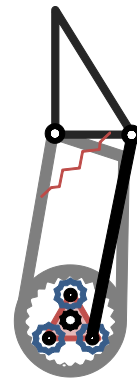
Note: No specific non-backdrivable mechanism was chosen.

**#17. Gear / Non-backdrivable / none**

This concept uses a non-backdrivable actuator and a planetary gear that distributes the actuation torque.

- When a torque is applied to the sun gear, the entire finger rotates.
- When the proximal phalanx touches the object, the finger stops rotating and the planet gears start to rotate within the housing causing the distal phalanx to rotate.
- When the distal phalanx makes contact with the object the actuator should maintain its constant actuation force.

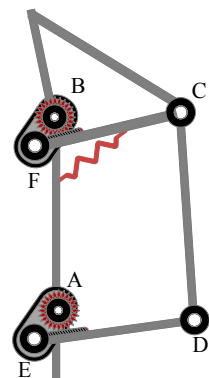
Note: There is probably still a relative movement possible between the proximal and distal phalanx.

**#18. Linkage / Mechanical stop, joints / Threshold force**

This concept uses two toothed joints in A and B.

- When a torque is applied to link DE the entire finger rotates around joint A.
- When the proximal phalanx touches the object the preload of the spring at joint B is overcome and the distal phalanx rotates around joint B.
- When the distal phalanx touches the object a threshold force should be overcome which causes links DE and CF to rotate around joint E and F and lock joint A and B respectively.

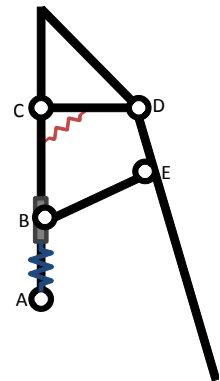
Note: The exact mechanism to make this concept work still has to be determined.



#19. Linkage / Mechanical stop, links / Threshold force

This concept uses a singular position of the transmission linkage to remove a degree of freedom from the mechanism.

- When a torque is applied to link FG the entire finger rotates around joint A.
- When the proximal phalanx makes contact with the object the preload of the linear spring at joint C is overcome and the distal phalanx rotates around joint C.
- When the distal phalanx makes contact with the object the preload of the linear spring which connects joint A and the linear slider B on link AC is overcome and slider B moves towards joint A until link BE and EF are in line, which locks the joints.

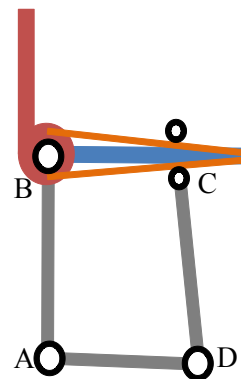


Note: Joint A still has to be locked.

#20. Linkage / non-backdrivable+effective length / separate actuator

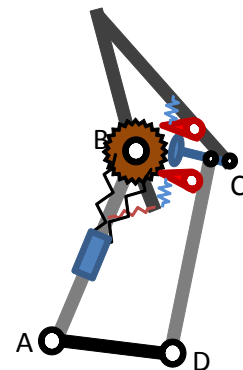
In this concept the distal phalanx is connected to the transmission linkage via a passive element. The distal phalanx can rotate freely around joint B and is attached to link BC via two leaf springs whose effective length can be controlled by a separate actuator.

Note: The rotational stiffness of the finger around joint A still has to be adjusted.

**#21. Linkage / non-backdrivable+antagonistic / separate actuator**

This concept combines non-backdrivable mechanism with the antagonistically working principle. The brown sprocket can freely rotate around joint B and is connected by 2 nonlinear springs to a slider. The pretension of the springs can be adjusted by moving the slider along link AB which controls the rotational stiffness of the sprocket. The distal phalanx rotates around joint B and is connected to the sprocket by a non-backdrivable mechanism.

Note: The rotational stiffness of the finger around joint A still has to be adjusted.

**#22. Pulley-tendon / antagonistic couple / threshold force**

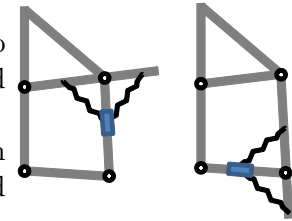
With this concept the proximal and distal phalanges are connected by two nonlinear springs in an antagonistic setup. The two springs of a single joint are not identical, but the left spring has a slightly higher stiffness. For each joint both springs are connected to a linear slider. Moving the slider will rotate the phalanges due to the different stiffness values of the springs. The contact force is determined by the difference in stiffness of the nonlinear springs. After the phalanges make contact with the object, the spring force is increased, which increases the apparent stiffness of the joints.



#23. Linkage/antagonistic couple / separate actuator

If two links of an underactuated finger could be connected using two nonlinear springs in an antagonistic setup, the apparent stiffness could be varied by changing the length of the springs.

Note: Since all the links also have to be able to freely rotate with reference to each other, it is hard to connect two links directly and maintain zero resultant torque around the joint.

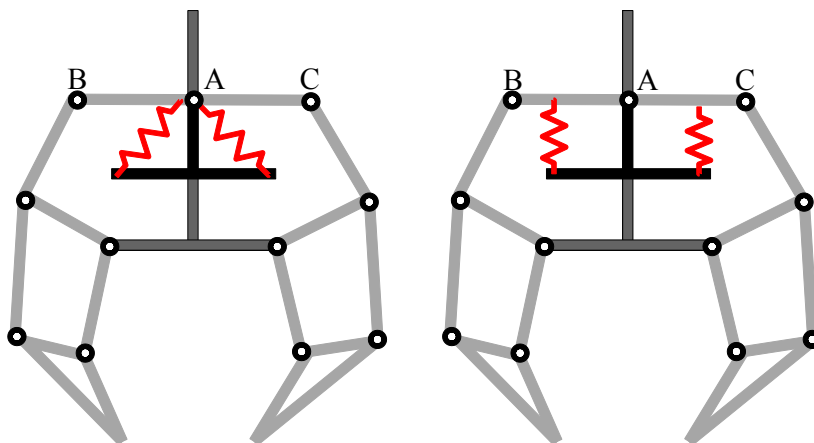
**A-5-3 GrasperLevelConcepts**

The third level in which concepts were generated was the grasper level. On this level it is intended to implement a single mechanism which adjusts the stiffness of the entire grasper in once.

#24. Linkage / Adjustable moment arm / separate actuator

With this concept the stiffness of the entire grasper is adjusted by adjusting the rotational stiffness of the differential mechanism. For the individual rotation of both the proximal and distal phalanx the links of the transmission linkage also rotate. Both transmission linkages are connected to each other by the differential mechanism. Increasing the rotational stiffness of the differential mechanism could therefore have an effect on the stiffness of the entire grasper. With this concept a rotational joint in A connects the differential to a prismatic joint which can translate along the vertical axis. The differential is also connected to the prismatic joint via two preloaded compression springs in points B and C. These springs exert a torque around joint A. The distance between the attachment points B and C and joint A can be varied using a second actuator. By changing this distance the rotational stiffness of the differential is adjusted.

However there is still a coupled movement between the proximal and distal phalanx possible which does not require the differential mechanism to rotate. Therefore this concept does not adjust the stiffness of all available degrees of freedom.



A-6 Concept selection

From the list of concepts a number of promising concepts were selected. Two groups of concepts could be distinguished based on the possible configurations in which the stiffness can be adjusted. With one group of concepts the stiffness could only be adjusted in a predetermined number of configurations. This group consisted of the concept solutions which used ratchet-like mechanisms, where the number of teeth of the gears limits the number of possible configurations. With the other group the stiffness could be adjusted in any configuration. It was stated that it is desirable if the grasper is able to adjust the stiffness for any configuration. Therefore the ratchet based concepts were declined. Furthermore it was stated that it is desirable to obtain a high stiffness without using friction forces. Using friction forces could lead to wear of components which is undesirable. As a result concepts 3, 4 and 24 were chosen to elaborate more on the design.

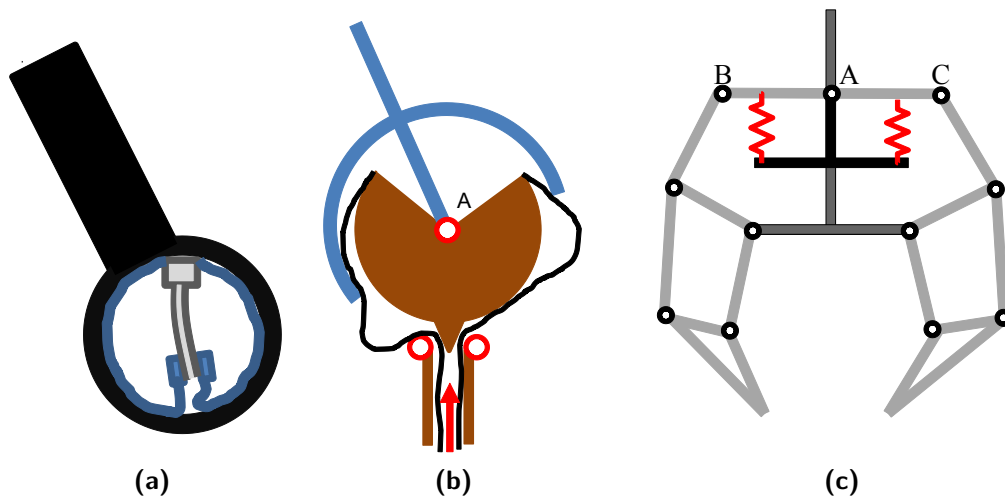


Figure A-3: Schematic representation of the selected concepts 3 (a), 4 (b) and 24 (c).

A-7 Proof of concept

A-7-1 Concept 3

In order to obtain a rough estimation of the forces and angular deflections that occur when a torque is applied to concept 3 some calculations were done. The resulting torque on the flexible member and its angular deflection caused by an external force were estimated. Fig. A-4 illustrates the dimensions used in the calculation and Fig. A-5 shows the free body diagram. The values of the parameters used in the calculations can be found in Table A-3. The required friction force and normal force that is needed to withstand the external force was calculated using equations A-1 and A-2. The magnitude of the horizontal forces acting on the cantilever beam was estimated using equations A-3 to A-6. For simplicity it was assumed that the vertical forces F_{Ay} , F_{By} , F_{Cy} and F_{Dy} were counteracted by the actuator that moves the slider across the cantilever beam and do not contribute to the deflection of the cantilever beam.

$$F_{\mu} = \frac{F(L + R)}{2R} \quad (\text{A-1}) \quad F_{Bx} = \frac{F_p l + F_{\mu} R}{2l} \quad (\text{A-3}) \quad F_{Ax} = \frac{F_p l - F_{\mu} R}{2l} \quad (\text{A-5})$$

$$F_p = \frac{F_{\mu}}{\mu} \quad (\text{A-2}) \quad F_{Dx} = F_{Bx} \quad (\text{A-4}) \quad F_{Cx} = F_{Ax} \quad (\text{A-6})$$

Where F represents the external force applied to the phalanx, w the width of the cantilever beam, l the effective length of the cantilever beam, R the radius of the joint, $L + R$ the length of the moment arm of the external force and μ represents the static friction coefficient of the used materials. Using the pseudo rigid body model a rough estimate of the angular deflection ϕ of the cantilever beam was calculated using equation A-7 and A-8.

$$K = \frac{\gamma K_{\theta} EI}{l} \quad (\text{A-7}) \quad \phi = \frac{(F_{Dx} - F_{Ax})l}{K} \quad (\text{A-8})$$

with

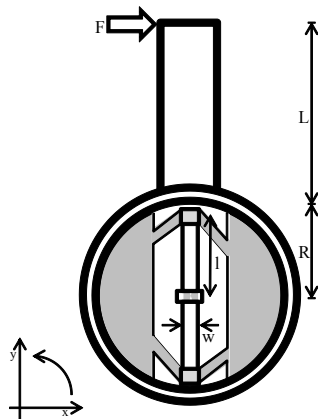


Figure A-4: Dimensions used for calculation.

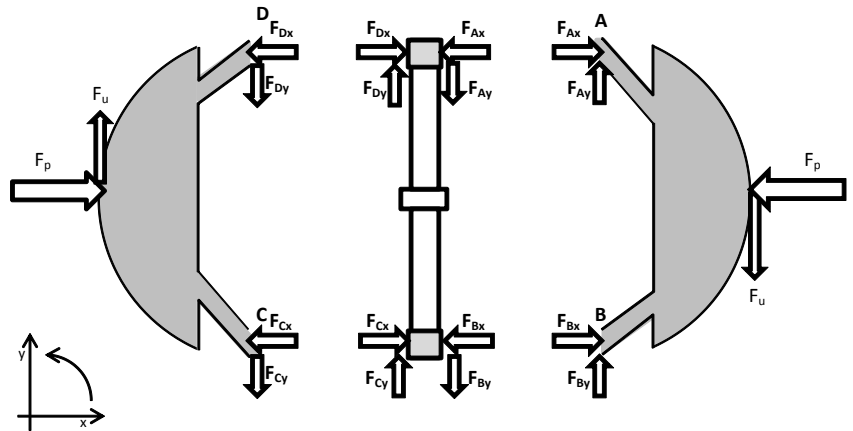


Figure A-5: Free body diagram of concept solution.

Table A-3: Parameter values and results

Constants			Parameter	Steel	Polycarbonate	Unit
L	0.06	[m]	w	0.0005	0.001	[m]
R	0.04	[m]	E	200	2.6	[GPa]
l	0.03	[m]	μ	0.8	0.31	[-]
t	0.01	[m]	F_p	7.8	20.16	[N]
F	5.00	[N]	K	1.56	1.30	[Nm/rad]
			ϕ	0.16	0.19	[rad]

$$I = \frac{tw^3}{12}$$

$$\gamma = 0.85$$

$$K_\theta = 2.65$$

Where t represents the thickness, γ the characteristic radius and K_θ the characteristic stiffness of the cantilever beam. This set of equations was used to obtain a rough estimate of the force F_p and the thickness t that is required to withstand external force F and result in an angular deflection of approximately 10 degrees. The calculation was done for a steel and polycarbonate cantilever beam. The results are shown in Table A-3 indicate that for both materials the force F_p which is needed to obtain the required friction force is already quite large for a joint radius R of 0.04m. Additional to the calculations a proof of concept model was constructed using Lego for the body and a plastic sheet folded like a harmonica to act as a cantilever beam. The sliders of the mechanism had to be moved by hand to adjust the effective length of the cantilever beam. The proof of concept model is illustrated in Fig. A-6.

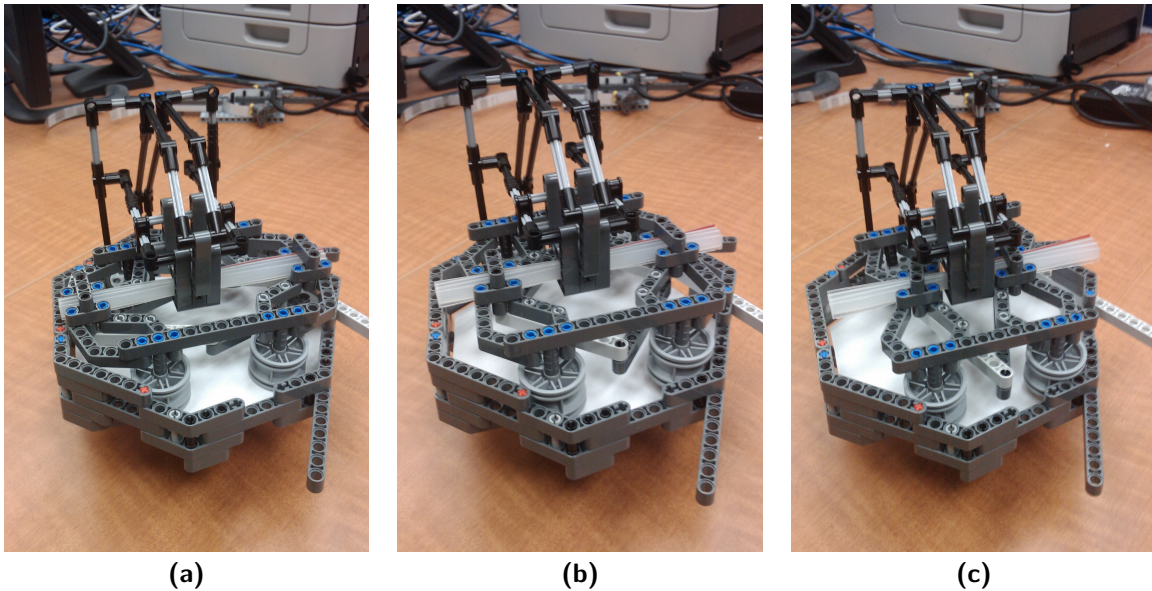


Figure A-6: Proof of concept model of concept 3 in the idle state (a) where the outer ring can freely rotate without, in the low stiffness state (b) where the outer ring is connected to the cantilever beam with a large effective length and high stiffness state (c) where the outer ring is connected to the cantilever beam with a small effective length.

The proof of concept model showed that the concept works. In the idle configuration the outer ring can rotate freely. When the sliders are half way the cantilever beam a connection is made between the inner mechanism and the outer ring. This connection is maintained while the slider moves further to the origin of the cantilever beam. It can be noticed that the stiffness changes while the slider moves along the cantilever beam, however the change in stiffness is quite low. This could be changed by using another material for the cantilever beam. A downside of this mechanism is that the inner mechanism and the outer ring could slip. As mentioned the amount of friction force that is needed to counteract the joint torque applied by external force F is relatively high. Also the size of a joint is commonly quite small. The calculations were done with a joint radius of 0.04m which is quite large. This concept will therefore be very hard to realize on a small scale.

Concept 4

Concept 4 makes use of buckling of a flexible member. The force that is required to buckle an element can be calculated, however the force needed to deform an element once it is buckled is unknown. Therefore no rough calculations were done for this concept, but only a proof of concept model was made. Lego was used to build a ground frame and a phalanx with two extended links. A plastic sheet was used as the flexible member. Fig. A-7 illustrates the three components of the proof of concept model. Fig. A-8a to A-8c illustrates the concept in the idle state, the state where buckling has occurred and the deflection is small and the model with a larger deflection respectively.

The proof of concept model showed that the rotational stiffness of the lever can be adjusted. In the idle state the lever can freely rotate. After buckling has occurred the flexible member makes contact with the lever which increases its rotational stiffness. However the flexible member seems to force the joint to an equilibrium position which is found when the buckling of the flexible member is symmetrical. Friction in the model prevents the joint from reaching this equilibrium point. Also the force that is needed to buckle the flexible member is quite large. Once the member buckles, the force needed to maintain the size of the 'buckle' is much lower than the buckling force itself. Therefore the actuator will need some force control algorithm in order to make this concept work. Also it seems that the rotational stiffness of the joint does not increase significantly when the size of the deflection increases. It was found that the rotational stiffness of the state illustrated in Fig. A-8c was smaller than the state illustrated in Fig. A-8b. Again the small size of a joint will result in large forces between the phalanx and the flexible member. Therefore scaling down this concept could be difficult.

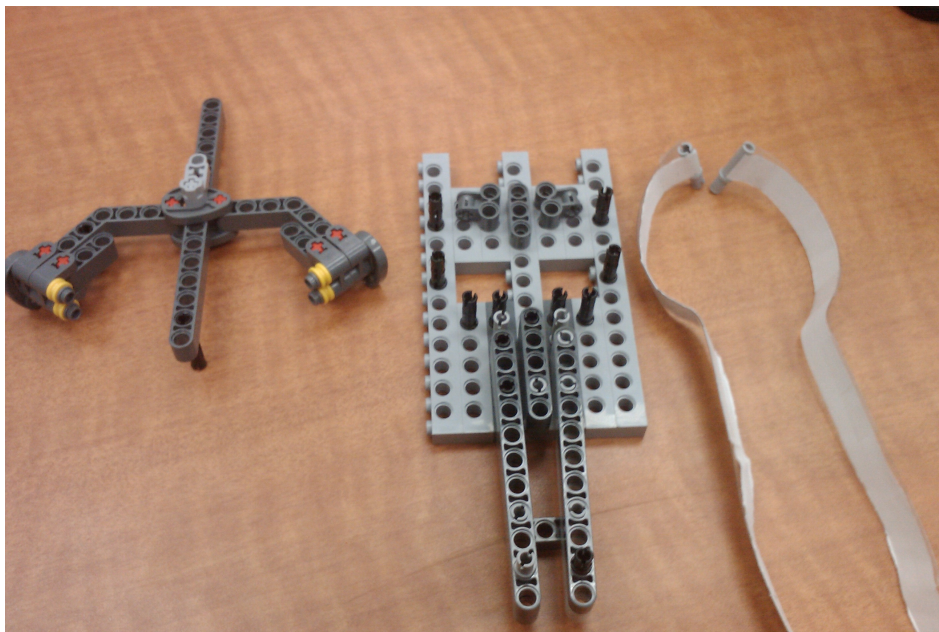


Figure A-7: Lego proof of concept model of concept 4 where illustrating the three components of the model: the lever with two extensions, ground frame with guiding for the flexible member and the flexible member itself

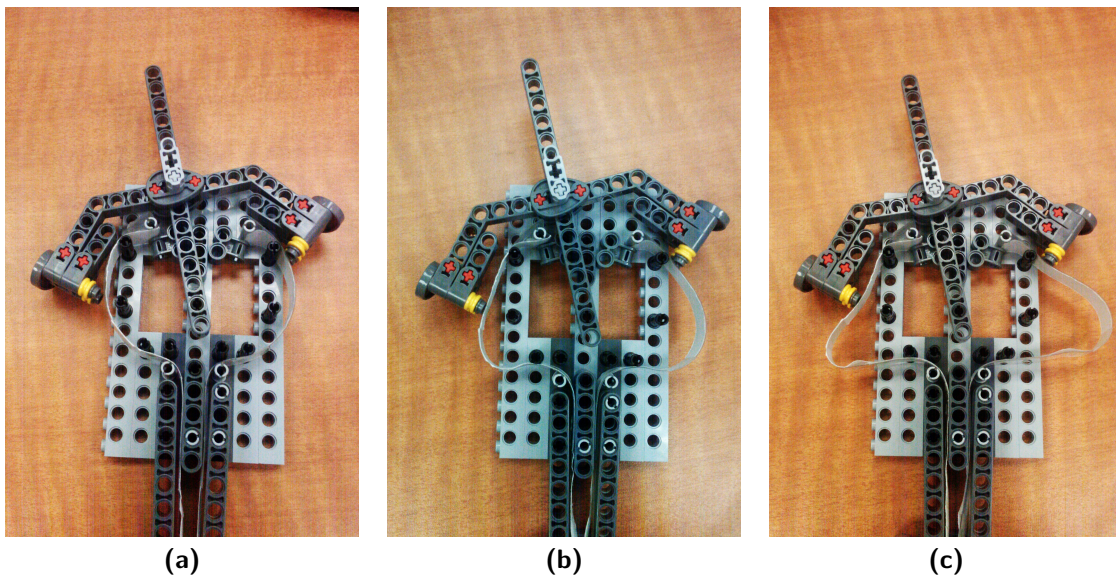


Figure A-8: Lego proof of concept model illustrating the idle state (a), small buckle state (b) and large buckle state (c).

A-7-2 Concept 24

Concept 24 makes use of compression springs with an adjustable moment arm to change the rotational stiffness of the differential mechanism of the grasper. In order to estimate the change in rotational stiffness which can be obtained with this method some calculations were done. Fig. A-9 illustrates a lever which can rotate around joint A . Two compression springs of length L_1 and L_2 exert a force to the lever with a moment arm equal to r which results in a torque around joint A . Length L_0 is the free length of the compression springs and angle α represents the angle of the lever. The rotational stiffness of the lever around joint A was calculated for different lengths of r . Table A-4 lists the values of the parameters used in this calculation. Using equations A-9 to A-14 the resulting moment around joint A and the rotational stiffness were calculated.

$$L_1 = L - r \tan \alpha \quad (\text{A-9}) \quad L_2 = L + r \tan \alpha \quad (\text{A-12})$$

$$F_1 = P_0 + k(L_0 - L_1) \quad (\text{A-10}) \quad F_2 = P_0 + k(L_0 - L_2) \quad (\text{A-13})$$

$$M_A = 2Kr^2 \tan \alpha \quad (\text{A-11}) \quad \frac{\delta M_A}{\delta \alpha} = \frac{2Kr^2}{\cos^2 \alpha} \quad (\text{A-14})$$

Fig. A-10a and A-10b show the results of the analysis illustrating the resulting torque and the rotational stiffness of the lever around joint A respectively. The graphs show that the rotational stiffness of the differential can be adjusted quite well by controlling the moment arm of the compression springs. The exact value of the rotational stiffness can off course easily be adjusted by adjusting the parameters of the compression springs.

A proof of concept model was build using Lego. Fig. A-11a and A-11b illustrate the model in the compliant and stiff configuration respectively. The location of the attachment points of

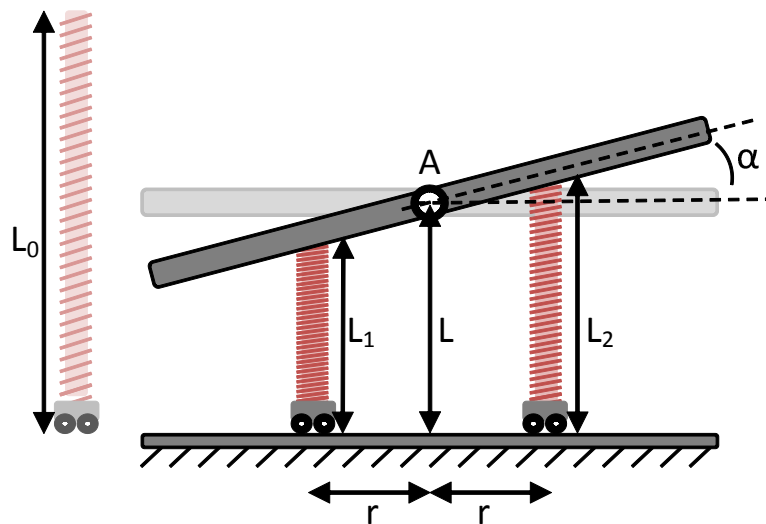


Figure A-9: Schematic representation of a lever with angle α which can rotate around joint A . Two compression springs of lengths L_1 and L_2 apply a moment around joint A with a moment arm equal to r .

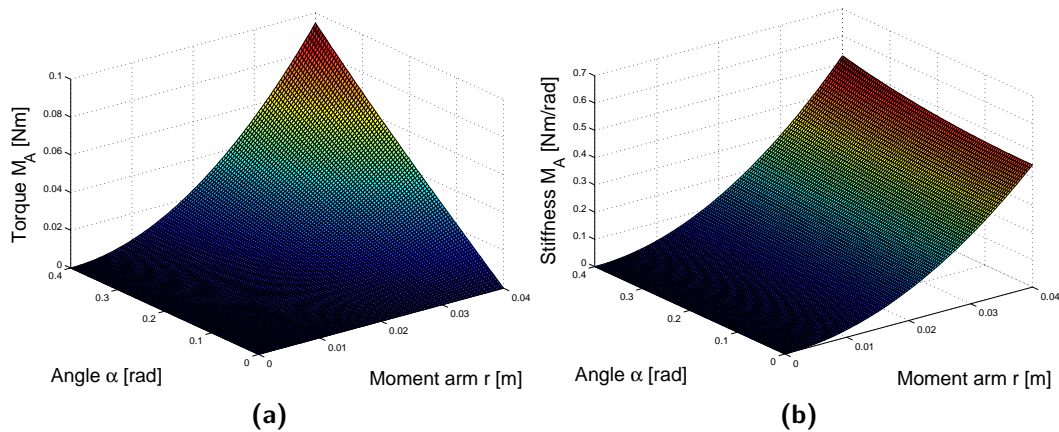
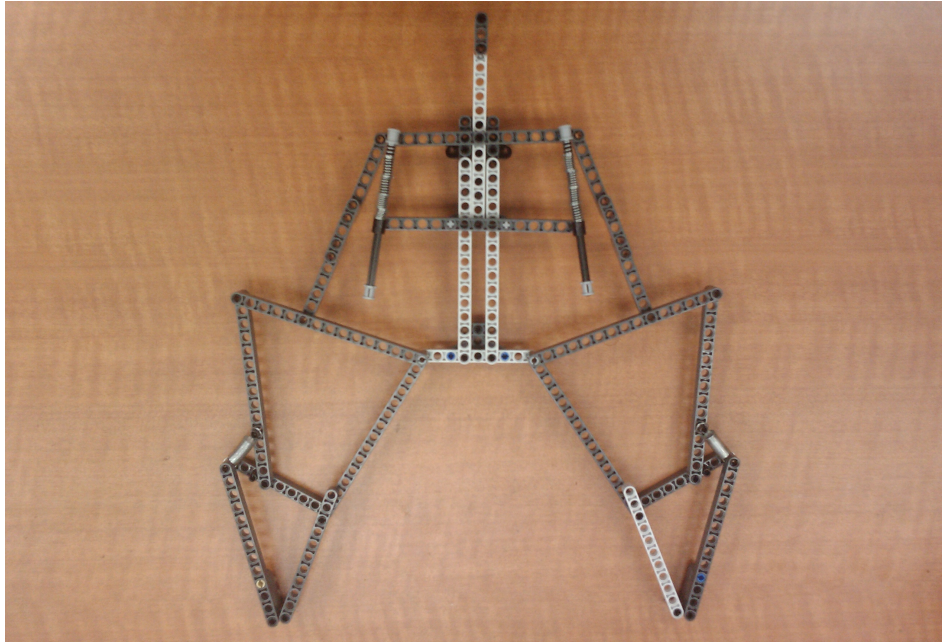


Figure A-10: Resulting torque (a) and rotational stiffness of the lever (b) around joint A for various lengths of the moment arm r and lever angle α

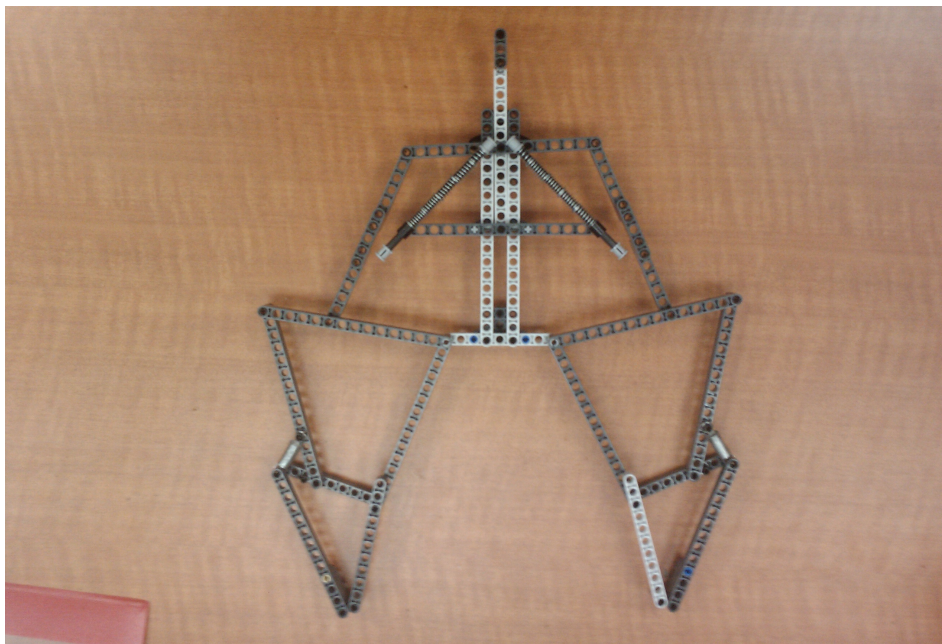
the springs was adjusted manually. When grasping an object the change in rotational stiffness of the differential mechanism could be noticed very well when trying to pull the object out of the grasper in the direction parallel to the palm. When the object was pulled in the direction perpendicular to the palm no change in stiffness was noticed since the differential does not rotate. With this concept only a few components were added to a conventional design of a grasper. Because of this simplistic, yet functional mechanism to adjust the stiffness this concept was considered to be promising.

Table A-4: Constant values used in calculations

Parameter	Value	Unit
L_0	0.06	[m]
P_0	0.00	[N]
k	140	[N/m]
L	0.04	[m]
r	0:0.04	[m]
α	0:0.4	[rad]



(a)



(b)

Figure A-11: Lego proof of concept model of concept 24 in which the grasper is in the low stiffness state (a) and the high stiffness state (b).

A-8 Final concept

Concept 24 was considered the most promising concept. Therefore it was elaborated more on the design of this concept. The design was changed such that it could be actuated with a single actuator. One particular concept design is illustrated in Fig. A-12. With this design the differential of the grasper is connected to a second prismatic joint via four springs. Two of the springs are the compression springs which are used to adjust the rotational stiffness of the differential as discussed in section A-7-2. However the moment arm of these springs is adjusted by rotating the springs instead of translating like in concept 24. The stiffness of the grasper increases once the actuation force exceeds a certain threshold value. The threshold value was determined by two additional preloaded tension springs on top of the differential. Once the actuator force overcomes this threshold value the moment arm of the compression springs increases.

This concept design proved the potential of actuating the grasper with a single actuator. However it consisted of a number of drawbacks. The stiffness could not be maintained when the grasper opened and also in the compliant state the line of force of the two compression springs did not always intersect the rotational joint of the differential. Also the use of four springs was considered unnecessary. Therefore the design was adjusted which led eventually to the concept of which Fig. A-13 illustrates two proof of concept models made out of Lego and components that were manufactured with a 3d-printer. This concept uses a jack-like mechanism with a single preloaded tension spring to obtain a bi-stable behavior. The two stable positions of the bi-stable mechanism result in either a compliant or a stiff state of the grasper. Fig. A-14 illustrates the grasping sequence of the final concept. The dimensional design of the concept will be discussed in Appendix B-2.

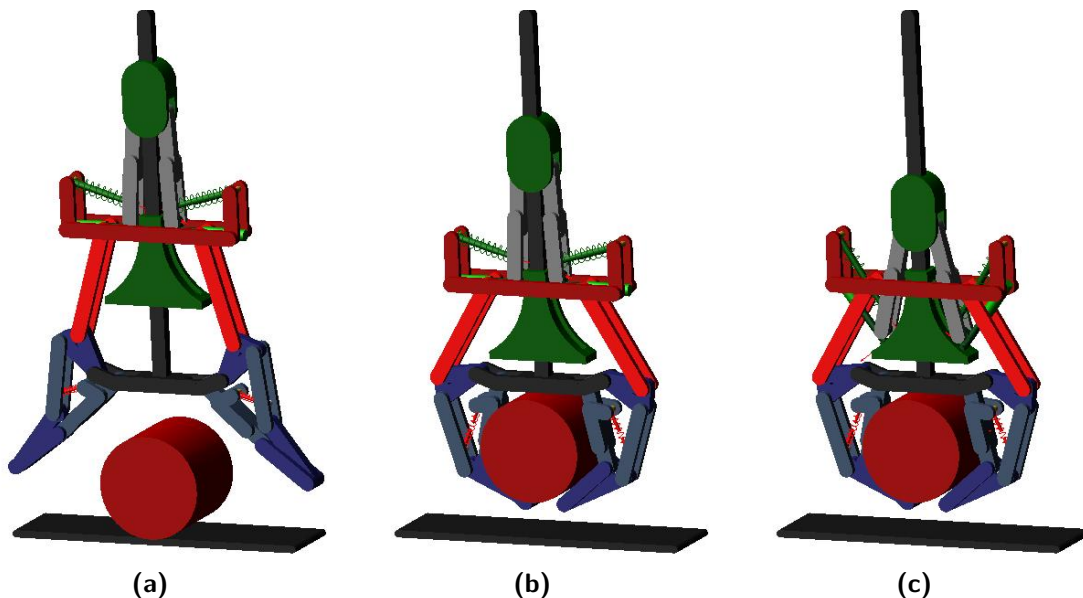


Figure A-12: Grasping sequence of a concept solution where the grasper is illustrated in the opened position (a), closed compliant position (b) and closed stiff position (c). Four springs connect the differential to the input mechanism.

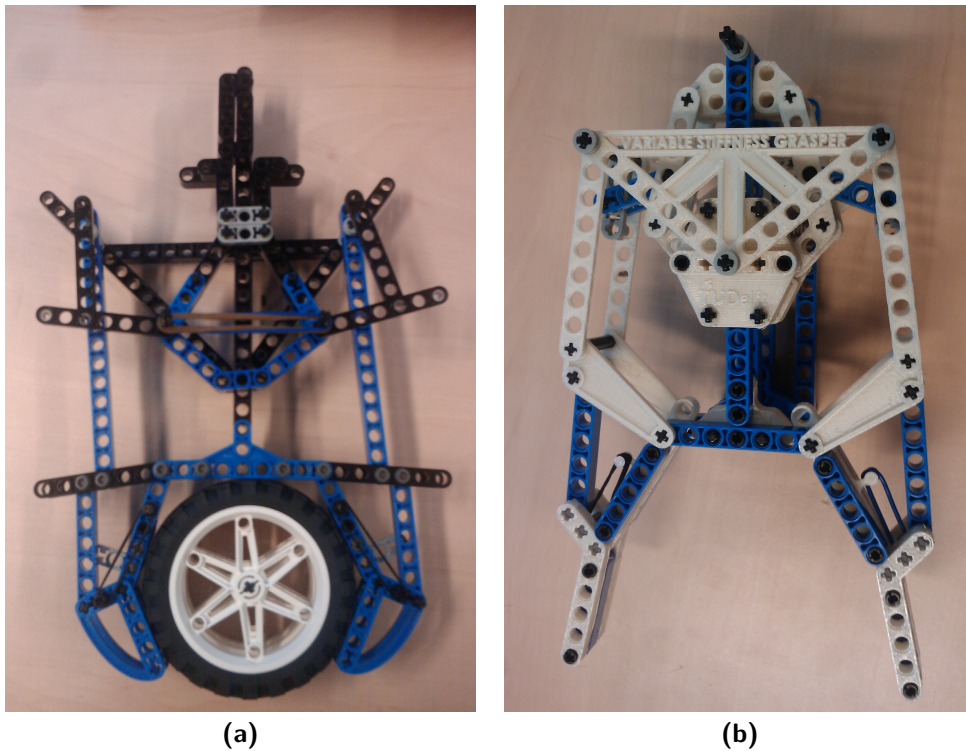


Figure A-13: Two additional proof of concept models made out of lego (a) and partially made out of lego complemented with parts constructed with a 3d printer (b).

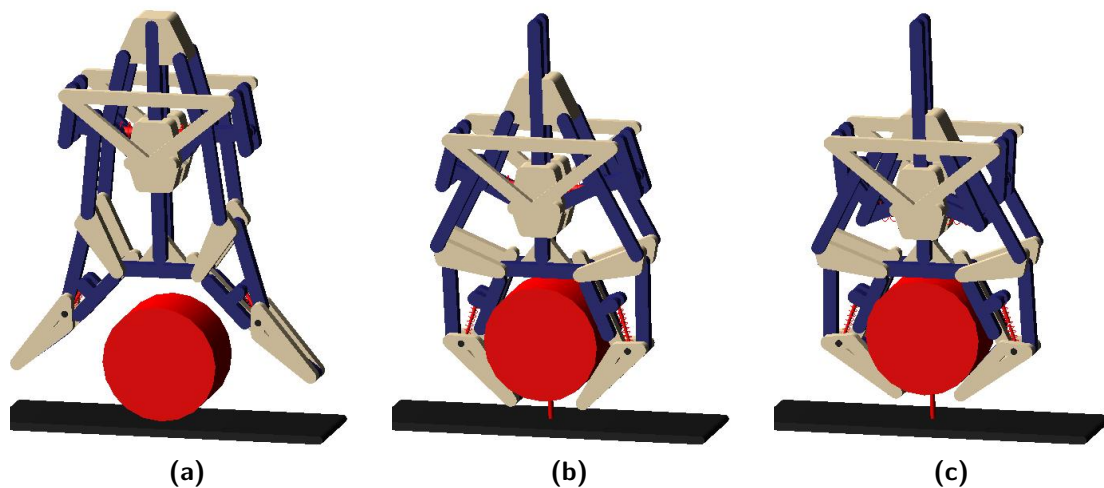


Figure A-14: Grasping sequence of the final concept where the grasper is illustrated in the opened position (a), closed compliant position (b) and closed stiff position (c).

Appendix B

Analytical Modeling

B-1 Experiments

A Matlab model was made to analytically determine the static equilibrium position of the grasper and object for a given object displacement. Two types of experiments were modeled which resembled a pullout of the object in either the direction perpendicular or parallel to the palm of the grasper. For each object displacement the configuration of the grasper and the magnitude of the contact forces were determined. The model was able to switch between different grasp types in the case that an unstable solution was found. This section elaborates more on the Matlab model which is used by discussing the main files of the Matlab model and illustrating the results of a simulation. The Matlab files itself can be found on the data-DVD which is provided with this thesis.

B-1-1 Matlab files

GrasperModel.m

The file *GrasperModel.m* is the main file of the model. In this file the value of the constant parameters describing the grasper and the object is determined. For the grasper the parameters such as the link lengths, the magnitude of the actuation force and the state of the grasper can be set. For the object the parameters such as the diameter and the object displacement can be determined. All parameter values are stored in global data structures which allow other functions to easily read, add or modify parameter values and it results in a clear overview of all available parameters.

Another setting that is determined in this file is the type of experiment that has to be modeled. A choice can be made between three types of experiments. The first type of experiment resembles a single grasp. With this experiment the static equilibrium position of the grasper is determined based on a given object displacement perpendicular and parallel to the center of the palm. The other two experiments resemble the situation in which the grasper has obtained a stable grasp and the object is pulled away from the center of the palm. With the second type of experiment the object is moved in the direction parallel to the palm. In this case the configuration of the grasper and the object displacement perpendicular to the palm in which a static equilibrium position is obtained are determined. With the third type of experiment the object is moved in the direction perpendicular to the palm. In this case the configuration of the grasper and the object displacement parallel to the palm in which a static equilibrium position is obtained are determined. The value of the maximum object displacement and the number of iterations can be determined in this Matlab file. Executing this file will result in the full analytical analysis of the selected experiment.

DoExperiment.m

The function *DoExperiment.m* is executed by *GrasperModel.m*. The main task of this function is to execute the selected experiment and store the calculated data after each iteration. For each iteration this file subsequently executes the functions *CalculateGrasp.m* and *CalculateJointCoordinates.m*.

CalculateGrasp.m

In the function *CalculateGrasp.m* the nonlinear solver `fmincon` is used to determine the static equilibrium position of the grasper and object. For each grasp type the input variables of the nonlinear solver are determined, the nonlinear solver is executed and the results are stored in global data structures. The input variables mainly consist of the link angles of the grasper which can not be calculated using geometric equations. For each grasp type a different set of input variables was used, minimizing the number of unknown variables. This was done in order to reduce the calculation time of the solver and to increase the probability of finding the correct solution.

The file contains a nested function *SwitchGrasp* which is used to check whether the right grasp type was used. This is done by analyzing the solution proposed by the solver by checking whether this solution fulfills a list of criteria. In the case that the solution meets all the criteria the grasp type is considered correct. In the case that the solution does not meet all the criteria a new grasp type is suggested based on the criterion that is not fulfilled. An example of such a criterion is that the magnitude of none of the phalanx contact forces can be negative. In the case that the solver proposes a solution which contains negative contact forces a new grasp type is suggested based on the specific phalanx.

CalculateCoordinates.m

This function is used to calculate the joint coordinates of the grasper based on the joint angles and link lengths.

GrasperEquations.m

The function *GrasperEquations.m* describes all the loop closure and contact force equations and is used as the objective function which the nonlinear solver `fmincon` tries to minimize. The output value of this function is the sum of the loop closure and force equations that correspond to the selected grasp type.

PlotGrasper.m

This function provides a graphical representation of the proposed solution. It shows the configuration of the grasper, the object position and the values of the contact forces of the phalanges and the resulting force of the object.

PlotData.m

This function gives an overview of the analytical results illustrating the contact forces of the phalanges and the resulting force of the object for each object displacement.

B-1-2 Analytical results

Fig. B-1 illustrates the analytical results of a Matlab simulation in which the object undergoes a displacement parallel to the palm of the grasper. In this particular simulation the total object displacement of 0.02m is simulated in 80 steps. For each step the contact forces and resulting force is calculated.

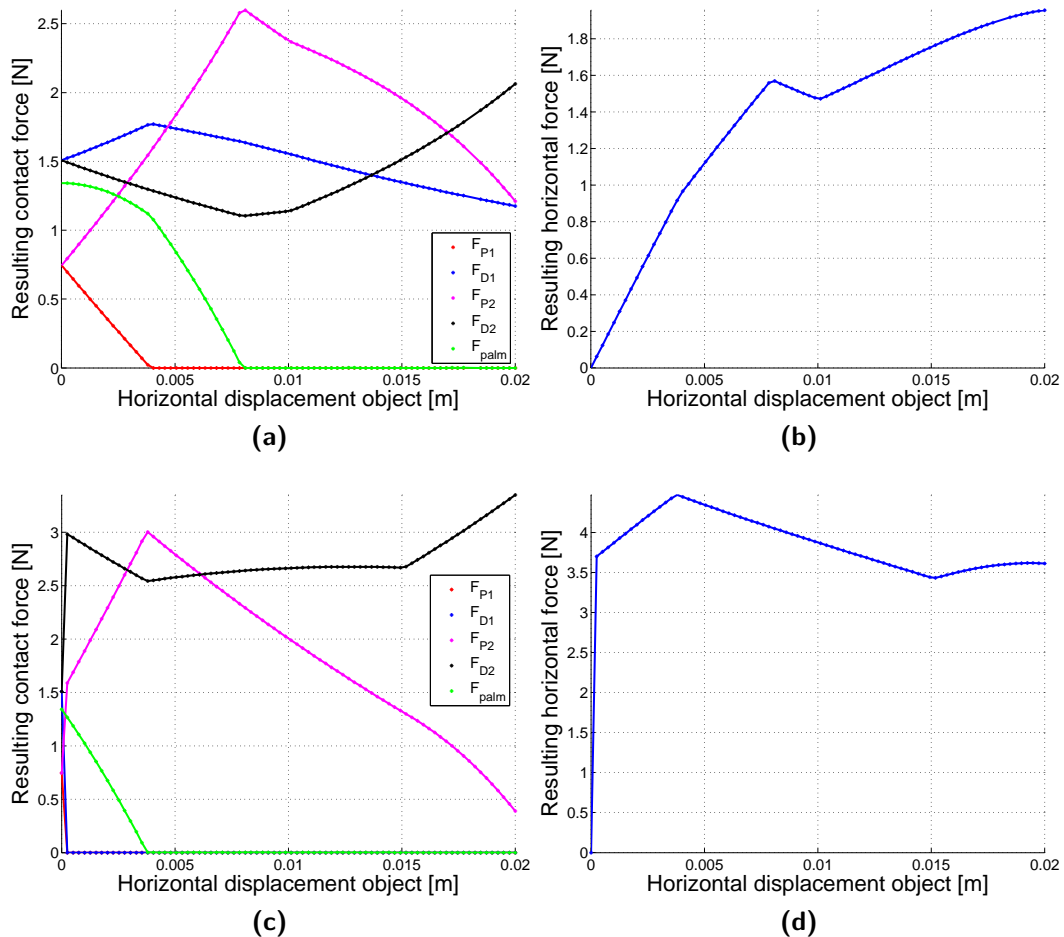


Figure B-1: Results of an analytical simulation of an object displacement parallel to the palm of the grasper for both the compliant (a)(b) and stiff (c)(d) state. Figures (a) and (c) illustrate the contact forces of the phalanges and the palm, where figures (b) and (d) illustrate the resulting force of the object parallel to the palm of the grasper.

B-2 Optimization

The dimensional design of the grasper was done in three stages. First the lengths of the phalanges and the width of the palm were determined, second the dimensions of the links of the transmission linkage and the seesaw mechanism were determined and third the dimensions of the bi-stable mechanism were determined. The following sections will discuss the dimensional design of each stage

Phalanx lengths

Two design parameters were chosen as a basis for the dimensioning of the phalanges. The maximum radius of the object that had to be grasped in a five point grasp $r_{obj,5}$ was set at 0.060m and the total length of the finger L_{tot} was set at 0.090m. Equation B-2 as described in [2] relates the object radius that can be grasped in a five point grasp to the length of the proximal phalanx L_1 and half the width of the palm L_0 .

$$L_{tot} = L_1 + L_2 \quad (B-1)$$

$$r_{obj,5} \leq \frac{1}{2} \left(L_1 + \sqrt{L_1^2 - 4L_0^2 + 4L_0L_1} \right) \quad (B-2)$$

According to B-2 the radius $r_{obj,5}$ is at its maximum when the length of the proximal phalanx is equal to half the width of the proximal phalanx. Substituting $L_0 = \frac{1}{2}L_1$ into equation B-2 results in:

$$r_{obj,5} = \frac{1}{2}L_1 (1 + \sqrt{2}) \quad (B-3)$$

using $r_{obj,5} = 0.060m$ the length of L_1 equals 0.05m. As a result the link length of the distal phalanx L_2 and half the width of the palm L_0 equal 0.04m and 0.025m.

Transmission linkage and seesaw

In order to determine the link lengths of transmission linkage and the differential a genetic algorithm was used. A total of 9 input variables was used consisting of the lengths and fixed angles of links of the transmission linkage and the differential. Each variable was restricted by a lower and upper bound of which the values were chosen in such a way that only feasible solutions could be obtained.

The objective function that was used consisted of three analytical simulations: the first simulation modeled the grasper in its opened position, the second simulation resembled a horizontal pullout of the object and the third simulation resembled a vertical pullout of the object. Every set of input variables proposed by the genetic algorithm was used to subsequently perform these three simulations for two different object sizes of $r_{obj}=0.032m$ and $r_{obj}=0.040m$. A list requirements was set up:

- The relative angles between the input links of the fingers and the coupler links that connect the differential with the input links were restricted. At all times the values of $\beta_1 - \alpha_1$ and $\alpha_2 - \beta_2$ had to be larger than $\frac{1}{12}\pi$ rad. This was done in order to prevent singularities.
- The minimal distance between joint A and the palm was set at 0.015m. This was done in order to take the thickness of the links into account and to reserve some space for the bi-stable mechanism.

Bi-stable mechanism

Once the link lengths of the grasper were known the bi-stable mechanism was designed. First of all the requirements of the mechanism were set. The bi-stable mechanism has two threshold force values which have to be overcome in order to switch between states. The threshold force required to switch from the compliant to the stiff state has to be lower than the actuation force of 4N. Therefore this value was set at 3.5N. Another requirement was that the bi-stable mechanism should prevent the differential from rotating for any external force. Therefore the mechanism was designed in such a way that the prismatic joint of the differential translates before the differential starts to rotate. This translation occurs when the actuation force is counteracted.

Fig. B-3 illustrates a schematic overview of the bi-stable mechanism and the differential of the grasper. The magnitude of the force F_2 which is required to prevent the differential from rotating is described in eq.B-4 to B-7 using the sum of the moments around joint A:

$$\sum M_A = 0 : F_{3X}l_8 \sin \theta_1 + F_{3Y}l_8 \cos \theta_1 + F_{2X}l_7 \sin \theta_1 - F_{2Y}l_7 \cos \theta_1 = 0 \quad (\text{B-4})$$

where

$$F_{2Y} = F_2 \sin(\theta_4) \quad (\text{B-5})$$

$$F_{2X} = F_2 \cos(\theta_4) \quad (\text{B-6})$$

Substituting B-5 and B-6 into eq.B-4 gives:

$$F_2 = \frac{l_8(F_{3X} \sin \theta_1 + F_{3Y} \cos \theta_1)}{l_7(\sin \theta_4 - \theta_1)} \quad (\text{B-7})$$

where F_{2Y} equals the magnitude of the actuator force F_{ACT} and F_{3X} and F_{3Y} represent the maximum horizontal and vertical force that are applied to the differential mechanism as a result of an object displacement. The value of F_{3Y} is equal to the actuator force F_{ACT} since it was stated that the differential will translate vertically which occurs when F_{3Y} exceeds the value of the actuator force. In the equilibrium position that follows the value of F_{3Y} will be equal to the actuator force. The value of F_{3X} is dependent of the angle of the coupler link that connects the differential to the input link of the finger. Using Matlab model the values of F_{3X} and F_{3Y} were found 1.2N and 4N respectively. In order to prevent the rotation of the differential the sum of the moments around joint V should be less or equal than 0N as described by eq.B-8:

$$\sum M_V \leq 0 : F_{2Y}l_6 \cos \theta_2 + F_{2X}l_6 \sin \theta_2 - F_{1Y}l_3 \cos \theta_2 + F_{1X}l_3 \sin \theta_2 - 2F_S l_4 \sin \theta_2 \leq 0 \quad (\text{B-8})$$

where

$$F_{1Y} = F_1 \sin \theta_3 \quad (\text{B-9})$$

$$F_{1X} = - F_1 \cos \theta_3 \quad (\text{B-10})$$

$$F_S = F_{S0} + (l_S - l_{S0})K \quad (\text{B-11})$$

substituting B-5, B-6, B-9 and B-10 into B-8 gives:

$$F_S \geq \frac{F_2 l_6 \sin(\theta_2 + \theta_4) - F_1 l_3 \sin(\theta_2 + \theta_3)}{2l_4 \sin \theta_2} \quad (\text{B-12})$$

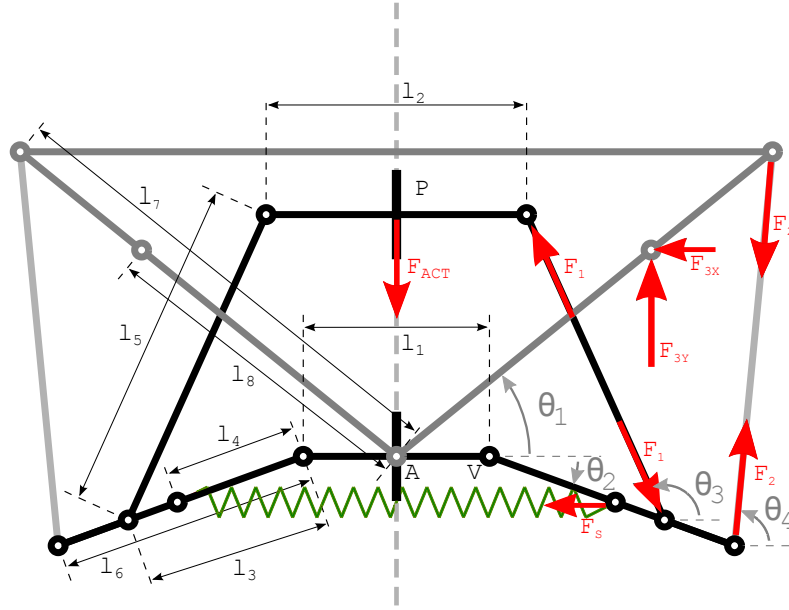


Figure B-3: Schematic representation of the bi-stable mechanism and the differential, where l_i and θ_i indicate the lengths and angles of the links. F_{act} , F_S and F_i represent the actuator force, spring force and internal forces. Note that the schematic does not represent a complete free body diagram, the force vectors only indicate the forces that are present in the equations

where F_{S0} is the spring preload in Newton, l_S and l_{S0} are the true and free length of the spring in meters and K is the spring stiffness in Newton per meter. Note that the spring force F_S is multiplied with a factor 2 in eq. B-8. This is due to the fact that the spring prevents a translation of prismatic joint P relative to prismatic joint A via both the left and right side of the bi-stable mechanism. By multiplying F_S with a factor 2 the effect of the left side of the bi-stable mechanism can be neglected and the required spring force can be calculated using the sum of the moments around joint V . The actuator force that is needed to transfer between the stiff and compliant state can be expressed using the sum of the moments around joint V as described in B-8, substituting B-13 into the equation and discarding the effect of force F_2 :

$$F_{1X} = \frac{F_{1Y}}{\tan(\pi - \theta_3)} \quad (\text{B-13})$$

$$F_{1Y} = \frac{-2F_S l_4 \sin \theta_2}{l_3 \cos \theta_2 - \frac{l_3 \sin \theta_2}{\tan(\pi - \theta_3)}} \quad (\text{B-14})$$

The link lengths and the minimum and maximum angles of θ_2 of the bi-stable mechanism were determined using trial and error. An initial guess was done for all the parameters and using B-12 and B-14 the required spring force and the corresponding threshold value were determined. Based on the estimated spring force a suitable spring was selected and used to calculate the actual spring force using B-12. The parameter values were optimized by comparing the required spring force with the actual spring force and comparing the desired threshold with the actual threshold until the requirements were met. An overview of the link lengths, spring characteristics and threshold torques of the bi-stable mechanism can be found in Table B-2.

Table B-2: Specifications of the bi-stable mechanism where $F_{T,SC}$ and $F_{T,CS}$ indicate the threshold force required to transfer from the stiff to compliant state and from the compliant to the stiff state respectively. The angle θ_2 for both the compliant and stiff state is indicated by $\theta_{2,C}$ and $\theta_{2,S}$ respectively.

Link lengths			Spring characteristics			Mechanism characteristics		
l_1	0.025	m	F_0	1.15	N	$F_{T,SC}$	2.86	N
l_2	0.035	m	L_0	0.0304	m	$F_{T,CS}$	3.60	N
l_3	0.025	m	K	120	N/m	$\theta_{2,C}$	-0.70	rad
l_4	0.018	m				$\theta_{2,S}$	0.35	rad
l_5	0.045	m						
l_6	0.018	m						
l_7	0.065	m						

Appendix C

Experiments

C-1 Prototype

A prototype was built to be able to validate the theoretical results. The final concept was designed in such a way that it consisted out of links with a constant thickness. This way it was possible to fabricate all the components using laser cutting. A 3D-CAD model was drawn in Solidworks which is illustrated in Fig. C-1. A drawing was made in which all the components of the grasper were drawn side by side. This drawing was used as an input file for the laser cutting machine. Because of the tolerances of the laser cutting machine and the fact that the line of the cut is skew, the diameters of the holes of the links were drawn 0.2 mm smaller than the actual size. Therefore each hole had to be drilled afterwards in order to obtain the desired diameter. In order to be able to connect the links the diameter of the holes were drilled to size such that a tight or loose fit was obtained, dependent whether the link had to rotate around an axle or not. The links were connected using brass axles with a diameter of 4mm. Fig. C-3 and C-4 illustrate the grasper in its compliant and stiff state respectively. It can be seen that in the compliant state the links of the bi-stable mechanism are pulled against the mechanical stops by the preloaded spring. The coupler links that connect the differential with the bi-stable mechanism can freely rotate. In the stiff state it can be seen that the coupler links are forced in their maximum angle by the preloaded spring and the actuator force.



Figure C-1: Solidworks drawing of the final concept



Figure C-2: Prototype of the final concept

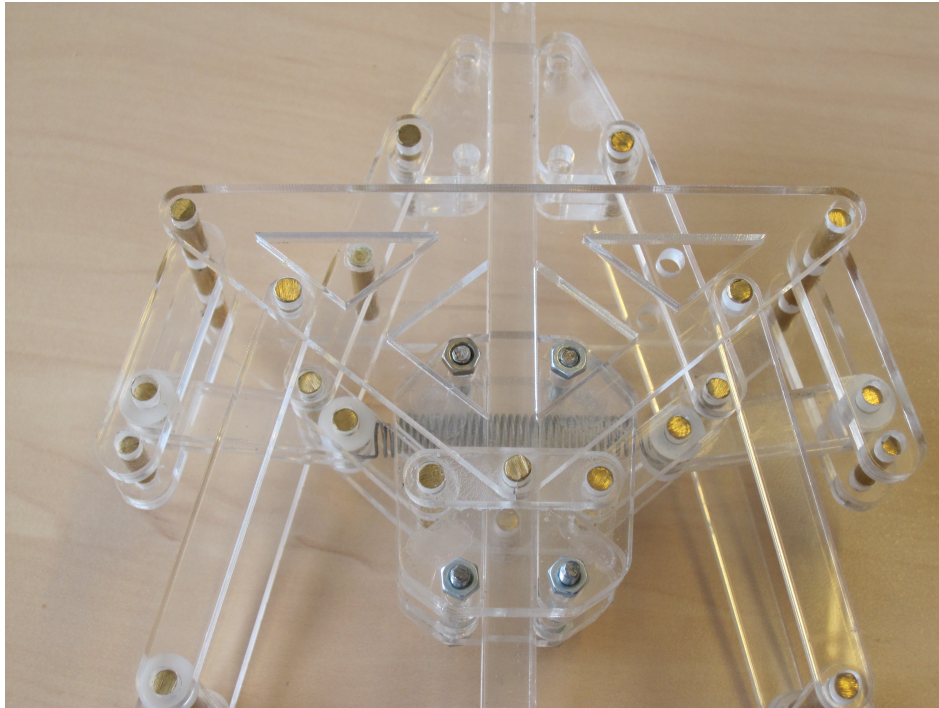


Figure C-3: Close up of the bi-stable mechanism in its compliant state where the preloaded spring of the bi-stable mechanism pulls the links against the mechanical stops.

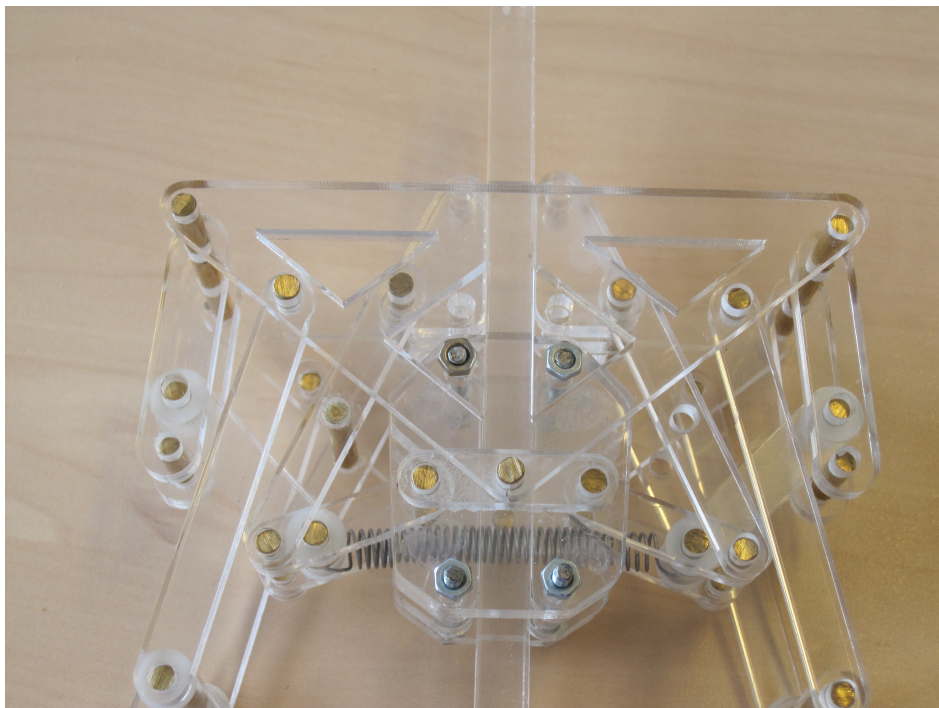


Figure C-4: Close up of the bi-stable mechanism in its stiff state. The coupler links that connect the bi-stable mechanism with the differential are kept in their maximum angle by the actuator force and the preloaded spring of the bi-stable mechanism.

C-2 Measurement setup

A measurement setup was assembled to quantify the robustness of the grasper in compliant and stiff state. This section will discuss two main parts of the measurement setup concerning the actuation of the grasper and the object.

C-2-1 Grasper

The ground link of the grasper was rigidly connected to the base plate of the measurement setup using M4 threaded rods and acrylic spacers. The upper prismatic joint of the bi-stable mechanism was connected to a prismatic joint using two M3 threaded rods and acrylic spacers. In order to actuate the grasper a constant force had to be applied coaxial to the joints. Since the bi-stable mechanism of the grasper was designed for a constant actuation force of 4N a constant weight of 400 grams was used to actuate the grasper. The actuation force was aligned with the prismatic joints of the bi-stable mechanism by connecting the weight to the actuator via a rope and pulley to the prismatic joints. In order to reduce the friction of the prismatic joints of the grasper ball bearings were implemented in the design. Fig. C-5 and C-6 illustrate in more detail how the grasper is connected to the base plate and how it is actuated.

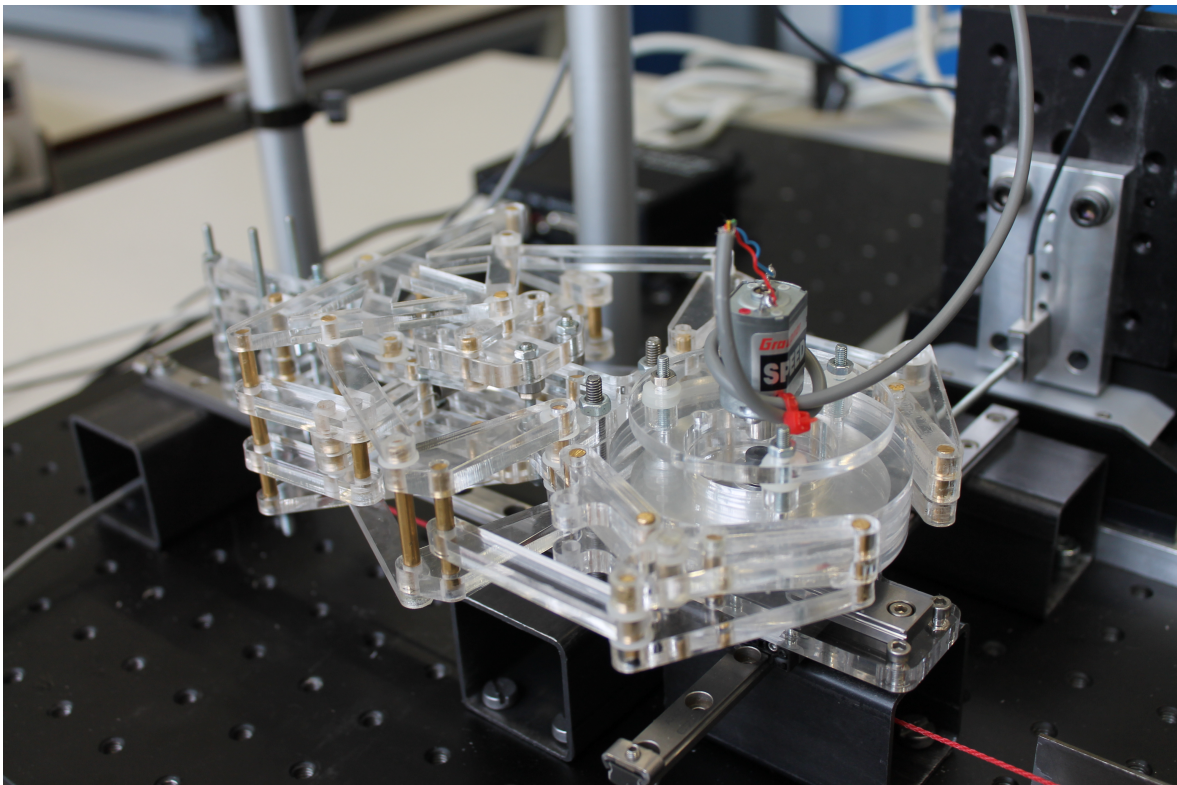


Figure C-5: Overview of the grasper mounted on the base plate

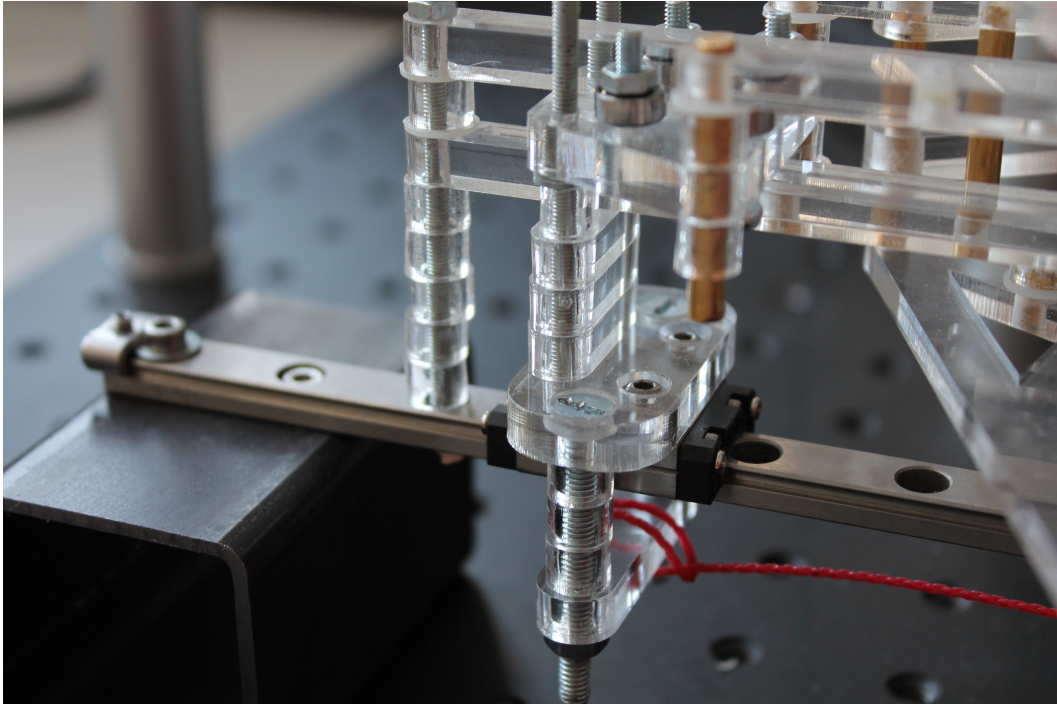


Figure C-6: Close up of the connection between the prismatic joints

C-2-2 Object

A cylindrical object was made by stacking three acrylic discs with a diameter of 35mm on top of each other and mounting it onto an aluminium frame. The frame was connected to a central axle using ball bearings. This allowed a smooth rotation of the object. The object was fixed onto a planar joint which was created by mounting two prismatic joints on top of each other. This planar joint was rigidly fixed to the base plate. During the experiment the resulting force of the object parallel to the palm had to be measured, therefore a linear actuator with a load cell was aligned parallel to the palm and mounted onto the base plate. The actuator was connected via the load cell to the planar joint using a threaded rod. In this configuration the position of the object parallel to the palm was controlled by the actuator, while the object could freely translate in the direction perpendicular to the palm. Because the object could freely translate in the direction perpendicular to the palm the resulting force of the object parallel to the palm was not always aligned with the actuator which results in an additional torque. It was assumed that this torque was counteracted by the prismatic joints and that it did not influence the force value measured by the load cell. A rotational actuator with an eccentric load was mounted on top of the object. This actuator was used to induce vibrations to the joints of the grasper once it had grasped the object. These vibrations were used to overcome static friction present in the joints of the grasper. Fig. C-7 to C-9 illustrate an overview of the object and the linear actuator and provide a more detailed image of the object, the rotational actuator and the planar joint.

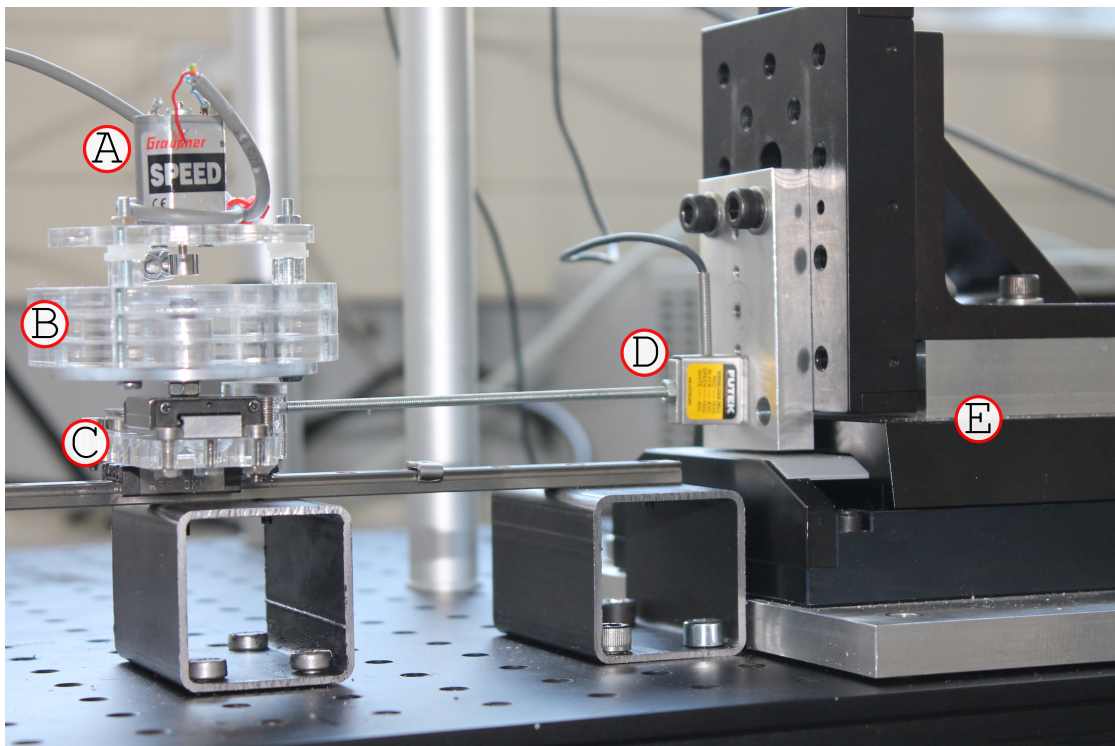


Figure C-7: Overview of the setup used to obtain a predefined object displacement and to measure the resulting force of the object parallel to the palm, illustrating the rotational actuator with eccentric load (A), the cylindrical object (B), the two prismatic joints which form a planar joint (C), the load cell (D) and the linear actuator (E).

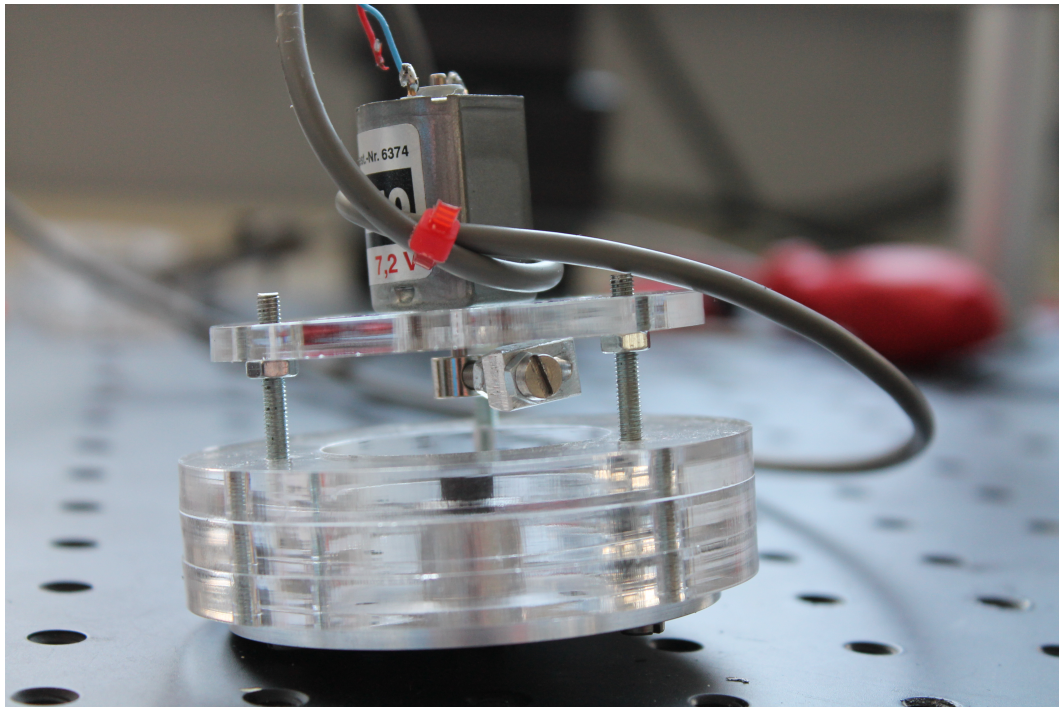


Figure C-8: Close up of the object

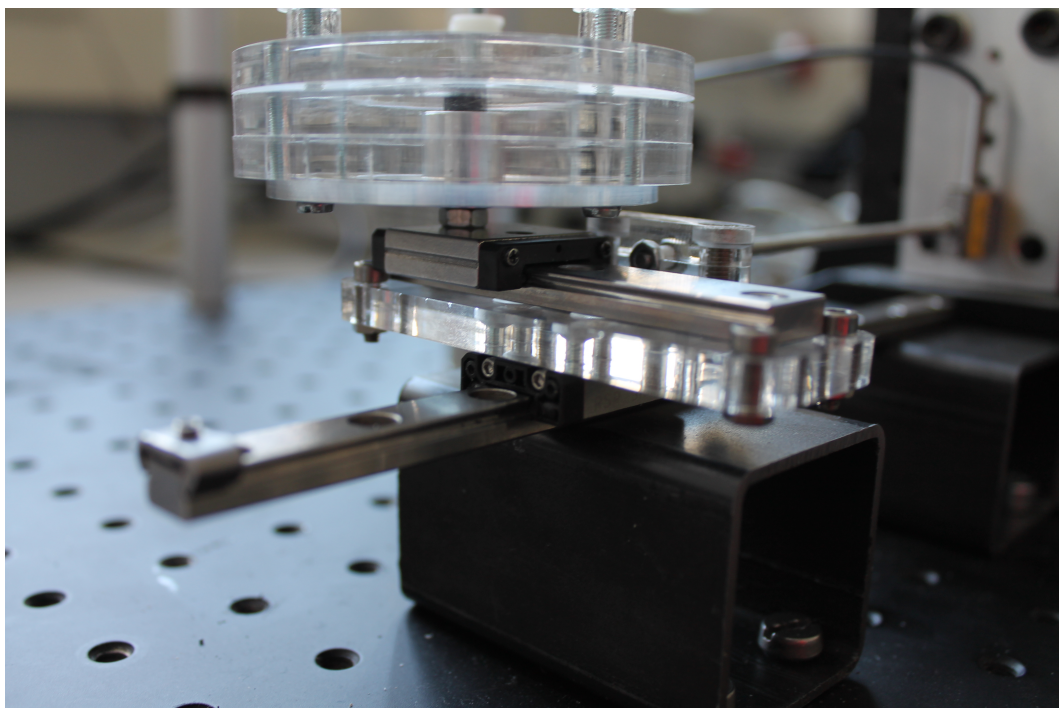


Figure C-9: Close up of the planar joint on which the object is mounted.

C-2-3 Control

Fig. C-10 illustrates the used hardware of the experimental setup. A desktop pc was connected to a National Instruments usb data acquisition module and to the controller of the linear actuator. The data acquisition module was connected to the power source of the rotational actuator and to the data amplifier of the load cell. A Labview program was used to execute the experiments. The Labview program was able to control the displacement of the linear actuator, to control the voltage of the rotational actuator that was attached to the object, to display a real time graphical representation of the force measured by the load cell and to store experimental data. The used Labview program can be found on the data-DVD which is provided with this thesis.

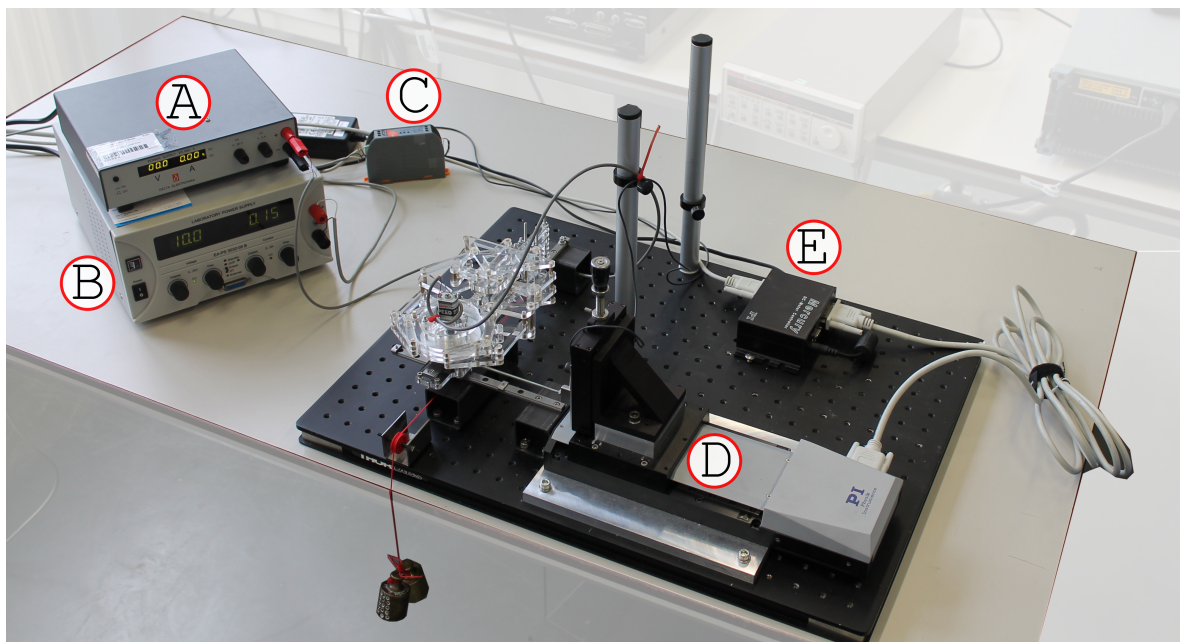


Figure C-10: Overview of the measurement setup illustrating the power source of the rotational actuator (A), the power source of the load cell (B), the data amplifier of the load cell (C), the linear actuator (D) and the controller of the linear actuator (E).

Appendix D

**Literature study: Performance
quantification of variable stiffness
actuator designs**

Submitted to *Robotics and Autonomous Systems*

Performance quantification of variable stiffness actuator designs

R.A.J. Stavenuiter^{a,b}, J.L. Herder^{a,c}

^a*Delft University of Technology, Delft, The Netherlands*

^b*Department of BioMechanical Engineering*

^c*Department of Precision and Microsystems Engineering*

Abstract

A variable stiffness actuator (VSA) is able to adjust its output position and apparent output stiffness independent of each other. Numerous actuator designs based on different working principles have been proposed in literature but no comprehensive performance comparison between designs has been done. Generalized data sheets are not widely used and can be improved. The limited number of performance indicators that are available and the absence in literature of the required measurement data to use these indicators are factors that contribute to the absence of wide spread performance comparison of VSA designs. We introduce the adjustment space ratio (*ASR*) and the linear regression coefficient (R^2) as two performance indicators of a VSA design. These indicators make use of data that is extracted from the torque-angular deflection graph, experimental data that is commonly published in literature. These indicators are used to quantify the performance of 19 actuator designs, showing differences between individual designs, but do not indicate clear differences between classes of designs classified by their working principle. By defining two performance indicators this research contributes to the ability of a large scale performance comparison of VSA designs.

Keywords: Variable stiffness actuators, passive compliance, performance comparison

1. Introduction

A variable stiffness actuator (VSA) is able to control its output position and output stiffness independent of each other. This means that both the output position and the effect that external forces have on the output position can be controlled. In the past years a large number of VSA designs have been proposed in literature and the question arises which of these VSA designs has the best performance. VSA designs have been compared on a large scale by discussing the differences in working principle [1] [2], but in order to quantify and compare the performance between VSA designs a set of indicators is required. Other than the indicators that describe the design criteria such as the allowable torque, angular deflection range and stiffness range, which are strongly dependent on the application, there is only a small number of

performance indicators described in literature:

- *Actuator energy consumption* [3]: By deriving the set of equations that analytically describe the energy consumption of the actuator, the theoretical energy consumption can be estimated using simulation.
- *Performance envelope volume (PEV)* [4]: In the torque-angular velocity-stiffness plot PEV is the total volume of all the possible torque- angular velocity-stiffness relations that the actuator can obtain.
- *Real working volume fitting (RWVF)* [5]: In the torque-angular velocity-stiffness plot RWVF is defined as the ratio between the volume of the torque-angular velocity-stiffness relations that is used by the VSA during operation and the volume of the PEV.
- *Stiffness velocity* [5]: The stiffness velocity is defined as the time which is needed to change

the stiffness from the minimum to the maximum stiffness setting.

- *Energy consumption to change stiffness* [6]: Using a port based analysis the amount of energy needed to change the stiffness setting of a VSA can be defined.

Some of these indicators have been used to compare the performance of a small number of VSA designs [3] [6], but no large scale performance comparison has been done. We believe that one of the reasons for this is caused by the absence of a general set of performance indicators for the objective performance quantification of VSA designs. Also experimental data of VSA designs as published in literature is often not sufficient to determine the value of the available performance indicators. A generalized data sheet [7] is composed and a template is available for use, but not all designers make use of this template when introducing a new VSA design. Besides, the template contains only a few indicators that quantify the performance of the VSA design independent of the design criteria. It is therefore difficult to conduct a large scale performance comparison between available VSA designs to see if a single design or group of designs has a better performance than others. If for every VSA design a generalized set of performance indicators is used, it is much easier to compare the performance between VSA designs on a large scale.

This paper proposes two generic performance indicators to enable large scale performance quantification of VSA designs. These indicators are extracted from the torque-angular deflection curve, experimental data which is commonly published in literature. These indicators will be used to quantify the performance of 19 actuator designs to identify if a single design or group of designs classified by their working principle has a better performance than other designs. The performance quantification is based on data extracted from images of the torque-angular deflection graph as found in literature.

The paper is structured as follows. In section 2 the desired characteristics of a VSA, the derivation of two performance indicators and the method used

to quantify and compare the performance of the VSA designs is discussed. Section 3 shows the results of the analysis which will be discussed in section 4. Conclusions are drawn in section 5.

2. Methods

2.1. Derivation of performance indicators

For the derivation of performance indicators it had to be determined what property of a VSA was suitable for the quantification of the performance. Because the main goal of this research is to compare the performance between VSA designs on a large scale, experimental data concerning this property should be available for a large number of designs. A literature study was done to make an inventory of the available VSA designs and for all designs that were found the type of experimental data that was published in literature was compared. As a result it turned out that the torque-angular deflection graph of the VSA was most often included in the research papers. This graph describes the passive deflection angle as a result of an external torque for the different stiffness settings of the VSA.

The next step of the derivation of a performance indicator was to determine what torque-angular deflection behavior is desired for VSA designs. According to [8] the desired behavior of a VSA consists of two main characteristics:

1. A wide range of the apparent output stiffness, provided by a nonlinear relation between the apparent output stiffness and a control parameter α .
2. A constant apparent output stiffness throughout the range of angular deflection while the parameter α is kept constant.

The first characteristic is desirable because having a wide range of output stiffness increases the versatility of the VSA. If the actuator can obtain many different characteristics the actuator can be applicable for a wide range of tasks. The nonlinear relation between the stiffness and the control parameter α allows the actuator to have a large variation in stiffness settings for a small variation of the parameter α . However the authors

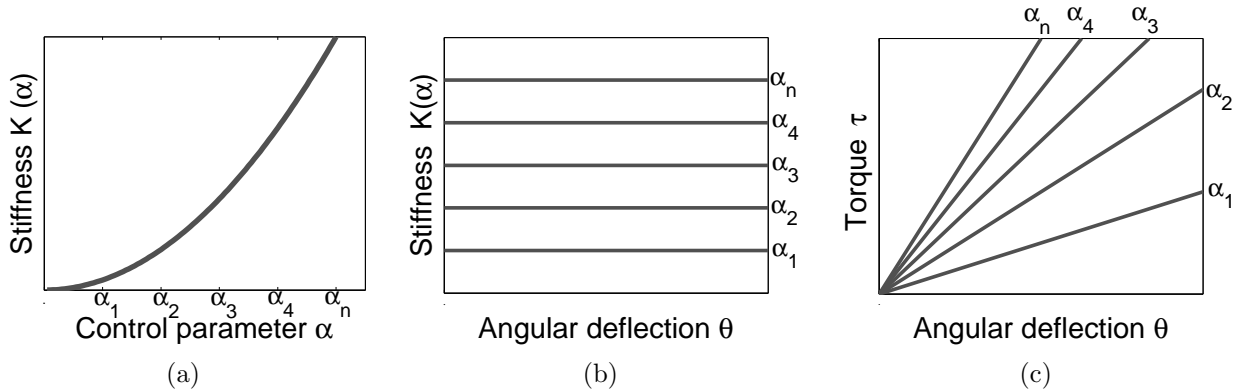


Figure 1: Two desired characteristics of a VSA: a wide range in the apparent output stiffness for different values of α (a) and a constant apparent output stiffness for various deflection angles when the parameter α is kept constant (b). The expression of these characteristics in the torque-angular deflection graph is illustrated in (c). The minimum and maximum stiffness setting are denoted by 1 and n.

believe that the wide range in output stiffness is mainly desired, independently of the type of relation between the stiffness setting and the control parameter α because this relation can be dependent of the application. The second characteristic is desirable because having a constant stiffness value for each setting of contributes to the simplicity of the control algorithm. Figure 1a and 1b show a graphical representation of these desired characteristics.

The extent to which the VSA design meets these desired characteristics can be found in the torque-angular deflection graph. The overall reason to have a wide range in apparent output stiffness is to obtain different torque-angular deflection relations. Therefore the number of the available torque-angular deflection relations within the limiting characteristics of the design can be used as a measure to quantify the range of apparent output stiffness.

In the torque-angular deflection graph a constant stiffness is expressed as a linear relation between the applied torque and the resulting angular deflection. Therefore a method to quantify if the relation between the apparent output stiffness and the angular deflection is constant is by determining to what extent there exists a linear relation between the applied torque and the resulting angular deflection. Figure 1c illustrates the representation of the desired characteristics in the

torque-angular deflection curve. Two indicators have been defined to quantify the performance of a VSA by analyzing to what extent the design meets the desired characteristics:

- Adjustment Space Ratio (ASR)
- Linear regression coefficient (R^2)

2.1.1. Adjustment Space Ratio

The ASR is used to quantify the number of the available torque-angular deflection relations within the limiting characteristics of the design. The adjustment space of a VSA is considered as all the torque-angular deflection relations within the range of a VSA and is defined as the bounded surface area between three functions:

$$T(\theta_{\alpha_1}) \quad for \quad \theta_{\alpha_1} : [0 \quad \theta_{\alpha_1,max}] \quad (1)$$

$$T(\theta_{\alpha_n}) \quad for \quad \theta_{\alpha_n} : [0 \quad \theta_{\alpha_n,max}] \quad (2)$$

$$T(\theta_{\alpha_i,max}) \quad for \quad \theta_{\alpha_i,max} : [\theta_{\alpha_1,max} \quad \theta_{\alpha_n,max}] \quad (3)$$

These three functions describe the relation between the torque T and (1) the angular deflection at the minimum stiffness setting θ_{α_1} , (2) the angular deflection at the maximum stiffness setting θ_{α_n} and (3) the maximum deflection angle for all of the stiffness settings $\theta_{\alpha_i,max}$ as illustrated in Figure 2a. With this definition it is assumed any stiffness setting between the minimum and maximum setting can be obtained.

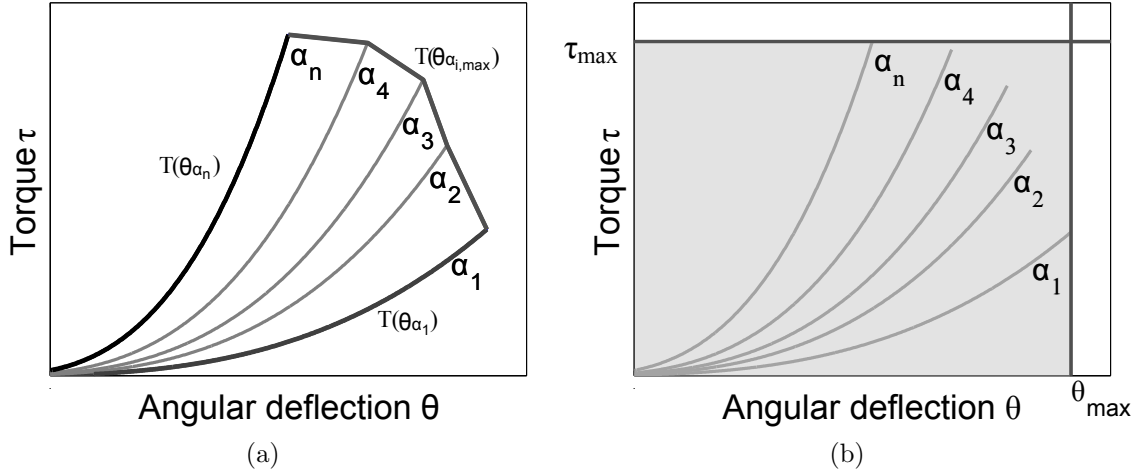


Figure 2: Graphic representation of the adjustment space (a) and the surface area bounded by the extreme values (b).

The *ASR* is defined as the ratio between the surface area of the adjustment space and the surface area of the box bounded by the origin of the torque-deflection curve, the maximum deflection angle θ_{max} and the maximum applied torque τ_{max} as shown in Figure 2. This results in an indicator that is normalized with reference to the maximum deflection angle and maximum torque.

According to the desired characteristics shown in Figure 1a and 1b all of the stiffness values should be available for all deflection angles. Theoretically, in the case of constant stiffness, the VSA should be able to resist an infinite amount of torque in order to obtain infinite stiffness at the maximum deflection angle. The maximum value of the *ASR* would then be 0.5. However when this desired torque-angular deflection characteristic is bounded by the maximum allowable torque τ_{max} of the VSA, the maximum value of the *ASR* will approach 1. Because the stiffness is adjusted to obtain a certain torque-angular deflection relation and a value of 1 indicates that all the torque-angular deflection relations within the range of the VSA can be achieved. The *ASR* can therefore be used to quantify the first characteristic.

2.1.2. Linear regression coefficient

A commonly used measure to quantify the linearity of a dataset is by applying a linear regression analysis. Using a least squares error method a linear function is found that fits the data the best.

An indicator that is used to express the overall quality of this fit is the linear regression coefficient R^2 , which is defined as:

$$R^2 = 1 - \frac{\sum_{i=1}^N [y_i - f_1(x_i)]^2}{\sum_{i=1}^N [y_i - \bar{y}]^2} \quad (4)$$

Where N equals the total number of data points, y_i equals the value of the applied torque of datapoint i , $f_1(x_i)$ equals the value of the torque of datapoint i corresponding to the linear fit and finally \bar{y} equals the mean value of the applied torque of the dataset. The value R^2 is dimensionless and varies between 0 and 1. It equals the value 1 when the dataset exactly matches the linear fit. It is therefore suitable for quantifying the second desired characteristic.

2.2. Performance quantification

In order to obtain the data for the performance quantification for each VSA design the image of the torque-angular deflection graph was taken from literature and analyzed using Adobe Photoshop and Matlab. The exact methods for the calculation of the values of the indicators are now discussed.

2.2.1. Adjustment space ratio

For the analysis of the *ASR* the torque-angular deflection graph of each VSA was copied from the article and opened in Adobe Photoshop. A mask was manually drawn covering the entire adjustment space where the values of $T(\theta_{\alpha_i, max})$ were

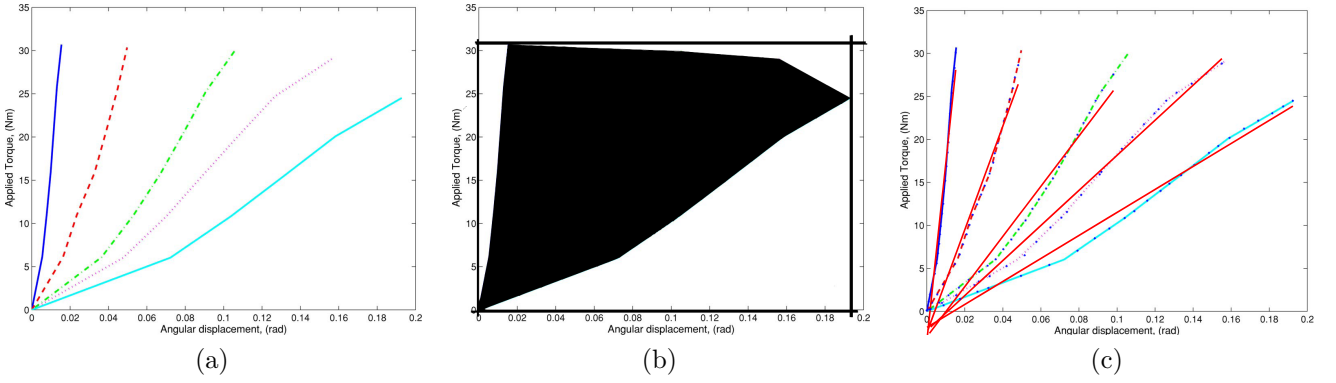


Figure 3: The torque-angular deflection characteristics of a VSA design as presented in literature [13] (a), the same characteristic covered by a mask which indicate the adjustment space and the extreme values used to calculate the ASR (b) and the same characteristic with the results of an indirect linear regression analysis (c).

linearly connected. If the data points were given, a mask was drawn by connecting all the data points. When no data points were given, a mask was drawn connecting the fitted curves. All of the pixels within this mask were colored black.

Two lines were drawn to indicate the absolute maximum value of both the torque and the deflection angle. The area within the axes frame and the two drawn lines was then saved, resulting in a binary image. A Matlab algorithm was used to calculate the ASR by calculating the ratio between the number of black pixels and the total amount of pixels of the image. Figure 3a shows the torque-deflection curve of a VSA design [9] and Figure 3b shows the same curve after the analysis where the adjustment space is covered by a mask and the boundaries of the extreme values are represented by two lines. As validation experiment the method used for the calculation of the ASR was applied ten times for a single actuator design.

2.2.2. Linear regression coefficient

For the linear regression analysis a Matlab algorithm was used to analyze the torque-angular deflection graph of all designs. In the case that the torque-angular deflection graph showed the actual data points these points of the characteristic corresponding to a fixed value of α were manually selected to obtain the coordinates. A linear regression analysis was then applied using the coordinates (direct regression analysis). This procedure was done for all of the curves corresponding

to different settings of α in the torque-deflection graph. When the graph did not show data points but only a curve fit, 25 points along the full length of the curve were manually selected in which it was attempted to spread the points evenly along the curve. These coordinates were then used in the linear regression analysis (indirect regression). Figure 3c shows the result of an indirect regression analysis of a torque-angular deflection curve for each stiffness setting. It was decided to use 25 data points based on an analysis where the linear regression coefficient of a third order polynomial was calculated for a number of data points increasing from 2 to 150. This analysis showed that the value of R^2 that was obtained when 25 data points were used was within 0.2% of the value obtained with 150 data points. Note that with the indirect regression analysis the outliers of the measurement data could have already been removed by a curve fit. Therefore the calculated value of R^2 could be higher using this analysis compared to the actual value. In order to obtain insight in the size of the error introduced by the analysis methods, the repeatability and validity of the methods were tested. The repeatability of the direct and indirect regression method was tested by analyzing a single graph of both regression methods for 15 times. As validation of the method a direct regression was applied on the torque-deflection graphs of two VSA designs [10] and [11] which showed the result of a linear regression analysis which was applied by their author.

2.3. Performance comparison

For each VSA design the values of the two indicators were calculated to quantify the performance. In order to determine if there is a difference in performance between VSA designs that are based on different working principles, all designs were classified according to the classification as defined in [1]. This classification distinguishes four working principles:

- *Equilibrium-controlled stiffness (ECS)*: A fixed stiffness spring is connected in series with a stiff actuator. By actively changing the equilibrium position of the spring the output force which relates to the desired stiffness can be controlled.
- *Antagonistic controlled stiffness (ACS)*: Two actuators in series with two nonlinear springs are coupled antagonistically. Both the output position and stiffness settings are controlled by the two actuators.
- *Structure controlled stiffness (SCS)*: The stiffness is controlled by changing the physical structure of a spring by means of changing the effective length.
- *Mechanically controlled stiffness (MCS)*: The stiffness is controlled by changing the preload or the effective moment arm of a spring, always using the full length of the spring.

The overall performance of a class of designs was determined by calculating the mean values of the ASR and R^2 of all the VSA designs within a class. For each VSA design a data sheet was made including images showing design details, the torque-deflection graph that was used for analysis and data concerning the maximum torque, angular deflection and stiffness. It was also stated whether the full range of the torque-angular deflection graph was shown. This was done because it is most likely that the values of the ASR and R^2 are different when only a section of the torque-angular deflection graph is used for the calculation. No corrections were done to compensate for this, since the remaining part of the graph is unknown.

3. Results

The literature study resulted in 25 scientific articles in which a new VSA design was proposed.

For 19 out of the 25 designs the torque-angular deflection graph for different stiffness settings was given in literature. Table 1 shows the values of the ASR and R^2 of the each of the 19 VSA designs. Figure 4 illustrates the values of the ASR and R^2 for each design classified by their working principle. The majority of the designs was based on the MCS working principle, while none of the designs mentioned in Table 1 were based on the ECS working principle. Two VSA designs that stand out based on the values of the ASR alone are the VSA-HD [4] and AwAS II [12]. For both designs the ASR has a value close to 1, which indicates a good performance. However there is a large difference in value of R^2 between the two designs. Figure 5a and 5b illustrate the torque-angular deflection curves of the AwAS II and VSA-HD respectively. It shows that the torque-angular deflection characteristic for each stiffness setting of AwAS II is close to linear while the characteristics of the VSA-HD is highly nonlinear. Overall most

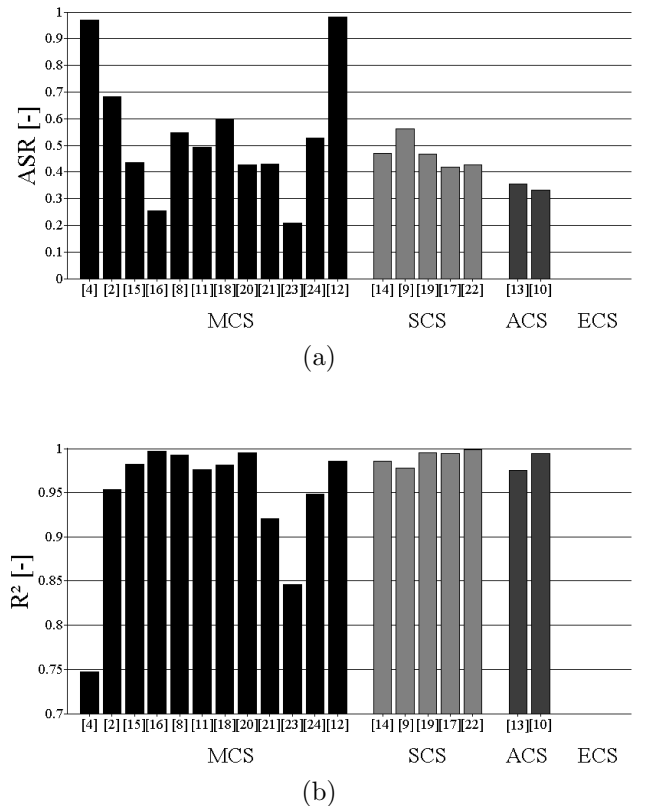


Figure 4: Overview of the values of the ASR (a) and R^2 (b) of all VSA designs classified by their working principle.

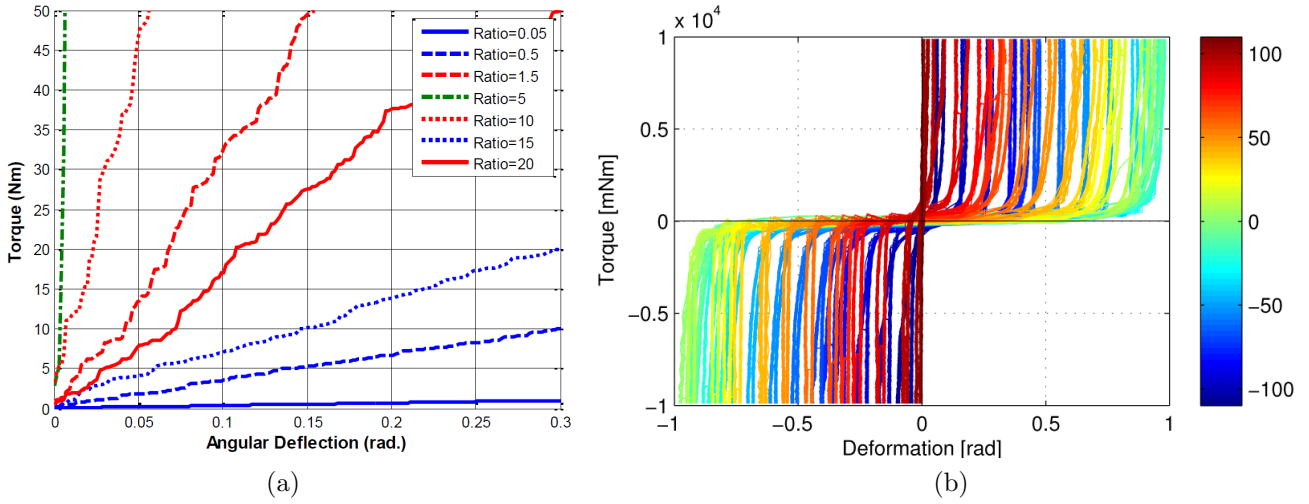


Figure 5: Torque-angular deflection characteristics of AwAS II (a) [12] and VSA-HD (b) [4].

Table 1: For every variable stiffness actuator design the working principle WP , the value of the ASR and the minimum, maximum and mean value of the R^2 is given.

Design	WP	ASR [-]	R^2 [-]		
			Min	Max	Mean
VSA-HD [4]	MCS	0.970	0.643	0.867	0.747
VSA-Cube [13]	ACS	0.355	0.954	0.993	0.975
VSJ [14]	SCS	0.470	0.976	0.993	0.986
VSJ [9]	SCS	0.563	0.964	0.989	0.978
DLR QA-joint [2]	MCS	0.683	0.885	0.999	0.954
AwAS [15]	MCS	0.436	0.975	0.993	0.982
AwAS II [12]	MCS	0.982	0.965	0.999	0.986
MP-joint [16]	MCS	0.254	0.990	0.999	0.997
HDAU [8]	MCS	0.548	0.968	0.999	0.993
VSA [10]	ACS	0.331	0.985	0.997	0.994
MIA [17]	SCS	0.419	0.992	0.999	0.995
MESTRAN [11]	MCS	0.494	0.943	0.990	0.976
VSA-II [18]	MCS	0.598	0.974	0.988	0.981
VSA [19]	SCS	0.467	0.989	0.999	0.994
MACCEPA 1.0 [20]	MCS	0.427	0.993	0.999	0.995
MACCEPA 2.0 [21]	MCS	0.430	0.801	0.969	0.921
ADEA [22]	SCS	0.426	0.998	0.999	0.999
VS-joint [23]	MCS	0.207	0.776	0.901	0.846
DLR FSJ [24]	MCS	0.527	0.900	0.988	0.948

VSA designs have a high value of R^2 . Based on the two indicators it can be stated that AwAS II has the best performance of the VSA designs analyzed in this research.

Table 2 illustrates the mean values and stan-

dard deviations of the ASR and mean R^2 for each of the working principles. It shows that on average the VSA designs of the MCS type have the highest value of the ASR and the all designs of the SCS have a close to linear torque-angular displacement

Table 2: The mean values and standard deviation σ of the ASR and mean R^2 for each class, where n denotes the number of mechanisms of each class

Type	(n)	ASR		Mean R^2	
		Mean	σ	Mean	σ
MCS	(12)	0.546	0.240	0.944	0.075
ACS	(2)	0.343	0.017	0.985	0.013
SCS	(5)	0.469	0.057	0.990	0.008
ECS	(0)	-	-	-	-

characteristic. As a result of the repeatability experiments of the regression analysis the standard deviations were $1.72e-4$ and $7.6e-3$ for the direct and indirect regression analysis respectively. The repeatability experiment of the ASR resulted in a standard deviation of $8.42e-4$. For the validation experiment the calculated value of R^2 was compared with the given value of R^2 resulting in two values of the root mean square error of 0.008 and 0.002.

Only for six designs it was stated in literature that the torque-angular deflection graph showed the curves of all the stiffness settings up to the maximum values of the torque and angular deflection, thus the entire adjustment space. In five cases it was stated that it did not show the entire adjustment space and for the other eight designs it was unknown.

4. Discussion

Table 1 and Figure 4 indicate differences in performance between individual VSA designs based on the values of the ASR and R^2 alone. The classification of the VSA designs according to their working principles did not result in clear differences in performance based on the values of the ASR and R^2 alone. Although Table 2 shows that the ACS type of joints have the lowest value of the ASR , and the MCS type of joints have the lowest value of R^2 , the number of mechanisms in each class is not sufficient to draw clear conclusions. Also Figure 4 shows that within the MCS class the performance varies much between individual VSA designs. In order to investigate if there is a difference in performance between the classes

of the used designs, more performance indicators should be used.

The fact that none of the designs used in this research was based on the ECS principle can be explained, because with the ECS working principle the VSA actively controls the position and stiffness settings simultaneously. As a result there are no passive torque-angular displacement curves for each stiffness setting.

Table 1 shows that the largest part of the VSA designs have a value of the ASR between 0.4 and 0.6. The low torque-high deflection region is often not within the range of the VSA. One of the reasons for that could be that not all torque-angular deflection relations are desirable during operation, but only a certain region of interest is wanted. In the low torque-high deflection region small external forces will result in large deflections, which in many cases is undesirable behavior. It is likely that in many applications the VSA does not have to be able to achieve this torque-angular deflection relation. In this case the designer is not encouraged to design a VSA with a larger adjustment space than necessary. However, for safe human-robot interaction, this low stiffness setting could be desirable. Therefore we believe that the ASR as being a measure of the available operating range within the maximum allowable torque and angular deflection is a suitable indicator in order to express the versatility of a VSA.

The method of calculation of the ASR as applied in this research can be discussed. For the calculation of the adjustment space the extreme values of the torque-angular deflection characteristic for each stiffness setting were linearly connected. It is most likely that in practice this is not the case, but since the exact behavior is unknown, this assumption was used. The assumption that any stiffness setting between the minimum and maximum setting is possible and the resulting characteristics cover the entire adjustment space can also be questioned.

The use of the linear regression coefficient R^2 to express the linearity of the torque-angular deflection characteristic as applied in this paper can be discussed. As Table 1 shows, 14 out of 19 designs have a mean value of R^2 above 0.97. This indi-

cates that either these designs have a close to linear torque-angular deflection characteristic, or that the indicator R^2 is not sensitive enough to show the differences. The torque-angular-deflection characteristics of most designs do show a close to linear characteristic, however in the case of the VSA -HD the nonlinear torque-angular deflection characteristics that can be seen in Figure 5 scores a mean value of 0.747 for R^2 . This shows that although the value of R^2 can vary between 0 and 1, only a value close to 1 indicates that the torque-angular deflection characteristic is close to linear. During this research it was also investigated if the value of the root mean square error (RMSE) of a normalized torque-angular deflection characteristic could be used to either express the linearity of the characteristic or ratify the value of R^2 , but due to inaccuracies in the transformations from pixels to a normalized dimensionless value using the maximal allowable torque this method was not used. However we believe that the value of the normalized RMSE is a suitable indicator to ratify the value of R^2 if it can be calculated accurately using real measurement data. Because the linear regression coefficient R^2 is a commonly used indicator to express the linearity of a data set, we believe that this indicator is suitable for quantifying the desired characteristic of having a constant stiffness throughout the range of angular deflection while the parameter is kept constant.

As for the method that is applied to calculate the value of R^2 in this research, the manual selection of data points introduces errors. As discussed earlier, due to the low sensitivity of R^2 , errors could have a large effect on the results. However, based on the standard deviations of the repeatability experiments that do not indicate the presence of large errors we state that the results obtained in this research represent a good approximation of the linearity of the torque-angular deflection characteristics of the VSA designs.

Because the data used for the performance quantification was extracted from the torque-angular deflection graphs as presented in literature and only for six designs it was stated that the whole graph was shown, the values of ASR and R^2 can differ from the actual values based on the whole

graph. Although this is the case we believe that for each VSA design the region of interest of the torque-angular displacement graph is shown.

5. Conclusion

This paper has introduced two indicators for the objective performance quantification of VSA designs, the Adjustment Space Ratio ASR and the linear regression coefficient R^2 . The results were presented of a performance comparison between 19 variable stiffness actuator designs based on these indicators alone. Differences in performance between individual designs were found, but did not indicate clear differences between groups of designs, classified by their working principle. In order to determine if there is a difference in performance between VSA designs classified by their working principle a larger set of performance indicators is required for the analysis.

Although the VSA designs used in this research are diverse, most of them are constructed using the same elements, namely a linear spring and a mechanism to introduce nonlinearities. It is interesting to see the different characteristics that result from the different configurations of those elements. In conclusion we would like to state that comprehensive performance quantification of VSA designs will benefit from a standardized data sheet with performance indicators to describe the behavior of a VSA design.

References

- [1] R. v. Ham, T. Sugar, B. Vanderborght, K. Hollander, D. Lefeber, Compliant actuator designs, *Robotics & Automation Magazine, IEEE* 16 (3) (2009) 81–94.
- [2] O. Eiberger, S. Haddadin, M. Weis, A. Albu-Schaffer, G. Hirzinger, On joint design with intrinsic variable compliance: Derivation of the dlr qa-joint, in: *Robotics and Automation (ICRA), 2010 IEEE International Conference on, IEEE, 2010*, pp. 1687–1694.
- [3] B. Vanderborght, R. Van Ham, D. Lefeber, T. G. Sugar, K. W. Hollander, Comparison of mechanical design and energy consumption of adaptable, passive-compliant actuators, *The International Journal of Robotics Research* 28 (1) (2009) 90–103.
- [4] M. G. Catalano, G. Grioli, F. Bonomo, R. Schiavi, A. Bicchi, Vsa-hd: From the enumeration analysis to the prototypical implementation, in: *Intelligent*

- Robots and Systems (IROS), 2010 IEEE/RSJ International Conference on, IEEE, 2010, pp. 3676–3681.
- [5] M. G. Catalano, R. Schiavi, A. Bicchi, Mechanism design for variable stiffness actuation based on enumeration and analysis of performance, in: Robotics and Automation (ICRA), 2010 IEEE International Conference on, IEEE, 2010, pp. 3285–3291.
- [6] L. Visser, R. Carloni, S. Stramigioli, Variable stiffness actuators: a port-based analysis and a comparison of energy efficiency, in: Robotics and Automation (ICRA), 2010 IEEE International Conference on, IEEE, 2010, pp. 3279–3284.
- [7] Viactors web site, <http://viactors.eu/>, accessed: 2012-08.
- [8] B.-S. Kim, J.-B. Song, Hybrid dual actuator unit: A design of a variable stiffness actuator based on an adjustable moment arm mechanism, in: Robotics and Automation (ICRA), 2010 IEEE International Conference on, IEEE, 2010, pp. 1655–1660.
- [9] J. Choi, S. Hong, W. Lee, S. Kang, M. Kim, A robot joint with variable stiffness using leaf springs, Robotics, IEEE Transactions on 27 (2) (2011) 229–238.
- [10] S. A. Migliore, E. A. Brown, S. P. DeWeerth, Biologically inspired joint stiffness control, in: Robotics and Automation, 2005. ICRA 2005. Proceedings of the 2005 IEEE International Conference on, IEEE, 2005, pp. 4508–4513.
- [11] H. V. Quy, L. Aryananda, F. I. Sheikh, F. Casanova, R. Pfeifer, A novel mechanism for varying stiffness via changing transmission angle, in: Robotics and Automation (ICRA), 2011 IEEE International Conference on, IEEE, 2011, pp. 5076–5081.
- [12] A. Jafari, N. G. Tsagarakis, D. G. Caldwell, Awas-ii: A new actuator with adjustable stiffness based on the novel principle of adaptable pivot point and variable lever ratio, in: Robotics and Automation (ICRA), 2011 IEEE International Conference on, IEEE, 2011, pp. 4638–4643.
- [13] M. G. Catalano, G. Grioli, M. Garabini, F. Bonomo, M. Mancinit, N. Tsagarakis, A. Bicchi, Vsa-cubebot: a modular variable stiffness platform for multiple degrees of freedom robots, in: Robotics and Automation (ICRA), 2011 IEEE International Conference on, IEEE, 2011, pp. 5090–5095.
- [14] J. Choi, S. Park, W. Lee, S.-C. Kang, Design of a robot joint with variable stiffness, in: Robotics and Automation, 2008. ICRA 2008. IEEE International Conference on, IEEE, 2008, pp. 1760–1765.
- [15] A. Jafari, N. G. Tsagarakis, B. Vanderborght, D. G. Caldwell, A novel actuator with adjustable stiffness (awas), in: Intelligent Robots and Systems (IROS), 2010 IEEE/RSJ International Conference on, IEEE, 2010, pp. 4201–4206.
- [16] S. Kajikawa, K. Abe, Robot finger module with multidirectional adjustable joint stiffness, Mechatronics, IEEE/ASME Transactions on 17 (1) (2012) 128–135.
- [17] T. Morita, S. Sugano, Development of 4-dof manipulator using mechanical impedance adjuster, in: Robotics and Automation, 1996. Proceedings., 1996 IEEE International Conference on, Vol. 4, IEEE, 1996, pp. 2902–2907.
- [18] R. Schiavi, G. Grioli, S. Sen, A. Bicchi, Vsa-ii: A novel prototype of variable stiffness actuator for safe and performing robots interacting with humans, in: Robotics and Automation, 2008. ICRA 2008. IEEE International Conference on, IEEE, 2008, pp. 2171–2176.
- [19] S. Sugano, S. Tsuto, I. Kato, Force control of the robot finger joint equipped with mechanical compliance adjuster, in: Intelligent Robots and Systems, 1992., Proceedings of the 1992 IEEE/RSJ International Conference on, Vol. 3, IEEE, 1992, pp. 2005–2013.
- [20] R. Van Ham, B. Vanderborght, M. Van Damme, B. Verrelst, D. Lefeber, Maccopa, the mechanically adjustable compliance and controllable equilibrium position actuator: Design and implementation in a biped robot, Robotics and Autonomous Systems 55 (10) (2007) 761–768.
- [21] B. Vanderborght, N. G. Tsagarakis, C. Semini, R. Van Ham, D. G. Caldwell, Maccopa 2.0: Adjustable compliant actuator with stiffening characteristic for energy efficient hopping, in: Robotics and Automation, 2009. ICRA'09. IEEE International Conference on, IEEE, 2009, pp. 544–549.
- [22] R.-J. Wang, H.-P. Huang, Adeactive variable stiffness differential elastic actuator: Design and application for safe robotics, in: Robotics and Biomimetics (ROBIO), 2011 IEEE International Conference on, IEEE, 2011, pp. 2768–2773.
- [23] S. Wolf, G. Hirzinger, A new variable stiffness design: Matching requirements of the next robot generation, in: Robotics and Automation, 2008. ICRA 2008. IEEE International Conference on, IEEE, 2008, pp. 1741–1746.
- [24] S. Wolf, O. Eiberger, G. Hirzinger, The dlr fsj: Energy based design of a variable stiffness joint, in: Robotics and Automation (ICRA), 2011 IEEE International Conference on, IEEE, 2011, pp. 5082–5089.

Catalano [4]

VSA-HD

WORKING PRINCIPLE

DESIGN

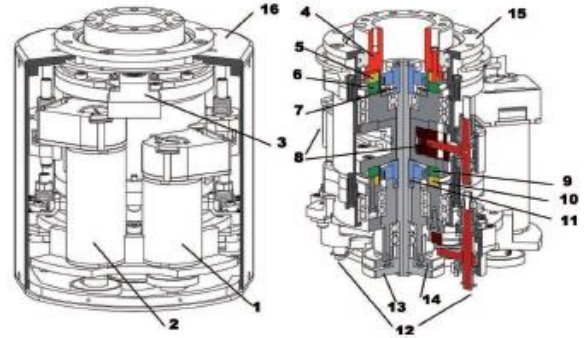
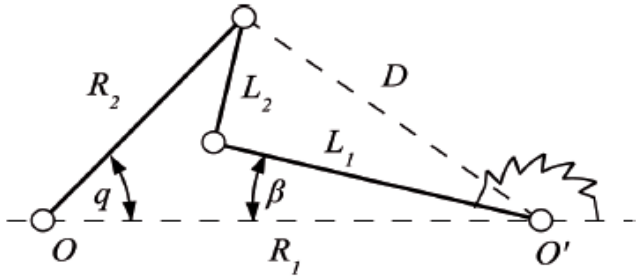
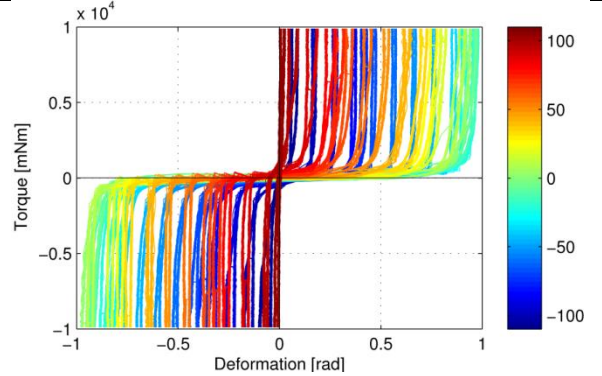


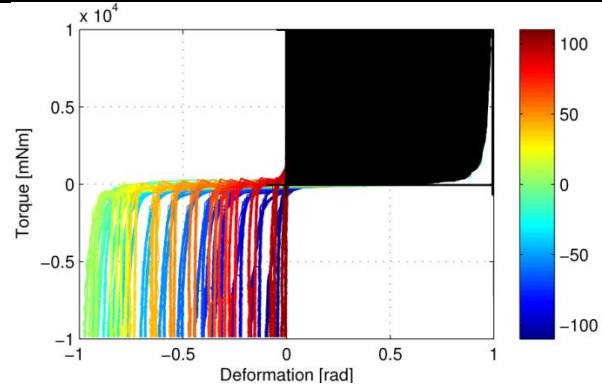
Fig. 9. Working principle of the non-linear spring used in the VSA-HD. Angle q is the interface between the non-linear elasticity and other system components. A linear spring is connected to the 4-bar linkages and excited by the angle β . The non-linearity comes from the variation in speed ratio between the cranks L_1 and R_2 , ranging from a finite value to 0 (4-bars fully opened), thus giving rise to a stiffness ranging up to infinity.

TORQUE - ANGULAR DEFLECTION

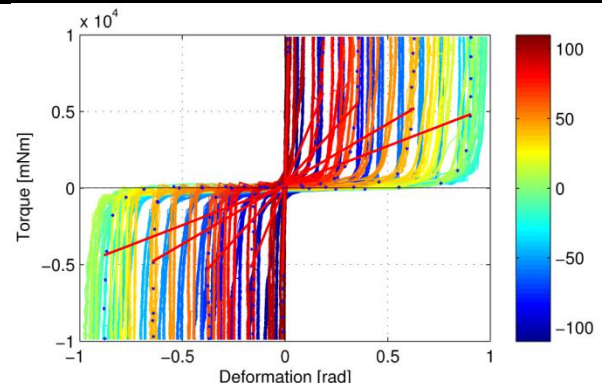
Quantity	Unit	Value
Torque	$[N \cdot m]$	Max 14
Angular deflection	$[rad]$	Max 1
Stiffness	$[N \cdot m/rad]$	Min 0
		Max 8000
ASR	$[-]$	0.970
R^2	$[-]$	Min 0.643
		Max 0.867
		Mean 0.747
Working principle		MCS
Datapoints		No
Full range	Torque	Unknown
	Angular deflection	Unknown
	Stiffness settings	Yes



ASR



LINEARITY



WORKING PRINCIPLE

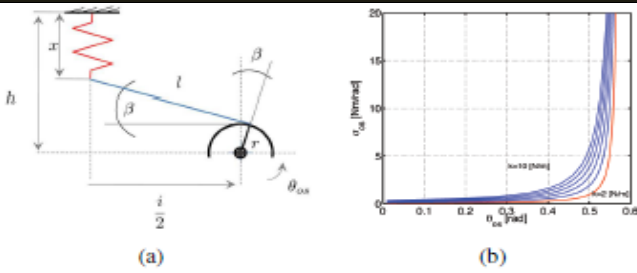
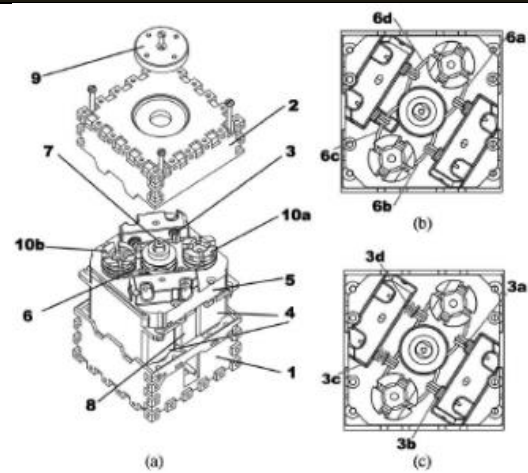
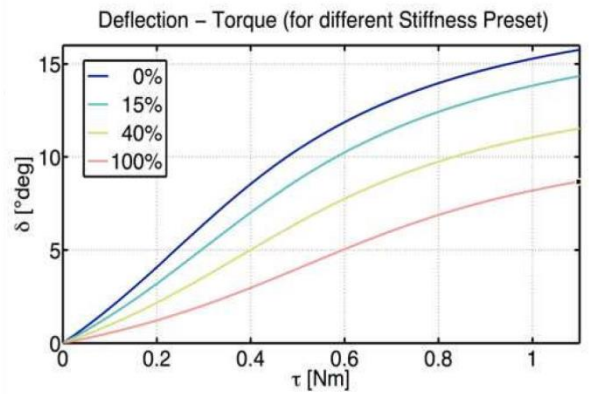


Fig. 7. Scheme of the stiffness regulation mechanical principle, (a), and stiffness characteristic of the Cube VS mechanism, (b). Symbols in panel (a) represent: i the distance between centres of the pulleys; l distance between free end of the spring and point in which the tendon is tangent to the pulley; r radius of the pulley; β the angle between i and l ; h the distance between fixed end of the spring and i ; x the length of the spring; θ_{os} the angular position of output shaft; k is the spring elastic constant. Different lines on panel (b) correspond to different values of the elastic constant of the springs, the red line matches the value of the springs adopted in the prototype.

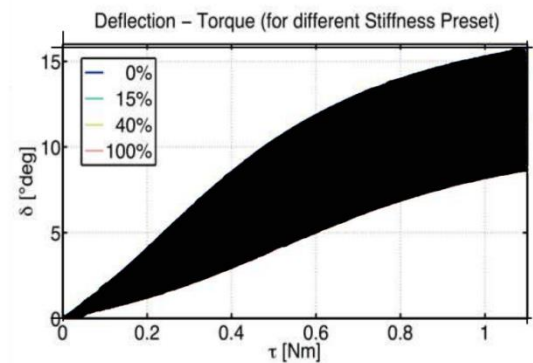
DESIGN



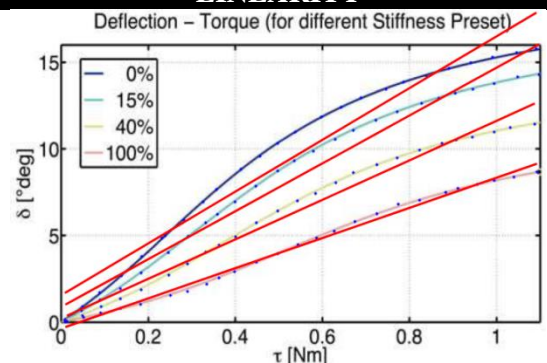
TORQUE - ANGULAR DEFLECTION



ASR



LINEARITY



Quantity	Unit		Value
Torque	$[N \cdot m]$	Max	1.1
Angular deflection	$[rad]$	Max	15.8
Stiffness	$[N \cdot m/rad]$	Min	3
		Max	14
ASR	$[-]$		0.355
R^2	$[-]$	Min	0.954
		Max	0.993
		Mean	0.975
Working principle			ACS
Datapoints			No
Full range	Torque		Yes
	Angular deflection		Yes
	Stiffness settings		Yes

WORKING PRINCIPLE

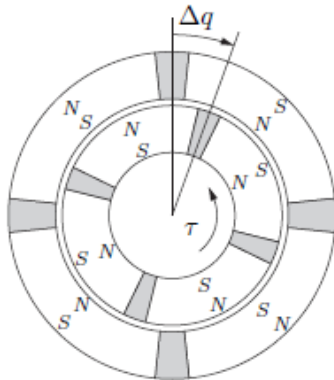
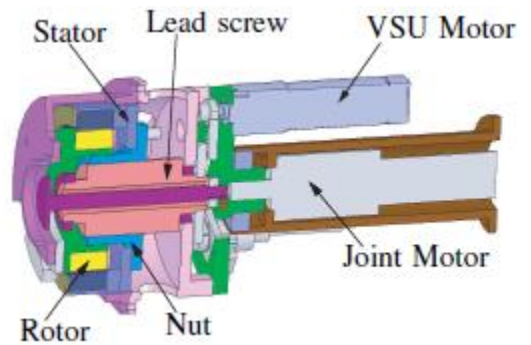
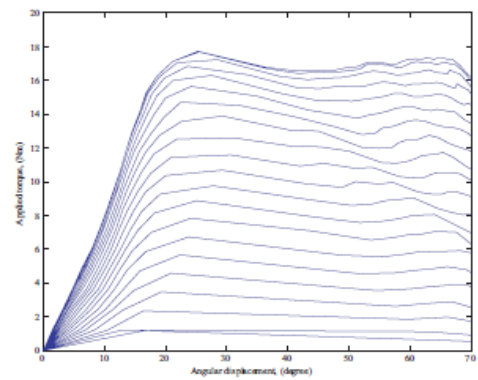


Fig. 1. Two concentric ring composed of magnets. Two adjacent magnets are magnetized in the opposite direction. Gray parts between the magnets are spacers, which are not magnetized. Δq is displacement from the neutral position. τ is the torque generated by the magnets.

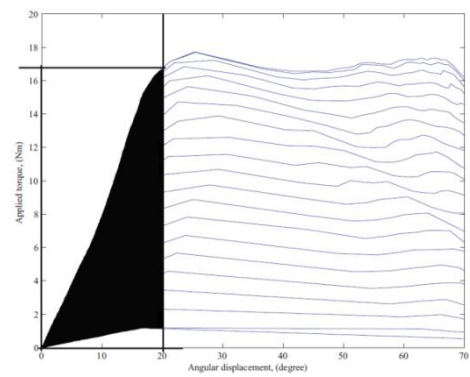
DESIGN



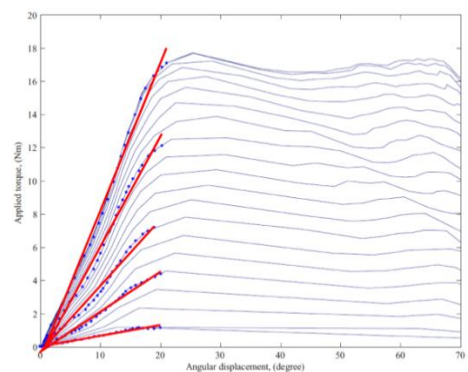
TORQUE-DEFLECTION



ASR



LINEARITY



Quantity	Unit	Value	
Torque	[N · m]	Max	18
Angular deflection	[rad]	Max	0.35
Stiffness	[N · m/rad]	Min	4.08
		Max	49.4
ASR	[-]		
R ²	[-]	Min	
		Max	
		Mean	
Working principle			SCS
Datapoints			No
Full range	Torque		Unknown
	Angular deflection		Yes
	Stiffness settings		Unknown

WORKING PRINCIPLE

DESIGN

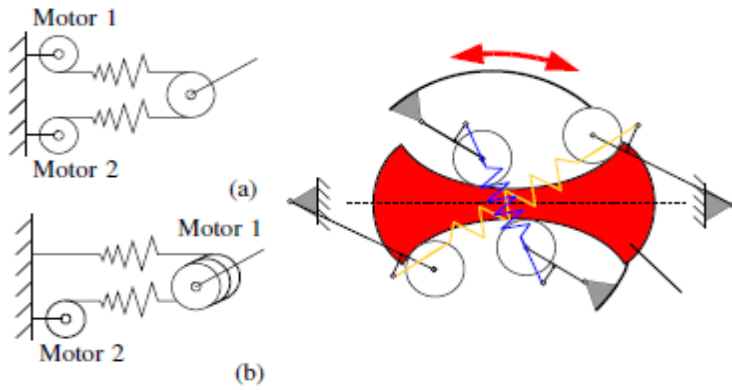


Fig. 4. Variable Stiffness Actuator with nonlinear progressive springs in antagonistic (a) and quasi antagonistic (b) realization. Principle of the elastic mechanism (right).

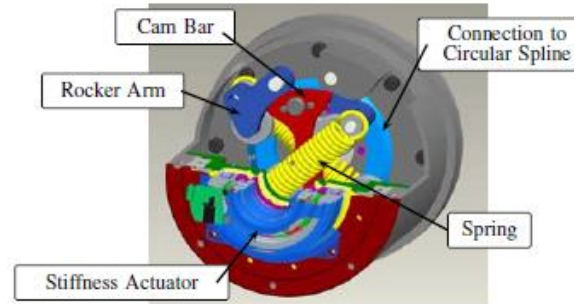
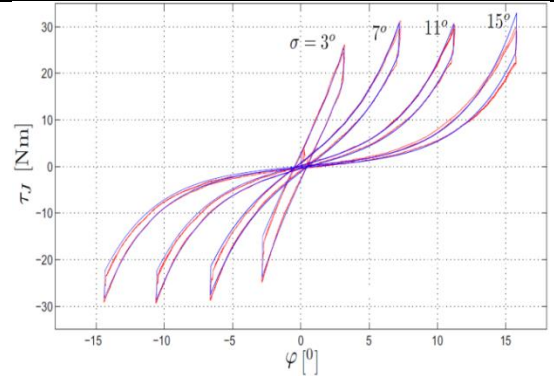


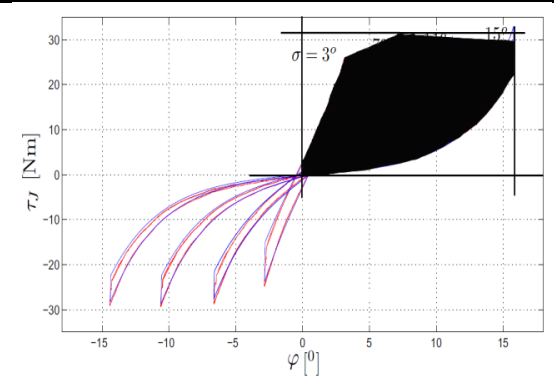
Fig. 5. Cross section of the Quasi Antagonistic Joint design.

Quantity	Unit	Value
Torque	$[N \cdot m]$	Max 40
Angular deflection	$[rad]$	Max 0.26
Stiffness	$[N \cdot m/rad]$	Min 20
		Max 750
ASR	$[-]$	0.683
R ²	$[-]$	Min 0.885
		Max 0.999
		Mean 0.954
Working principle		MCS
Datapoints		No
Full range	Torque	Yes
	Angular deflection	Yes
	Stiffness settings	Yes

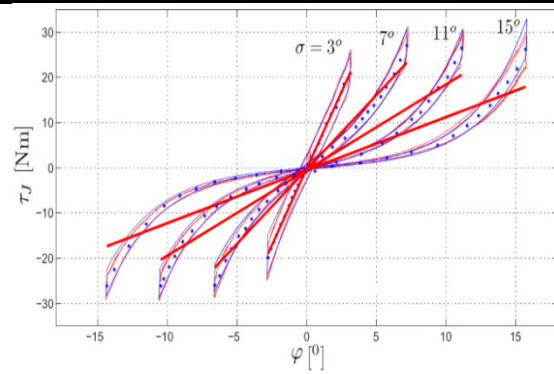
TORQUE - ANGULAR DEFLECTION



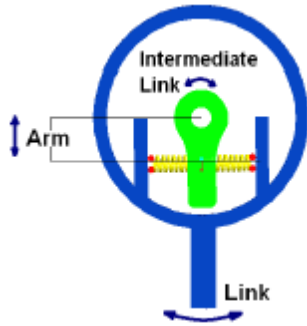
ASR



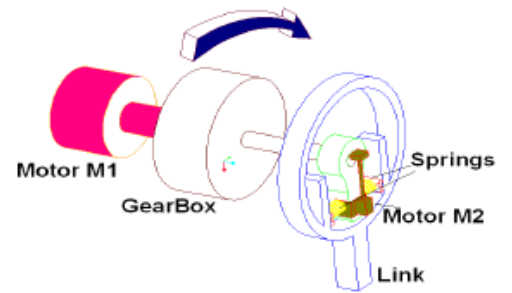
LINEARITY



WORKING PRINCIPLE

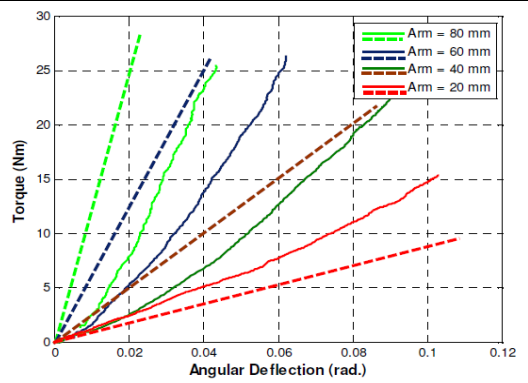


DESIGN

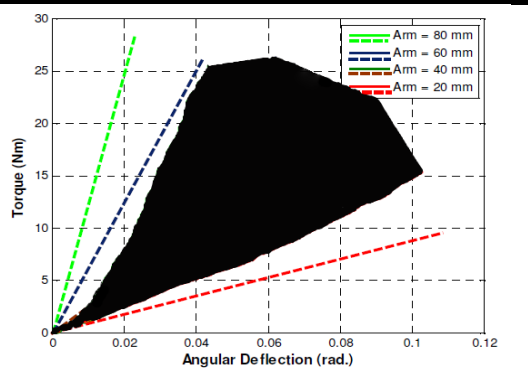


Quantity	Unit	Value
Torque	$[N \cdot m]$	Max 26
Angular deflection	$[rad]$	Max 0.2
Stiffness	$[N \cdot m/rad]$	Min 30
		Max 1300
ASR	$[-]$	0.463
R ²	$[-]$	Min 0.975
		Max 0.993
		Mean 0.982
Working principle		MCS
Datapoints		No
Full range	Torque	Unknown
	Angular deflection	No
	Stiffness settings	No

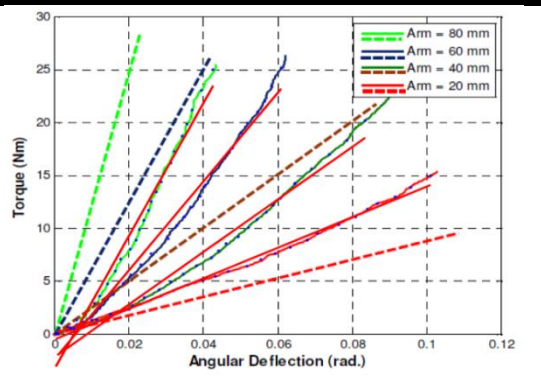
TORQUE - ANGULAR DEFLECTION



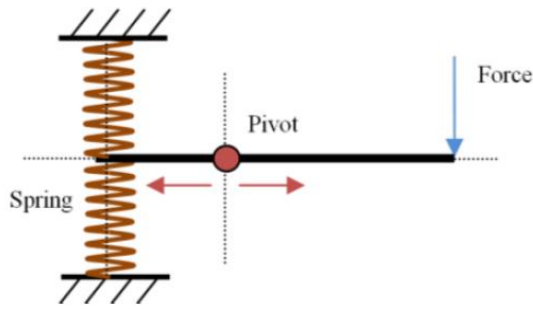
ASR



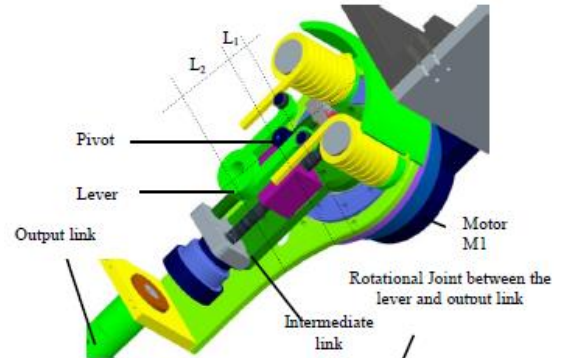
LINEARITY



WORKING PRINCIPLE

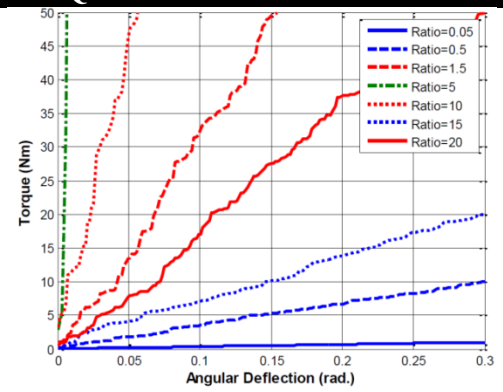


DESIGN

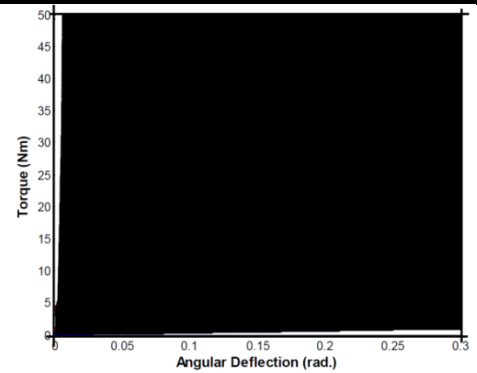


Quantity	Unit	Value
Torque	$[N \cdot m]$	Max 80
Angular deflection	$[rad]$	Max 0.3
Stiffness	$[N \cdot m/rad]$	Min 0 Max ∞
ASR	$[-]$	0.982
R ²	$[-]$	Min 0.999
		Max 0.965
		Mean 0.986
Working principle		MCS
Datapoints		No
Full range	Torque	No
	Angular deflection	Yes
	Stiffness settings	Yes

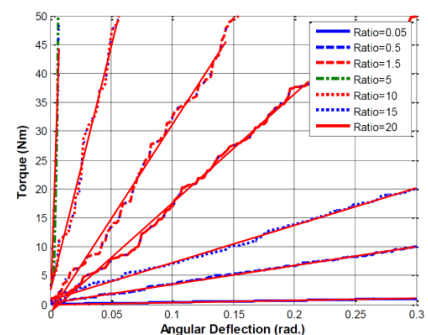
TORQUE - ANGULAR DEFLECTION



ASR



LINEARITY



WORKING PRINCIPLE

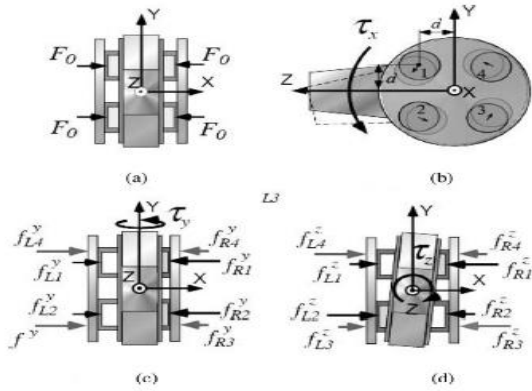
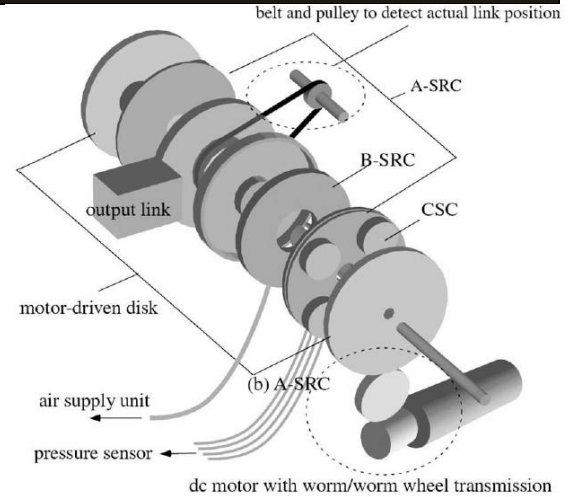


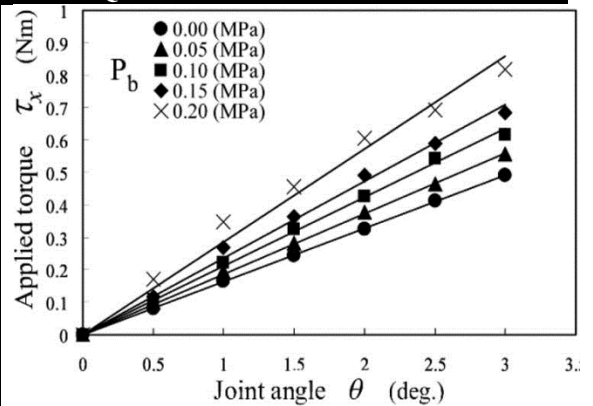
Fig. 2. Deformation of A-SRC under different conditions of external force application. (a) Initial condition when no external force is applied. (b) External force τ_x is applied around the X-axis. Deformation and slippage of A-SRC occur. (c) and (d) External forces τ_y and τ_z are applied around the Y- and Z-axes, respectively.

DESIGN

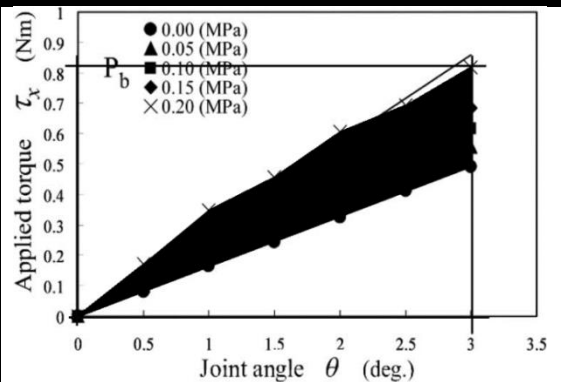


Quantity	Unit	Value
Torque	[N · m]	Max 0.8
Angular deflection	[rad]	Max 0.05
Stiffness	[N · m/rad]	Min 9.17
		Max 16.62
ASR	[-]	0.254
R ²	[-]	Min 0.990
		Max 1.000
		Mean 0.997
Working principle		MCS
Datapoints		Yes
Full range	Torque	Unknown
	Angular deflection	Unknown
	Stiffness settings	No

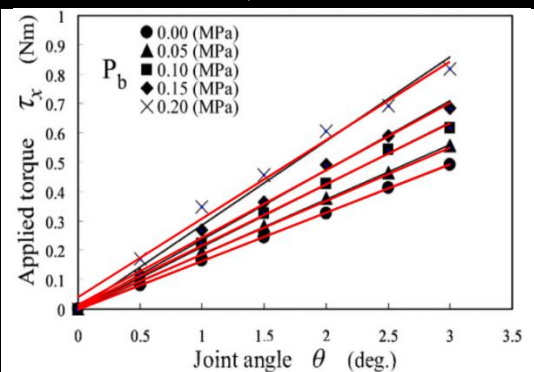
TORQUE - ANGULAR DEFLECTION



ASR



LINEARITY



WORKING PRINCIPLE

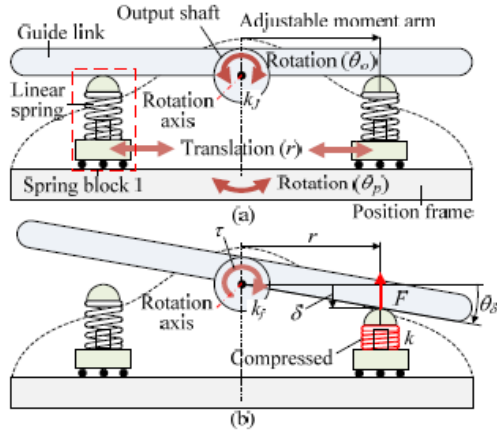
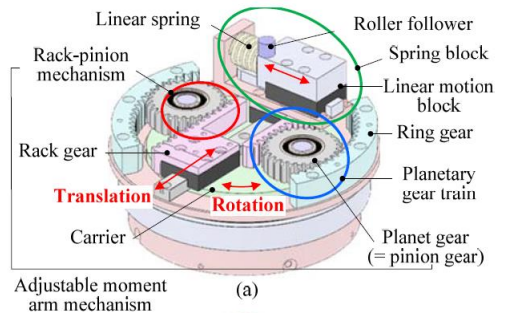


Fig. 3. Principle of variable stiffness mechanism based on adjustable moment arm: (a) initial state, and (b) rotated state.

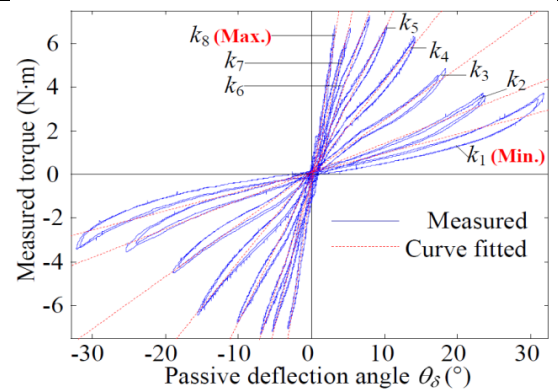
DESIGN



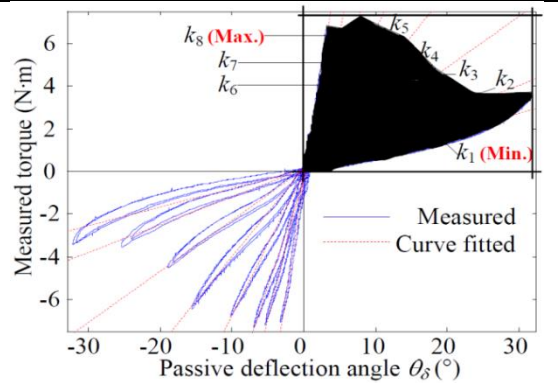
Adjustable moment arm mechanism (a)

Quantity	Unit	Value
Torque	$[N \cdot m]$	Max 8.50
Angular deflection	$[rad]$	Max 0.52
Stiffness	$[N \cdot m/rad]$	Min 3.90
		Max 123.42
ASR	$[-]$	0.548
R ²	$[-]$	Min 0.968
		Max 0.999
		Mean 0.993
Working principle		MCS
Datapoints		No
Full range	Torque	Yes
	Angular deflection	Yes
	Stiffness settings	Yes

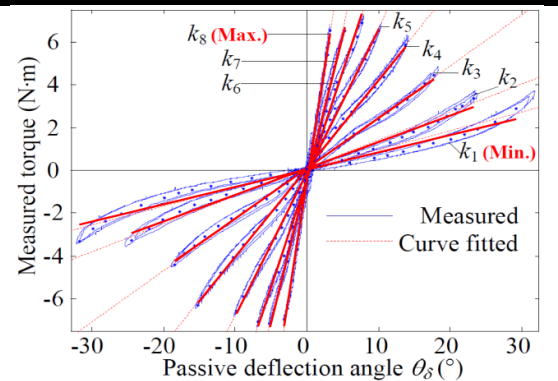
TORQUE - ANGULAR DEFLECTION



ASR



LINEARITY



WORKING PRINCIPLE

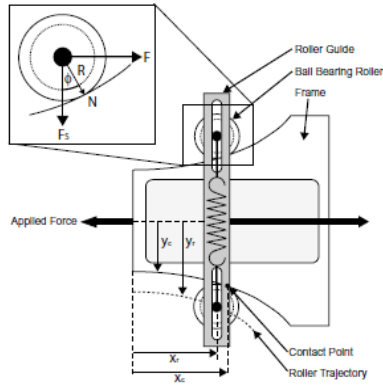
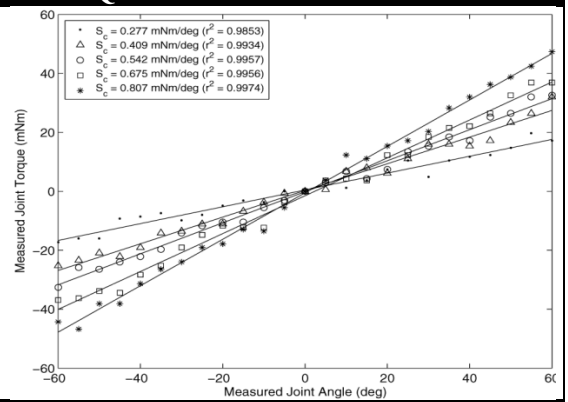


Fig. 2. The design of the nonlinear elastic device. When a stretching force is applied to the device, the rollers are forced along the expanding contour and stretch is applied to a pair of linear springs (one is not visible in background).

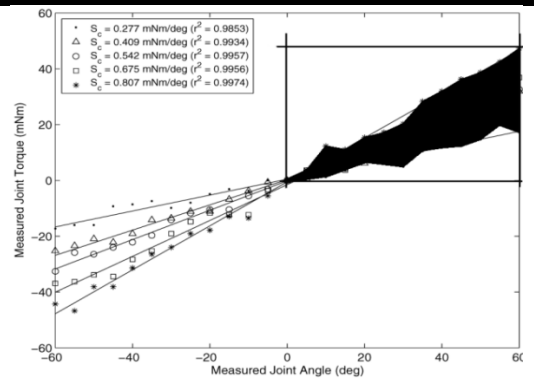
DESIGN



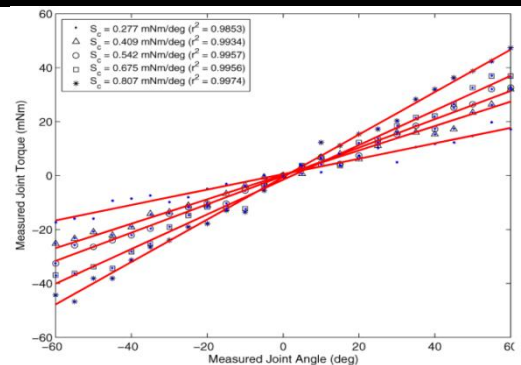
TORQUE - ANGULAR DEFLECTION



ASR



LINEARITY



Quantity	Unit	Value
Torque	$[N \cdot m]$	Max 0.045
Angular deflection	$[rad]$	Max 1.05
Stiffness	$[N \cdot m/rad]$	Min 0.016 Max 0.046
ASR	$[-]$	0.331
R^2	$[-]$	1 0.985 Measured 0.969 2 0.993 0.987 3 0.996 0.992 4 0.996 0.991 5 0.997 0.995 Min 0.985 0.969 Max 0.997 0.995 Mean 0.994 0.987
Working principle		ACS
Datapoints		Yes
Full range	Torque	Unknown
	Angular deflection	Unknown
	Stiffness settings	Unknown

WORKING PRINCIPLE

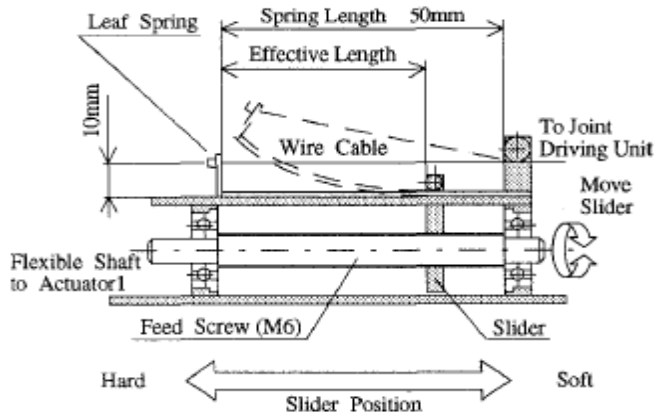
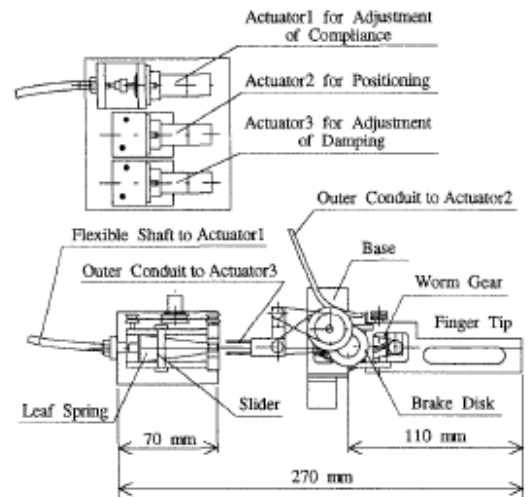


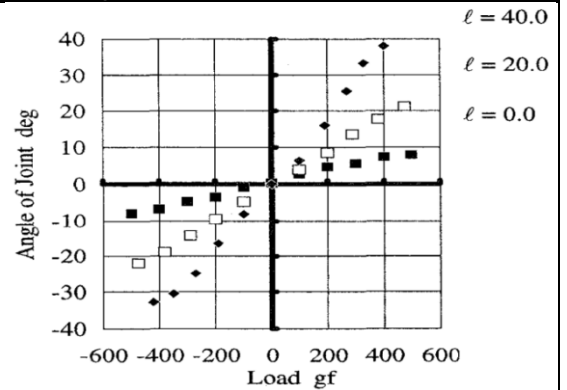
Figure 2: Structure of Mechanical Compliance Adjuster

DESIGN

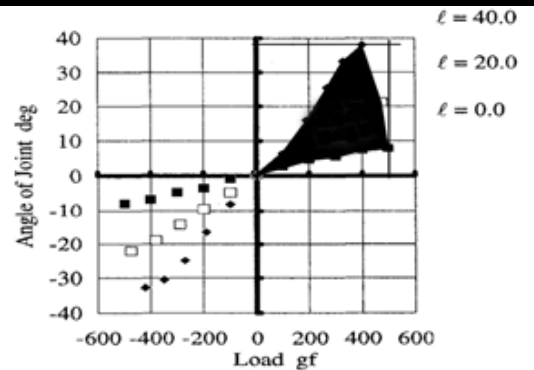


Quantity	Unit	Value
Torque	[N · m]	Max 0.49
Angular deflection	[rad]	Max 0.66
Stiffness	[N · m/rad]	Min 0.65
		Max 3.12
ASR	[-]	0.419
R ²	[-]	Min 0.992
		Max 0.999
		Mean 0.995
Working principle		SCS
Datapoints		Yes
Full range	Torque	Unknown
	Angular deflection	Unknown
	Stiffness settings	No

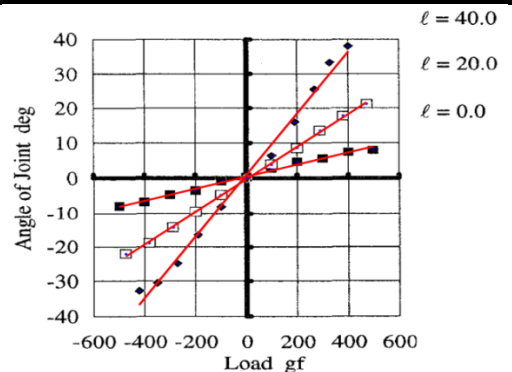
TORQUE - ANGULAR DEFLECTION



ASR



LINEARITY



WORKING PRINCIPLE

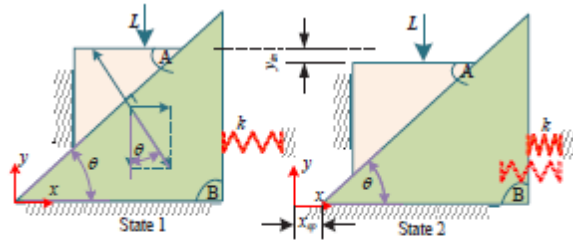
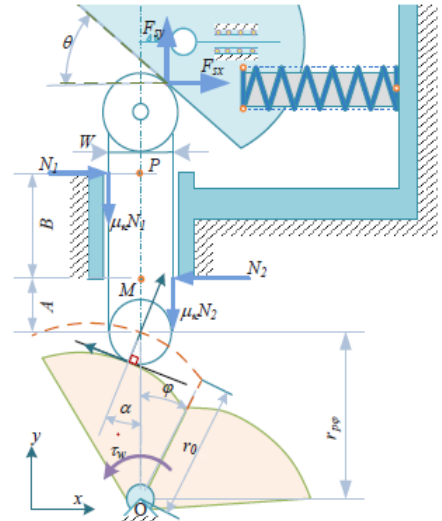


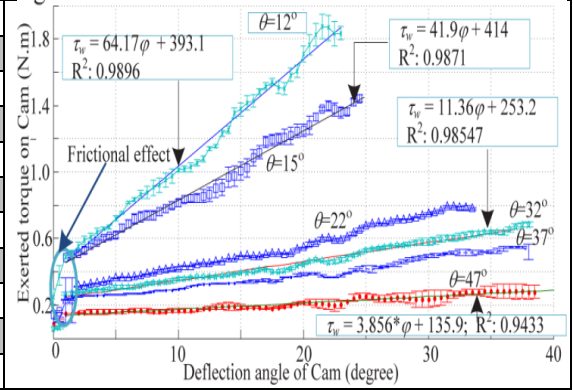
Fig.1 Concept of force transmission via slopes. L : pressing force; θ slope angle (transmission angle); x_0 : spring deflection; y_0 : displacement; k : stiffness of spring. Block A can slide on block B freely.

DESIGN

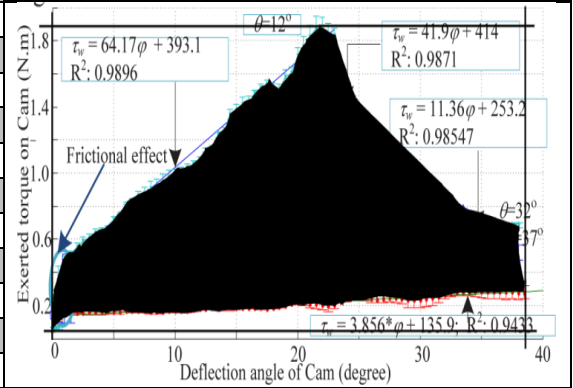


TORQUE - ANGULAR DEFLECTION

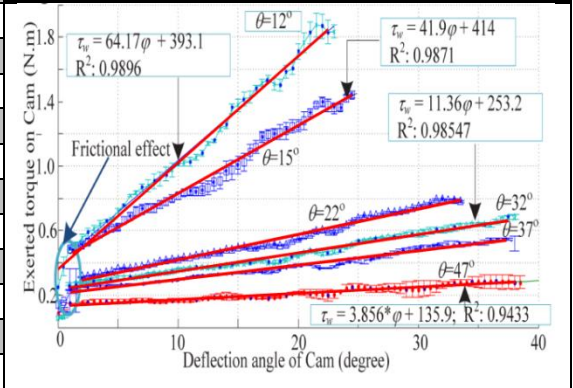
Quantity	Unit	Value		
Torque	$[N \cdot m]$	Max	1.8	
Angular deflection	$[rad]$	Max	0.70	
Stiffness	$[N \cdot m/rad]$	Min	0.22	
		Max	3.68	
ASR	[-]		0.494	
		Given	Measured	
R ²	[-]	1	0.990	0.988
		2	0.987	0.988
		3	-	0.987
		4	0.985	0.982
		5	-	0.978
		6	0.943	0.944
		Min	0.943	0.944
	Max	0.990	0.988	
	Mean	0.976	0.978	
Working principle			MCS	
Datapoints			Yes	
Full range	Torque		Unknown	
	Angular deflection		Unknown	
	Stiffness settings		Unknown	



ASR



LINEARITY



WORKING PRINCIPLE

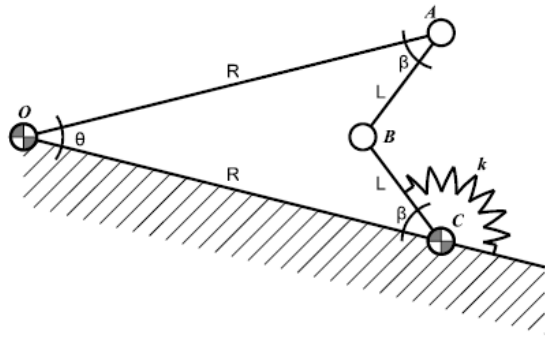


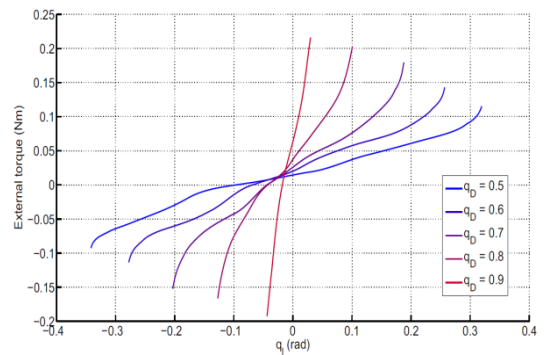
Fig. 2. Line diagram of 4-bar transmission mechanism of VSA II. Link OA of length R is driven by a motor at O . The torque spring k has a linear behaviour. Stiffness seen at O attains non-linearity through the geometry, where angle θ at O and transmission angle β are related non-linearly.

DESIGN

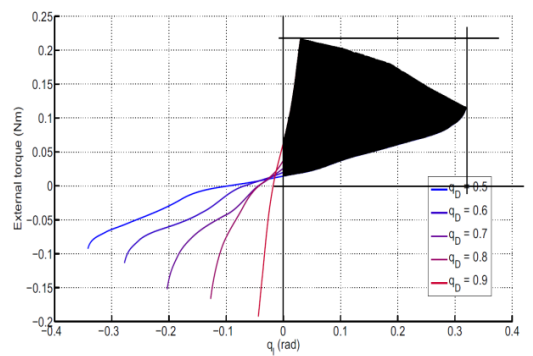


Quantity	Unit	Value
Torque	$[N \cdot m]$	Max 0.32
Angular deflection	$[rad]$	Max 0.22
Stiffness	$[N \cdot m/rad]$	Min 0.15
		Max 9.5
ASR	$[-]$	0.598
R^2	$[-]$	Min 0.974
		Max 0.988
		Mean 0.981
Working principle		MCS
Datapoints		No
Full range	Torque	Unknown
	Angular deflection	Unknown
	Stiffness settings	Unknown

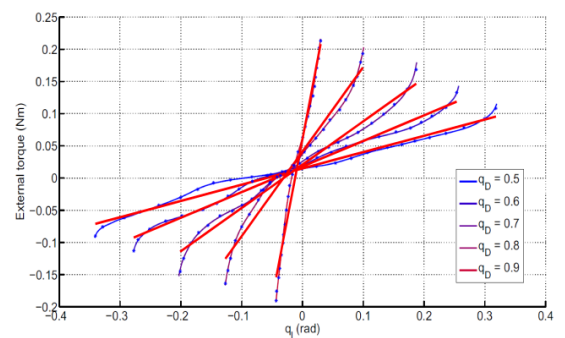
TORQUE - ANGULAR DEFLECTION



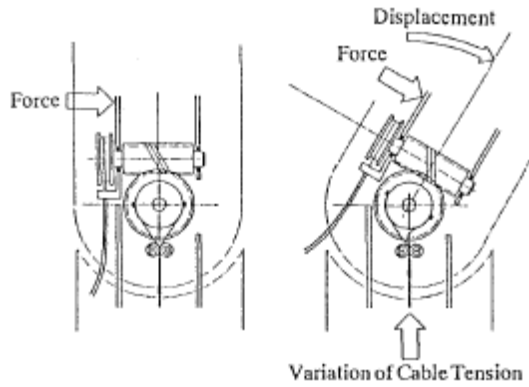
ASR



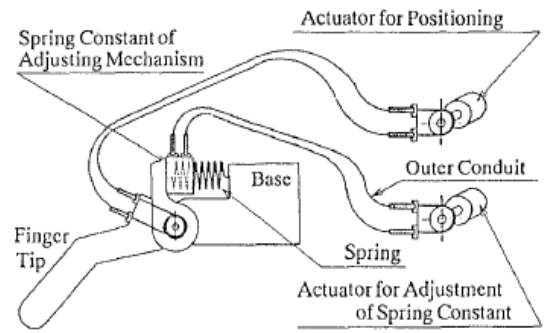
LINEARITY



WORKING PRINCIPLE

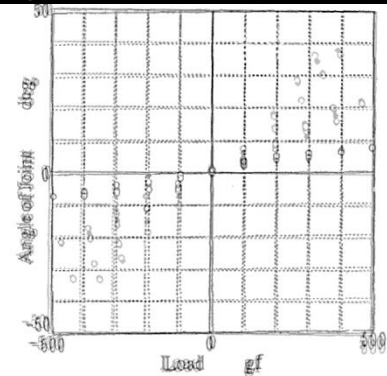


DESIGN

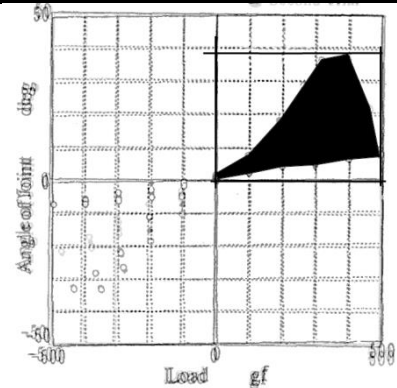


Quantity	Unit		Value
Torque	$[N \cdot m]$	Max	4.90
Angular deflection	$[rad]$	Max	0.75
Stiffness	$[N \cdot m/rad]$	Min	0.52
		Max	4.09
ASR	$[-]$		0.467
R^2	$[-]$	Min	0.989
		Max	0.999
		Mean	0.994
Working principle			SCS
Datapoints			Yes
Full range	Torque		Unknown
	Angular deflection		Unknown
	Stiffness settings		Unknown

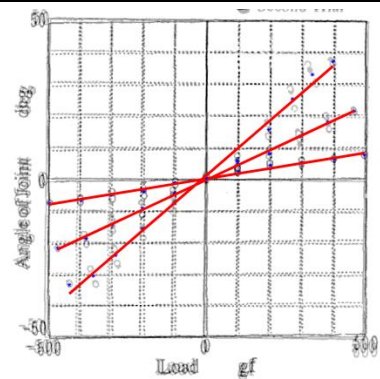
TORQUE - ANGULAR DEFLECTION



ASR



LINEARITY



WORKING PRINCIPLE

DESIGN

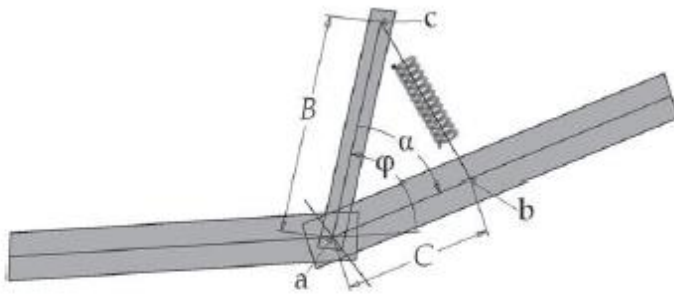
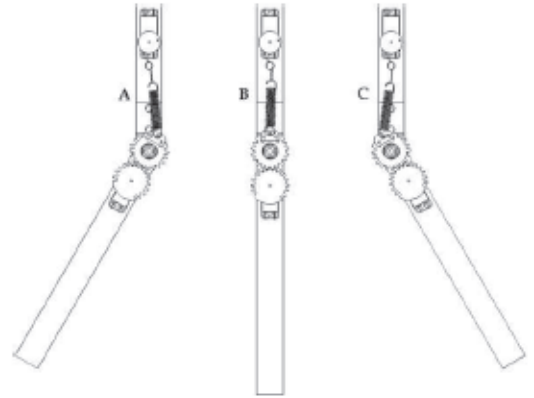
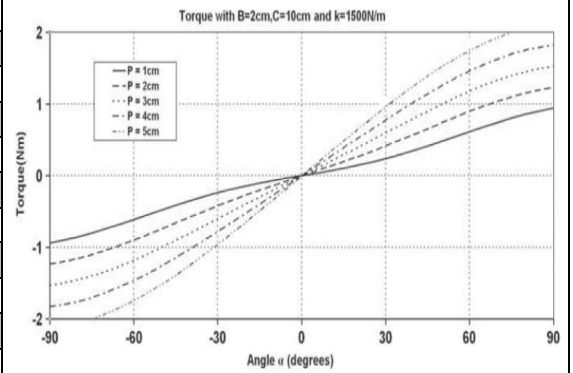


Fig. 1. Working principle of the MACCEPA.

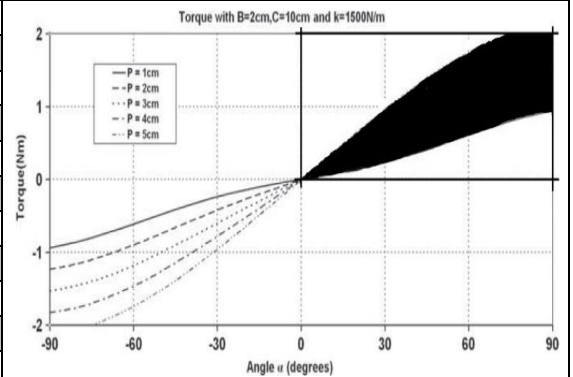


Quantity	Unit	Value
Torque	$[N \cdot m]$	Max 2
Angular deflection	$[rad]$	Max 1.57
Stiffness	$[N \cdot m/rad]$	Min 0.57
		Max 1.67
ASR	$[-]$	0.427
R^2	$[-]$	Min 0.992
		Max 0.999
		Mean 0.995
Working principle		MCS
Datapoints		No
Full range	Torque	Unknown
	Angular deflection	Unknown
	Stiffness settings	Unknown

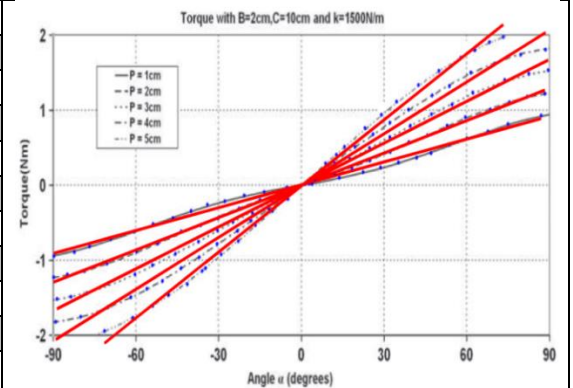
TORQUE - ANGULAR DEFLECTION



ASR



LINEARITY



Vanderborght [21]

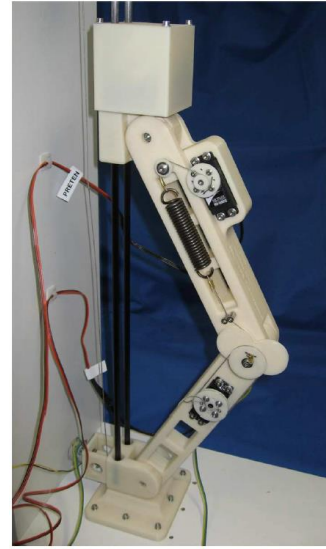
WORKING PRINCIPLE



Fig. 4. Working principle of the novel MACCEPA 2.0. Top: Out of equilibrium position (generating torque) Middle: At equilibrium position (not generating torque) Bottom: Changed pretension.

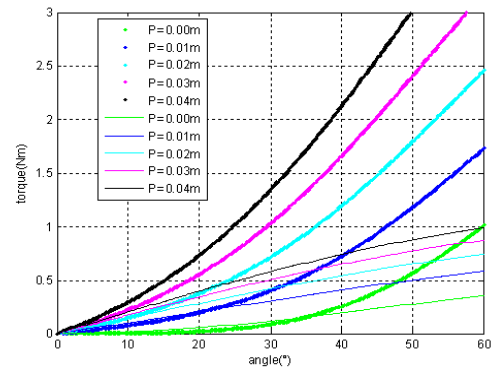
MACCEPA 2.0

DESIGN

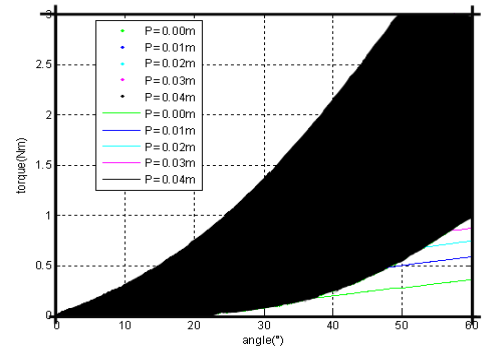


Quantity	Unit	Value
Torque	$[N \cdot m]$	Max 3
Angular deflection	$[rad]$	Max 1.05
Stiffness	$[N \cdot m/rad]$	Min 0
		Max 5.16
ASR	$[-]$	0.430
R ²	$[-]$	Min 0.801
		Max 0.969
		Mean 0.921
Working principle		MCS
Datapoints		No
Full range	Torque	Unknown
	Angular deflection	Unknown
	Stiffness settings	Unknown

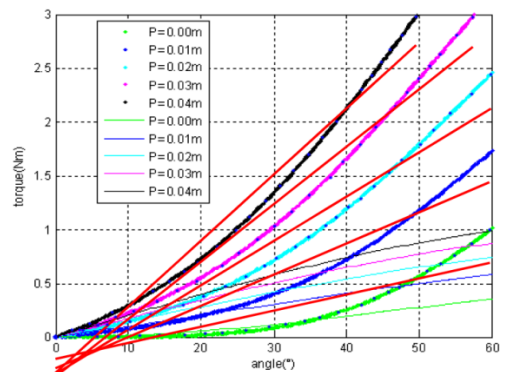
TORQUE - ANGULAR DEFLECTION



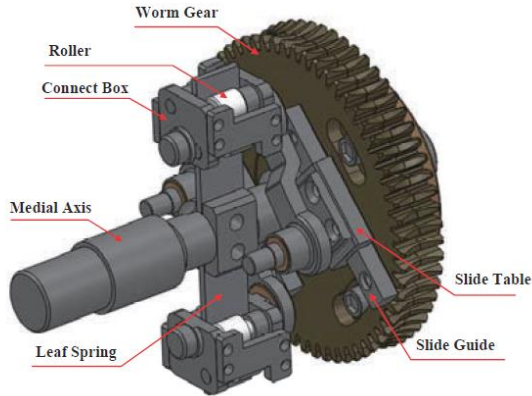
ASR



LINEARITY



WORKING PRINCIPLE

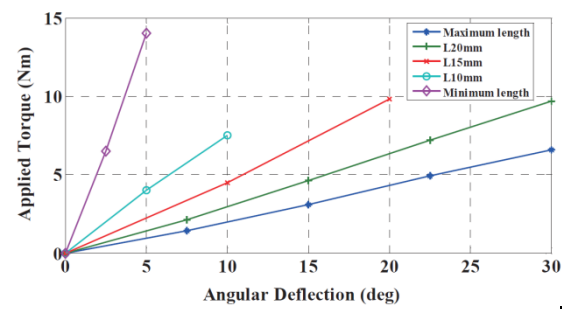


DESIGN

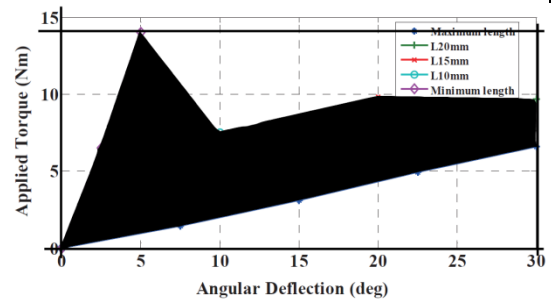


Quantity	Unit	Value
Torque	$[N \cdot m]$	Max 20.2
Angular deflection	$[rad]$	Max 0.52
Stiffness	$[N \cdot m/rad]$	Min 4.87
		Max rigid joint-like
ASR	$[-]$	0.426
R^2	$[-]$	Min 0.998
		Max 0.999
		Mean 0.999
Working principle		SCS
Datapoints		
Full range	Torque	No
	Angular deflection	Yes
	Stiffness settings	Yes

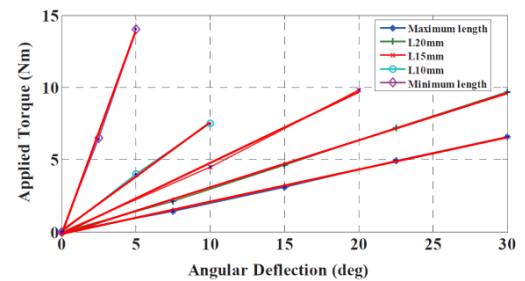
TORQUE - ANGULAR DEFLECTION



ASR



LINEARITY



WORKING PRINCIPLE

DESIGN

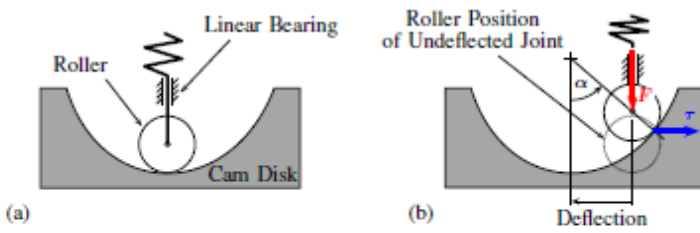
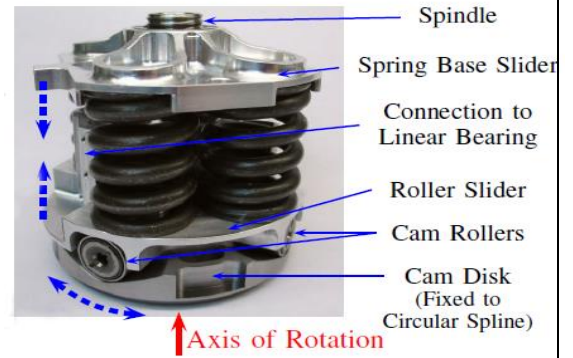
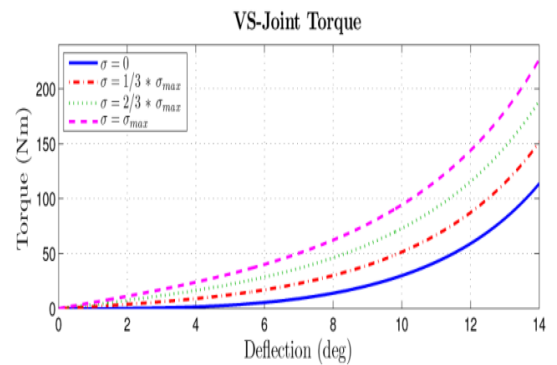


Fig. 4. Unwinded schematic of the VS-Joint principle in centered (a) and deflected (b) position. A deflection of the joint results in a horizontal movement of the cam disk and a vertical displacement of the roller. The spring force generates a centering torque on the cam disk

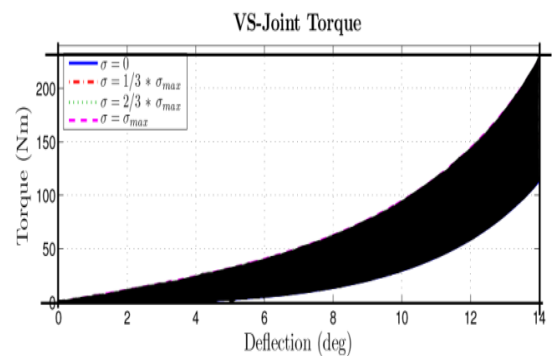


Quantity	Unit	Value
Torque	$[N \cdot m]$	Max 225
Angular deflection	$[rad]$	Max 0.24
Stiffness	$[N \cdot m/rad]$	Min 0
		Max 3036
ASR	$[-]$	0.207
R ²	$[-]$	Min 0.776
		Max 0.901
		Mean 0.846
Working principle		MCS
Datapoints		No
Full range	Torque	Yes
	Angular deflection	Yes
	Stiffness settings	Yes

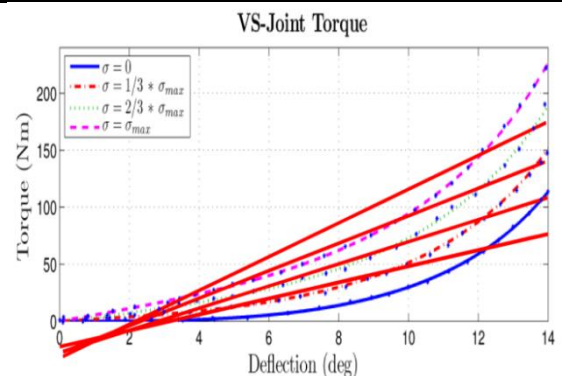
TORQUE - ANGULAR DEFLECTION



ASR

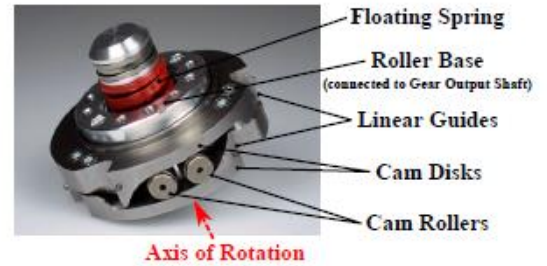
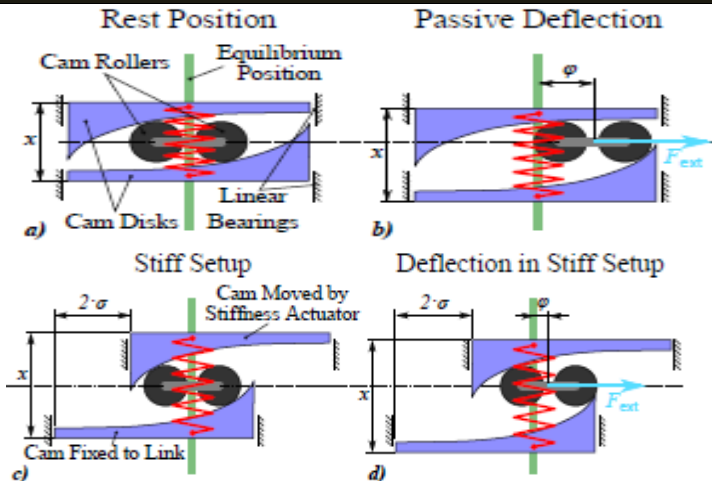


LINEARITY



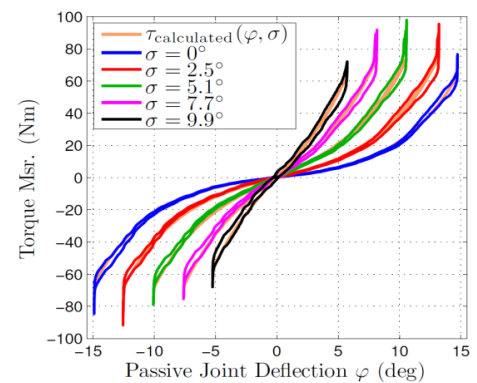
WORKING PRINCIPLE

DESIGN

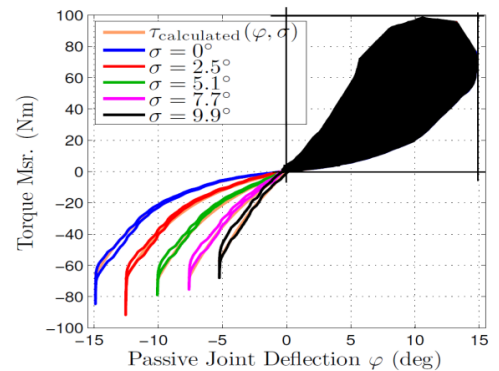


Quantity	Unit	Value
Torque	[N · m]	Max 67
Angular deflection	[rad]	Max 0.26
Stiffness	[N · m/rad]	Min 52.4
		Max 826
ASR	[-]	0.527
R ²	[-]	Min 0.900
		Max 0.988
		Mean 0.948
Working principle		MCS
Datapoints		No
Full range	Torque	Yes
	Angular deflection	Yes
	Stiffness settings	Yes

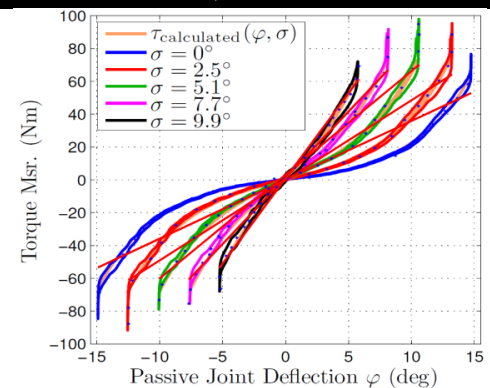
TORQUE - ANGULAR DEFLECTION



ASR



LINEARITY



Bibliography

- [1] R. v. Ham, T. Sugar, B. Vanderborght, K. Hollander, and D. Lefeber, “Compliant actuator designs,” *Robotics & Automation Magazine, IEEE*, vol. 16, no. 3, pp. 81–94, 2009.
- [2] G. A. Kragten and J. L. Herder, “A platform for grasp performance assessment in compliant or underactuated hands,” *Journal of Mechanical Design*, vol. 132, p. 024502, 2010.

